The Influence of Copper and Zinc on the Self-assembly of Amyloid-β from Alzheimer's Disease

Christian James Matheou

A thesis submitted to

QUEEN MARY, UNIVERSITY OF LONDON

for the degree of

DOCTOR OF PHILOSOPHY

School of Biological and Chemical Sciences Queen Mary, University of London September 2015

STATEMENT OF ORIGINALITY

I, Christian James Matheou, confirm that the research included within this thesis is my own work or that where it has been carried out in collaboration with, or supported by others, that this is duly acknowledged below and my contribution indicated. Previously published material is also acknowledged below.

I attest that I have exercised reasonable care to ensure that the work is original, and does not to the best of my knowledge break any UK law, infringe any third party's copyright or other Intellectual Property Right, or contain any confidential material.

I accept that the College has the right to use plagiarism detection software to check the electronic version of the thesis.

I confirm that this thesis has not been previously submitted for the award of a degree by this or any other university.

Signature:

Date: 06/09/15

Details of collaboration and publications:

Matheou CJ, Younan ND, Viles JH (2015) Cu^{2+} accentuates distinct misfolding of Abeta(1-40) and Abeta(1-42) peptides, and potentiates membrane disruption. *Biochem J* **466:** 233-242

ABSTRACT

Alzheimer's disease is characterised by the misfolding and aggregation of a native peptide, Aβ, for which there are several isoforms, $A\beta_{(1-40)}$ being the most common, and $A\beta_{(1-42)}$ being most closely associated with Alzheimer's disease. Upon misfolding, Aβ self-associates to form a number of aggregate species. What triggers this process of misfolding-aggregation, and determines which aggregate species forms, is not known. One possible determinant is metal homeostasis, which in Alzheimer's patients is deregulated.

Chapter 3 characterises how physiologically relevant levels of Cu^{2+} influence the misfolding pathway of Aβ. A ThT fluorescence assay found that Cu^{2+} is able to accelerate formation of $A\beta_{(1-40)}$ amyloid fibres; however, for $A\beta_{(1-42)}$, Cu^{2+} abolished fibre formation. Electron microscopy revealed that this is because Cu^{2+} stabilised $A\beta_{(1-42)}$ oligomers. These oligomers more readily disrupted lipid membranes than mature amyloid fibres, suggesting that the elevated levels of Cu^{2+} and the greater $A\beta_{(1-42)}$ synaptotoxicity in Alzheimer's disease may be related. Chapter 4 investigates the effect of Zn^{2+} on Aβ misfolding. Trace levels of Zn^{2+} are demonstrated to entirely abolish fibre growth, for both $A\beta_{(1-40)}$ and $A\beta_{(1-42)}$. It is found that that Zn^{2+} likely exerts such a dramatic effect through a rapid exchange of Zn^{2+} between Aβ molecules. Chapter 5 found that Cu^{2+} accelerated $A\beta_{(1-40)}$ fibre growth regardless of growth conditions, despite growth conditions influencing fibril morphology. It was also found that Cu^{2+} generated $A\beta_{(1-40)}$ fibres did not exhibit an altered stability, further suggesting that the effect of Cu^{2+} upon $A\beta_{(1-40)}$ is limited to fibril growth kinetics, in contrast to the effect of Cu^{2+} on $A\beta_{(1-42)}$, as well as the effect of Zn^{2+} upon either peptide. The present research has identified a diversity of significant interactions between Aβ, and Cu^{2+} and Zn^{2+}, highlighting a potential role for these metal ions in Alzheimer's disease.

ACKNOWLEDGMENTS

I would like to thank the Biotechnology and Biological Sciences Research Council for funding this PhD. Likewise, I am deeply grateful for Queen Mary University of London for hosting the project. To my two supervisors, Dr. John Viles and Dr. Caroline Brennan, I extend my sincerest appreciation, both for selecting me for such a fantastic experience, as well as for their encouragement and guidance throughout. I am also thankful to my research panel, Dr. Rachel Ashworth and Prof. Conrad Mullineaux, for their insight and advice during my 4 years.

I thank Graham McPhail and Giulia Mastroianni for their assistance with the transmission electron microscope. Similarly, the entire Dr. Viles group, Dr. Nadine Younan, Dr. Helen Stanyon, Miao Gu, Joseph Barritt, and David Bode, warrant a special thanks, as they too have assisted me with the various techniques presented herein, particularly Dr Nadine Younan, who mentored me when I started. Furthermore, they have all added to the overall experience, through their charm, wit, and ample supplying of caffeinated beverages. Similarly, I am grateful to every member of the Prof. Pickersgill group, Yumiko Tashiro, Dr. Shuang Gu, Dr. Allan Pang, Dr. Saima Rehman, Piers Rycroft, Junyi Qiu, Hui Zhang, and Ismail Uddin, for ensuring that my stay in G35 was a pleasant one.

Finally, I would like to thank my friends and family for the support and cheer they have provided me over the last four years. A special mention ought to be had for my parents, Dimitri Matheou and Jill Moon, who have never wavered in their enthusiasm. Likewise, despite having had to proofread my reports and listen to my presentations for the last 4 years of our 5 year relationship, Jessica Nicholson has at no time been any less than fantastic, for which I am truly grateful.

CONTENTS

LIST OF TABLES AND FIGURES

Figures

Tables

ABBREVIATIONS

Aβ – Amyloid β

Aβ*56 – A 56 kDa Aβ oligomeric assembly

αCTF – α-secretase cleaved APP C-terminal fragment

AD – Alzheimer's disease

ADDL – Aβ derived diffusible ligands

ADE – Amyloid degrading enzyme

AFU – Arbitrary fluorescence units.

AMPAR – α-amino-3-hydroxyl-5-methyl-4-isoxazolepropionic acid receptor

ANOVA – analysis of variance

APOE – Apolipoprotein E

APP – amyloid precursor protein

BASE-1 – β-site APP-cleaving enzyme-1

βCTF – β-secretase cleaved APP C-terminal fragment

CD – Circular dichroism

CREB – cAMP response element binding protein

CSF – Cerebrospinal fluid

DMSO – Dimethylsulfoxide

EDTA – Ethylenediaminetetraacetic acid

EM – Electron microscopy

EPR – Electron paramagnetic resonance

F-moc – *N*-(9-fluorenyl)methoxycarbonyl

GABA – γ-aminobutyric acid

GdnCl – Guanidinium Chloride

GM1 – Monosialotetrahexosylanglioside

HEPES – 2-[4-(hydroxyethyl)piperazin-1-yl] ethanesulfonic acid

HFIP – Hexaflouroisopropanol

LSD – Least significant difference

LTP – Long-term potentiation

LUV – Large unilamellar vesicle

MAPT – Microtubule-associated protein tau

nACHR – Nicotinic acetylcholine receptors

NMDAR - *N*-methyl-D-aspartate receptors

NMR – Nuclear magnetic resonance

PC – Phosphatidylcholine

PTA – Phosphotungstic acid

S.E.M – Standard error of the mean

ssNMR – Solid-state nuclear magnetic resonance

ThT – Thioflavin T

TEM – Transverse electron microscopy

UHQ – Ultra-high quality

UV – Ultraviolet

Vis – Visible

CHAPTER 1:

Introduction

1.1 ALZHEIMER'S DISEASE

1.1.1 Prevalence

Alzheimer's disease (AD) is a global concern; affecting approximately 30 million people worldwide, it is both the most common neurodegenerative disease and the second most burdensome chronic condition after blindness (Prince et al, 2009; Querfurth & LaFerla, 2010). This is reflected by its high economic impact, which is thought to be US$315 billion a year worldwide (Prince et al, 2009). Unfortunately, these numbers are set to rise, with it being estimated that by 2040 there will be 81.1 million cases of the disease (Ferri et al, 2005). This is largely because the risk of onset is much greater for individuals older than 65 years of age, with risk doubling for every 5 years after 65; thus, as life expectancy rises so too does AD incidence. However, there are other factors contributing towards increases in AD. For instance, high cholesterol and smoking lead to hypertension, which in turn is associated with elevated risk of AD (Breteler et al, 1998; Ravona-Springer et al, 2003), and there has been mounting evidence for the coincidence of AD and diabetes, with some even suggesting that AD should be considered as type-III diabetes (de la Monte & Wands, 2008). These factors are particularly worrisome for developing countries, as their adoption of westernised diets and smoking places them at much greater risk than previously; this is underscored by the forecast that AD incidence shall increase at a rate 3 fold greater in developing countries than developed countries (Ferri et al, 2005). However, perhaps the most significant contributor towards rising prevalence of AD is the fact that no effective treatments have been developed. From this it is clear that furthering our understanding of this disease is imperative.

1.1.2 Symptoms

Besides ultimately leading to death (typically within 8 years after diagnosis), AD is associated with a plethora of progressive symptoms (Forstl & Kurz, 1999; Prince et al, 2009). At early stages, it is very difficult to identify someone with AD, as initial symptoms include only mild impairment of both memory and executive functioning, which may be misattributed to stress or fatigue (Waldemar et al, 2007). Apathy may also be present at these early stages. Although typically overshadowed by the more dramatic symptoms that characterise AD, it is important to remember that apathy affects up to 92 % of individuals with AD (Mega et al, 1996), and may result in behaviours such as low social engagement, indifference, lack of insight, and blunted emotional response (Landes et al, 2001). Such behaviours may compound difficulty in identifying AD sufferers at early stages.

As the disease progresses, the symptoms become much more apparent, with impairment of recent memories becoming so severe that patients have been reported as appearing to “live in the past” (Beatty et al, 1988). Loss of vocabulary also occurs, which leads to increasing difficulty in communication, and motor impairment (apraxia) manifests, causing sufferers to struggle with both household tasks and balance. Long-term memory, which was initially intact, deteriorates, resulting in patients eventually becoming unable to recognise even close relatives (Forstl & Kurz, 1999). Additionally, apathy advances, leading to the requirement of support and management for patients, as they come to rely on others to initiate behaviours, even when they are still physically capable of carrying out the activities themselves (Landes et al, 2001). In late stage Alzheimer’s disease, symptoms worsen significantly, with patients completely losing the faculty of speech, and becoming physically incapable of manoeuvring or even feeding themselves, resulting in their full dependence upon care-givers (Förstl & Kurz, 1999).

1.1.3 Pathology and Diagnosis

Despite behavioural symptoms facilitating psychological testing of AD, alternative methods of diagnosis are often needed. At a neurological level, AD is characterised by a significant shrinkage in the brain areas associated with learning and memory, as shown in figure 1.01, due to a substantial loss of synapses and neurons. This enables imaging techniques, such as magnetic resonance imaging and positron emission tomography, to be used for diagnosis (Ballard et al, 2011). However, such imaging techniques are not entirely effective at differentiating between different forms of dementia. To improve accuracy, biomarkers in the cerebrospinal fluid (CSF), such as oxidative stress and inflammation, are at times used (Mattsson et al, 2009; Welge et al, 2009); however, the only definitive diagnosis available at present is post mortem. This relies on the identification of the two core pathological hallmarks of Alzheimer's disease first identified by Alois Alzheimer, the extracellular Amyloid-β (Aβ) plaques and intracellular tau tangles (Alzheimer et al, 1995).

1.2 AMYLOID-β AND TAU

1.2.1 Amyloid Precursor Protein

The characteristic plaques of AD are comprised of aggregated Aβ, a peptide which is cleaved from the amyloid-precursor protein (APP). The *APP* gene is located on chromosome 21, with the protein resembling a glycosylated cell-receptor (Kang et al, 1987). Alternative splicing yields several isoforms of APP which are differentially expressed, with the most prevalent neuronal isoform being 695 amino acids long (Mattson, 1997). The *APP* gene itself has been evolutionarily conserved in both sequence and expression (Wasco et al, 1992; Wasco et al, 1993), as has likely been its role, which has been supported by the observation that the human *APP* gene can

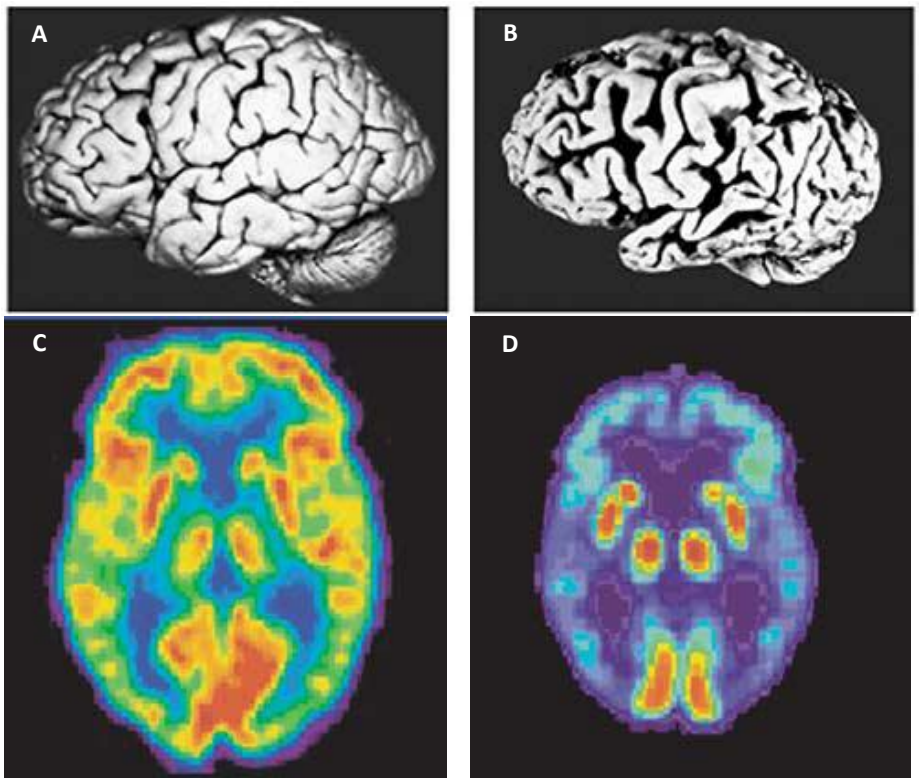

Figure 1.01 Shrinkage of Brain Regions in Alzheimer's Disease.

Alzheimer's disease causes shrinkage of brain regions involved in learning and memory; this is evident in this figure, as the individual with Alzheimer's disease portrays a marked shrinkage of gyri in the temporal and frontal lobes (A) compared to a healthy individual (B). Consequently, Alzheimer's patients suffer large decreases in their energy metabolism in the frontal and temporal lobes. This is evident in the positron emission tomography images (C & D) showing glucose uptake (red and yellow indicate high levels of glucose uptake), which compare a healthy individual (C) and an individual with Alzheimer's disease (D). Reprinted by permission from Macmillan Publishers Ltd: Nature, (Mattson, 2004), copyright (2004).

rescue *APP* knockout *Drosophila* (Luo et al, 1992). However, despite an apparent conservation of function across phyla, the precise role of APP is still not entirely clear, although it has been proposed that APP is important for neuronal development, as increases in APP expression coincide with neuronal differentiation and neurite outgrowth (Salbaum & Ruddle, 1994); this also supports the notion that APP is important for synaptic plasticity (Mattson, 1994). Notably, not only full-length APP is important for neuronal maintenance, as the proteolytically derived fragments also appear to exhibit critical physiological activities (Mattson et al, 1992). Understanding the proteolytic processing of APP is crucial for elucidating the origin of pathological Aβ.

1.2.2 Amyloid Precursor Protein Trafficking and Processing

APP undergoes classical N-glycosylation and O-glycosylation as it passes through the rough endoplasmic reticulum and Golgi apparatus (Mattson, 1997; Weidemann et al, 1989). As it exits from the late Golgi into secretory vesicles, and is ultimately inserted into the cell membrane, additions of sulphate and phosphate further increase APP complexity; these additions are dependent on such variables as cell-cycle, and regulate APP metabolism (Hung & Selkoe, 1994; Suzuki et al, 1994). Once at the cell surface, APP is rapidly internalised, due to its “YENTPY” domain; indeed, the estimated half-life for surface APP is less than ten minutes (Koo et al, 1996). After internalisation it is delivered to endosomes, where it may be recycled, or alternatively passed onto lysosomes for digestion (Haass et al, 1992). There are three proteinases, the secretases, which may cleave APP at various stages of the trafficking process.

Cleavage by α-secretase may occur in *trans*-Golgi vesicles, secretory vesicles, or the cell membrane itself. As its cleavage site resides within the Aβ sequence, it prevents Aβ production, and may be considered the principal step in “non-amyloidogenic” APP processing (Mattson, 1997), as shown in figure 1.02. Following cleavage, the

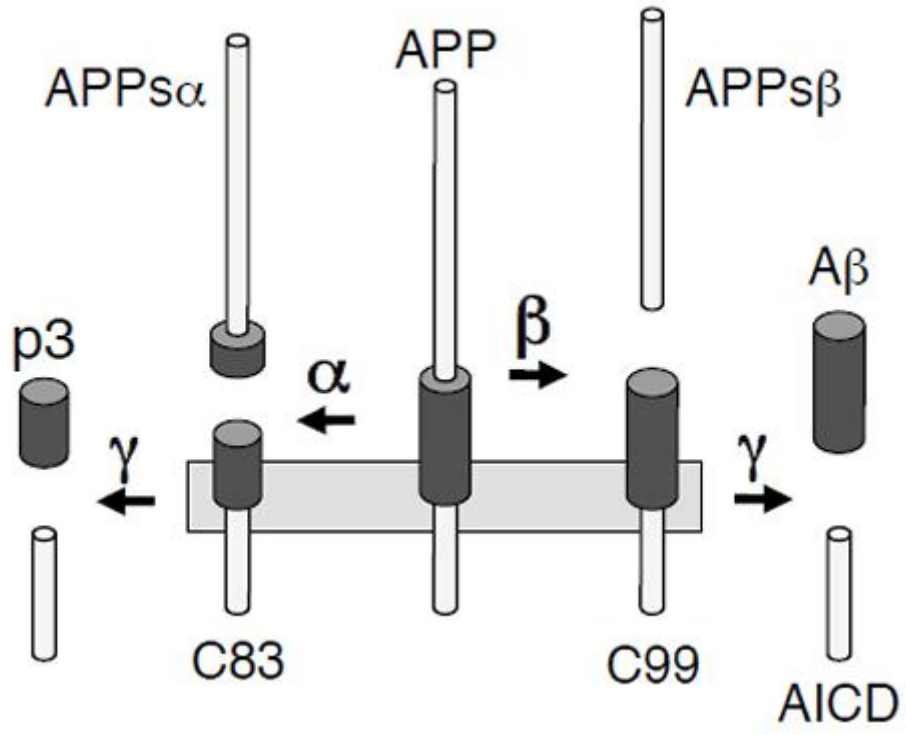

Figure 1.02 APP Cleavage.

Amyloidogenic processing of APP may commence with β-secretase, with Aβ being generated following subsequent γ-secretase cleavage. Alternatively, non-amyloidogenic processing may commence with α-secretase activity. This figure was reproduced from (Lichtenthaler, 2011), © 2010.

extracellular fragment, APPsα, is released, and the c-terminal fragment (αCTF) remains anchored to the membrane, where it may be cleaved further (De Strooper & Annaert, 2000). Interestingly, the activity of α-secretase appears to increase with electrical activity and activation of muscarinic acetylcholine receptors (Mattson, 1997), providing an explanation as to why neuronal activity has been found to be protective against AD.

The principal step in "amyloidogenic" processing is β-secretase cleavage. Cleavage by β-secretase, as for α-secretase, may occur at the t*rans*-Golgi vesicles, secretory vesicles, or cell membrane. Cleavage typically occurs at the Asp1 of the Aβ sequence, releasing APPsβ into the extracellular space, and retaining the βCTF in the membrane, which may be further cleaved to release Aβ. Several independent studies have identified a candidate β-secretase, BACE-1 (beta-site APP-cleaving enzyme-1); an aspartyl protease that functions optimally at low pH (Parvathy et al, 1999; Sinha et al, 1999; Vassar et al, 1999; Yan et al, 1999). Additionally, decline in BACE-1 activity has been found to coincide with lowered cholesterol level (Frears et al, 1999; Simons et al, 1998). This is as reduction in cholesterol causes loss of lipid "rafts"; these microdomains are thought to be crucial for coordinating the presentation of APP to BACE-1 (Simons et al, 1998). The correlation between cholesterol and β-site cleavage is particularly interesting, due to the correlation between high cholesterol diets and an increased risk of AD (Kivipelto & Solomon, 2006). BACE-1 has also been shown to cleave APP at the Glu11 of Aβ, releasing a shorter form of Aβ that has been identified to comprise the cores of Aβ plaques (Masters et al, 1985; Naslund et al, 1994); however, the significance of these shorter Aβ peptides are not yet understood.

In APP processing, γ-secretase is involved in both amyloidogenic and non-amyloidogenic processing, and is thought to occur after the endocytosis of both αCTF and βCTF, presumably as part of an endosomal-lysosomal compartment (Higaki et al, 1995; Knops et al, 1995). The γ-secretase cleavage site is within the transmembrane

region of αCTF and βCTF; thus, γ-secretase must hydrolyse a peptide bond in a hydrophobic environment, an impressive feat for which the molecular mechanism unfortunately remains unclear (De Strooper & Annaert, 2000). There is some flexibility within the γ-secretase cleavage site, which results in the generation of several Aβ peptides of varying length, typically between 38 and 43 residues long (Mattson, 1997).

1.2.3 Function of Aβ

In a healthy individual Aβ is found to be released at distal axons and synapses (Lazarov et al, 2002; Sheng et al, 2002); consequently, Aβ function is unlikely limited to the pathogenic. However, the physiological role of Aβ remains controversial (Hiltunen et al, 2009). Some research has demonstrated the capacity of Aβ to act as a neurotrophic factor, increasing the growth rate of neural stem cells independently of soluble factors released by the cells (Lopez-Toledano & Shelanski, 2004), suggesting that it may be important physiologically to neuronal survival. Others have also proposed that Aβ has a protective role *in vivo*, though through its inherent oxidative activity instead, as Aβ displays antioxidant properties capable of protecting against transition metal induced oxidation in the brain (Baruch-Suchodolsky & Fischer, 2009; Zou et al, 2002).

Alternatively, Aβ may be important for synaptic plasticity and memory formation, as siRNA and antibodies directed against Aβ reduce long-term potentiation (LTP) and memory, with addition of human Aβ able to rescue these functions (Puzzo et al, 2011). A role of Aβ in memory formation is supported by studies showing that levels of Aβ follow a circadian rhythm, increasing with wakefulness and falling in sleep (Kang et al, 2009), with sleep thought by many to have an important role in memory consolidation (Stickgold & Walker, 2005). Furthermore, it has been demonstrated that lack of sleep is associated with brain shrinkage and ventricle expansion akin to that which is typical in AD (Lo et al, 2014).

Adding to the broad repertoire of putative functions already proposed, Aβ has also exhibited the ability to influence transcription, specifically, increasing expression of BACE-1, which in turn regulates APP processing and its own production. It is thought Aβ does this through either itself acting as a transcription factor (Bailey et al, 2011), or, alternatively, as a signalling peptide (Tabaton et al, 2010). There is also the possibility that Aβ may function as a cholesterol transporter, with it being demonstrated that increases in Aβ were associated with a redistribution of cholesterol from the plasma membrane to the Golgi apparatus (Igbavboa et al, 2009). This possibility is particularly striking, as cholesterol is understood to be an important risk factor for AD (Kivipelto & Solomon, 2006).

Unfortunately, at this point it is not clear which possible role is correct, nor if Aβ may even have multiple functions. However, somewhat surprisingly, animal studies in mice demonstrate that Aβ is not essential, as complete depletion of Aβ through knockout of the *BASE-1* gene did not result in any major side effects (Luo et al, 2003).

1.2.4 Aβ Catabolism

In the brain, Aβ levels are controlled through a balancing of its production, from APP, and its removal, either via perivascular drainage, or by the action of amyloid-degrading enzymes (ADEs). In sporadic forms of AD, no change in Aβ production is observed; however, Aβ is seen to accumulate regardless (Funato et al, 1998). Furthermore, in mice with amyloid deposits the half-life of Aβ is seen to double, from ~2 hrs to ~4 hrs (Cirrito et al, 2003). For these reasons, there has been growing interest in Aβ catabolism.

There are more than 20 ADEs; however, the general consensus is that a zinc-metalloprotease, neprilysin, is the major ADE in Aβ catabolism (Nalivaeva et al, 2012;

Shirotani et al, 2001). Neprilysin levels are reduced in individuals with AD (Wang et al, 2005), and are also seen to decline in response to events that are associated with increased AD risk, such as ischemia and hypoxia (Fisk et al, 2007; Nalivaevaa et al, 2004). These studies highlight the potential importance of Aβ catabolism for a healthy brain.

1.2.5 Tau

Though not a focus of my PhD, the second hallmark of AD, the tau tangles, are not only notable for their coincidence with Alzheimer's disease, but for their importance in a range of neurodegenerative diseases, the "tauopathies". These include frontotemporal dementia, dementia puglistica, and progressive supranuclear palsy (Hutton et al, 1998; Roberts, 1988; Williams & Lees, 2009). Tau is not a single protein, but in fact a family of proteins, ranging from 352 – 441 amino acids in length, that are produced by the alternative splicing of a single gene on chromosome 17, *MAPT* (microtubule-associated protein tau) (Goedert et al, 1989). The tau proteins are abundant in the neurons, where they modulate both the flexibility and stability of axonal microtubules in distal axonal regions through their direct interaction with tubulin. It is this interaction that promotes the assembly of tubulin into microtubules.

Tau proteins are regulated through phosphorylation, with kinases such as PKN, which disrupts microtubule association (Taniguchi et al, 2001). There are a great number of potential phosphorylation sites in the tau proteins, 79 being present on the longest isoform. Of these, 30 have been found to be phosphorylated in non-pathological tau protein (Billingsley & Kincaid, 1997). Pathological tau is hyperphosphorylated, and aggregates into oligomers, β-sheets, and ultimately neurofibrillary tangles, though it is not clear whether hyperphosphorylation precedes or follows aggregation (Ballard et al, 2011). Whichever the case may be, once tau aggregation commences it perpetuates itself through recruiting more tau and spreading to additional brain regions. This has

been clearly demonstrated by the injection of pathological tau into wild-type mice, which induced formation of tau tangles consisting of endogenous tau (Clavaguera et al, 2009). Tauopathy symptoms do not arise from a loss of tau function, as tau knockout mice do not present neurodegenerative symptoms (Harada et al, 1994). Instead, the tau aggregates themselves are neurotoxic (Meraz-Rios et al, 2010).

Of particular interest is the interaction between Aβ and tau. The affinity of Aβ for tau is almost 1000-fold greater than the affinity of tau for itself, and formation of Aβ-tau promotes tau phosphorylation (Guo et al, 2006). Thus, it would seem that Aβ may be an important mediator of tau aggregation in AD. This is supported by the observation that phosphorylated tau is bound to both monomeric and oligomeric Aβ in the damaged neurons of AD patients and mouse models, and that these interactions are increased with disease progression (Manczak & Reddy, 2013), presumably with Aβ aggregation upstream of tau aggregation.

1.3 AMYLOID CASCADE HYPOTHESIS OF ALZHEIMER'S DISEASE

1.3.1 Genetic Support for an Amyloid Cascade

There has been some controversy as to the identity of the causative agent in Alzheimer's disease; however, there generally seems to be more to support Aβ aggregation preceding tau aggregation. The foundation for the "amyloid cascade hypothesis", which proposes that Aβ aggregation is the primary event in AD, may be considered to have first been laid down upon the observation that individuals with Down's syndrome invariably develop AD (Olson & Shaw, 1969). This discovery was particularly significant as those with Down's syndrome possess three copies of chromosome 21, the chromosome containing the *APP* gene. Consequently, individual's with Down's syndrome accumulate high levels of Aβ, as is characteristic of AD (Glenner & Wong, 1984). The concept of an amyloid hypothesis was further

established upon the discovery of a mutation within the Aβ sequence of *APP*, the Dutch mutation (E693Q). This was the earliest demonstration that mutations within *APP* may lead to enhanced amyloid deposition, while also illustrating the capacity of Aβ to aggregate independently of other AD correlates. The Dutch mutation leads to extensive Aβ plaque deposition in cerebral vessel walls, where it may lead to cerebral haemorrhage, apoptosis of cerebral endothelial cells, and AD itself (Levy et al, 1990; Miravalle et al, 2000; Van Broeckhoven et al, 1990).

Since the discovery of the Dutch mutation, there have been many more *APP* mutations found that are associated with AD, as shown in figure 1.03 (Benilova et al, 2012). Though these autosomal dominant mutations account for no more than 5 % of AD cases, and confer an “early-onset” form of the disease rather than a typical progression, they provide useful insights as to the role of Aβ in AD. For instance, it is apparent that many of these mutations cluster at secretase cleavage sites, where they promote the amyloidogenic pathway of APP, increasing Aβ production (Cai et al, 1993; Citron et al, 1992; Suzuki et al, 1994). This may be achieved through an inhibition of α-secretase activity, such as for the Flemish mutation (A692G), or a potentiation of β-secretase activity, as in the Swedish mutation (K670N/M671L) (Haass et al, 1995; Hardy, 1997). Additionally, several mutations in *APP* that lead to early-onset AD increase the aggregative properties of Aβ, such as the Arctic mutation (E693G) (Nilsberth et al, 2001). Additionally, there are over 100 mutations associated with early-onset AD that occur in the γ-secretase complex; these mutations influence the length distribution of Aβ peptides, promoting generation of longer, more hydrophobic alloforms, that aggregate more readily (Citron et al, 1997; Duff et al, 1996; Scheuner et al, 1996).

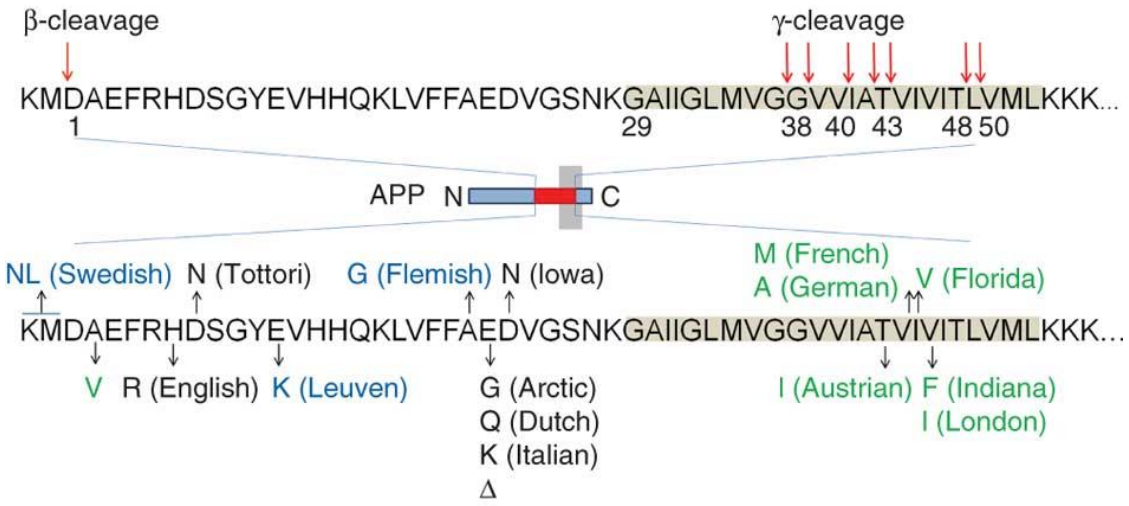

Figure 1.03 APP Mutations.

Red arrows indicate cleavage sites, and shaded grey indicates region within the plasma membrane. This figure shows mutations within *APP* that are associated with AD, some of which increase Aβ production (blue), increase Aβ self-association (black), or alter the ratio of Aβ isoforms (green). Reprinted by permission from Macmillan Publishers Ltd: Nature Neuroscience, (Benilova et al, 2012), copyright (2012).

There also exist mutations outside of *APP* that do not lead to early-onset forms of the disease, but still are strongly associated with disease risk. Most notable is the *ε4* allele of the *apolipoprotein E* (*APOE*) gene, which in heterozygotes increases AD risk by a factor of 4, and in homozygotes increases risk by a factor of 8 (Corder et al, 1993). *APOE* codes for a protein involved in cholesterol transport; however, for reasons that are not clear, the *ε4* allele reduces Aβ clearance, and elevates Aβ aggregation (Mattson, 2004; Roses, 1997); both of which are crucial to AD pathology.

The number of mutations that directly affect Aβ, and in turn are associated with AD, strongly supports amyloid deposition as the initiator of AD. However, a further observation that has been critical in establishing the amyloid cascade hypothesis involves mutations that directly affect tau. Such mutations are observed to cause frontotemporal dementia with parkinsonism, rather than AD (Poorkaj et al, 1998; Puzzo et al, 2011; Spillantini et al, 1998). As frontotemporal dementia is characterised by both an extensive deposition of tau tangles, and profound, fatal, neurodegeneration, but does not induce Aβ deposition, it may be concluded that even under the most extreme of circumstances tau is not able to induce Aβ aggregation. Thus, though AD is a multifaceted disease, there is much evidence to implicate Aβ accumulation as the primary factor from which everything else follows, including tau tangle formation, validating the use of an amyloid-centric model for AD pathology.

1.3.2 Amyloid Cascade Hypothesis

The amyloid cascade hypothesis, as shown in figure 1.04, posits that AD begins with the accumulation and aggregation of Aβ (in particular self-assembly into oligomeric and protofibrillar species), and that this may occur due to genetic mutations, reductions in Aβ catabolism, and yet to be identified triggers, which are likely to be numerous (Hardy, 2006). This basic premise is the cornerstone upon which every iteration of the amyloid cascade hypothesis has rested; however, the details of the steps that follow, and their

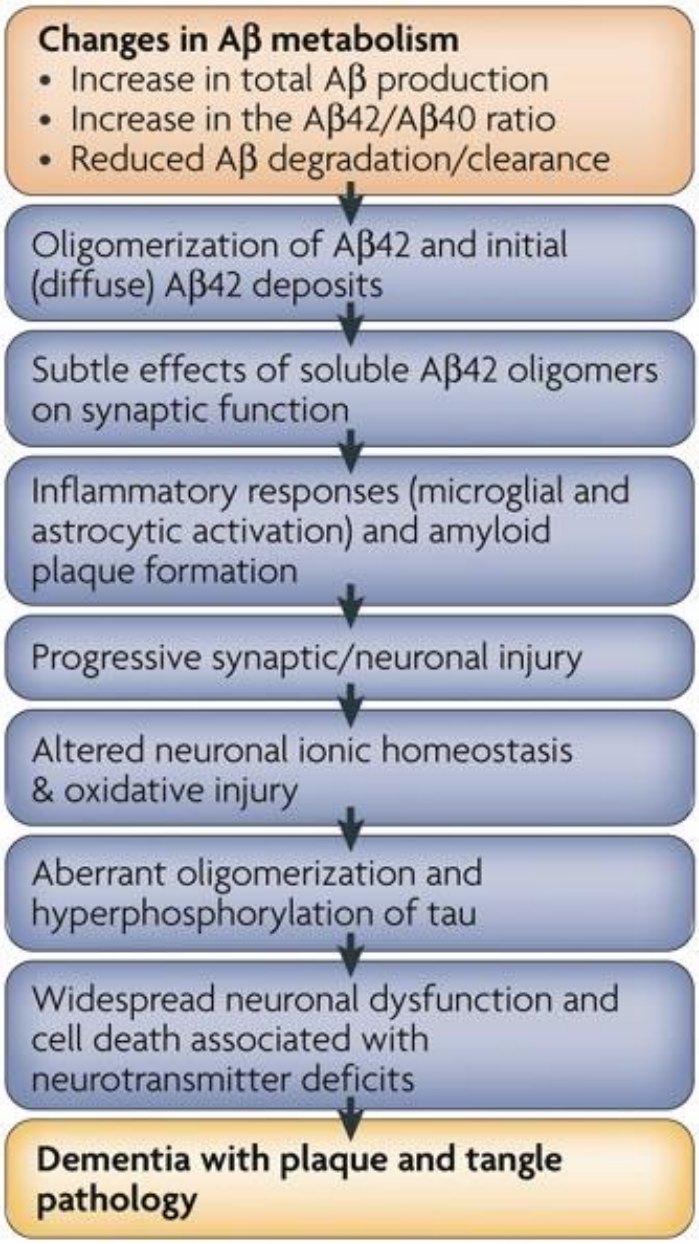

Figure 1.04 Amyloid Cascade Hypothesis.

A representative schematic of the amyloid cascade hypothesis. Reprinted by permission from Macmillan Publishers Ltd: Nature Reviews Molecular Cell Biology, (Haass & Selkoe, 2007), copyright (2007).

relative importance, are more contentious. Generally, it is believed that though the large Aβ plaques themselves may not be toxic, smaller intermediate species are, and these smaller assemblies can interact with and perturb synapses. In parallel to this, diffuse Aβ aggregates accumulate in the parenchyma, and incur inflammatory responses. This extended exposure to Aβ aggregates, both at the synapse and in the parenchyma, leads to neuronal degeneration, loss of ion homeostasis, and oxidative stress (Haass & Selkoe, 2007). Subsequently, the altered neurological environment, or perhaps a direct interaction between Aβ and tau (Guo et al, 2006), leads to hyperphosphorylation of tau, which then associates into tangles, exacerbating neuropathology through disruption of axonal transport and enhanced neurotoxicity (Haass & Selkoe, 2007). This culminates in a positive feedback of neurodegeneration, leading to the progressive symptoms of neuronal dysfunction typical of AD.

Though initially developed as a model for AD, the amyloid cascade hypothesis has now found broader application. This is as the misfolded structure of Aβ adopted in AD has been found to be a common feature of many protein misfolding diseases, including Parkinson's (Der-Sarkissian et al, 2003) and Huntington's (Scherzinger et al, 1999). As such, it is important for not just AD, but for protein misfolding diseases in general, to elucidate the misfolding pathway of Aβ.

1.4 AMYLOID-β MISFOLDING

1.4.1 Aβ Primary Sequence

As shall be discussed later, the two most notable alloforms of Aβ are 40 and 42 amino acids long, consisting of the following sequence:

```
     5        10        15        20        25        30        35        40
DAEFR HDSGY EVHHQ KLVFF AEDVG SNKGA IIGLM VGGVV / IA
```

Blue amino acids represent hydrophilic residues, whereas the red indicates hydrophobic. While the N-terminal is mainly hydrophilic, there are two major hydrophobic regions: the central hydrophobic core, from residues 17 – 21, and the C-terminus, from residues 29 – 40/42. The bulky side chains of these hydrophobic residues increase the propensity of Aβ to form β-sheet structures. Also of note are residues involved in Aβ's chelation of metal ions (particularly the histidines), indicated here by underlining.

1.4.2 Monomeric Aβ Structure

Monomeric Aβ is generally considered to be an intrinsically disordered peptide, having no defined tertiary structure, and exhibiting a high degree of flexibility (Uversky et al, 2008). Early nuclear magnetic resonance (NMR) data demonstrated that monomeric Aβ adopts a metastable "collapsed coil" secondary structure; a compact series of loops, turns, and strands, with no β-sheet or α-helical structure (Zhang et al, 2000). More recent studies have emphasised that there are in fact a diverse range of morphologies available for monomeric Aβ, with Aβ exhibiting a capacity to adopt both α-helical and β-sheet motifs (Sgourakis et al, 2011; Vivekanandan et al, 2011). The diverse ensemble of structures that are rapidly sampled by monomeric Aβ has been suggested to provide a starting point for misfolding and aggregation (Sgourakis et al, 2011; Yang & Teplow, 2008), which may proceed down two primary pathways, as shown in figure 1.05a (Faller et al, 2013).

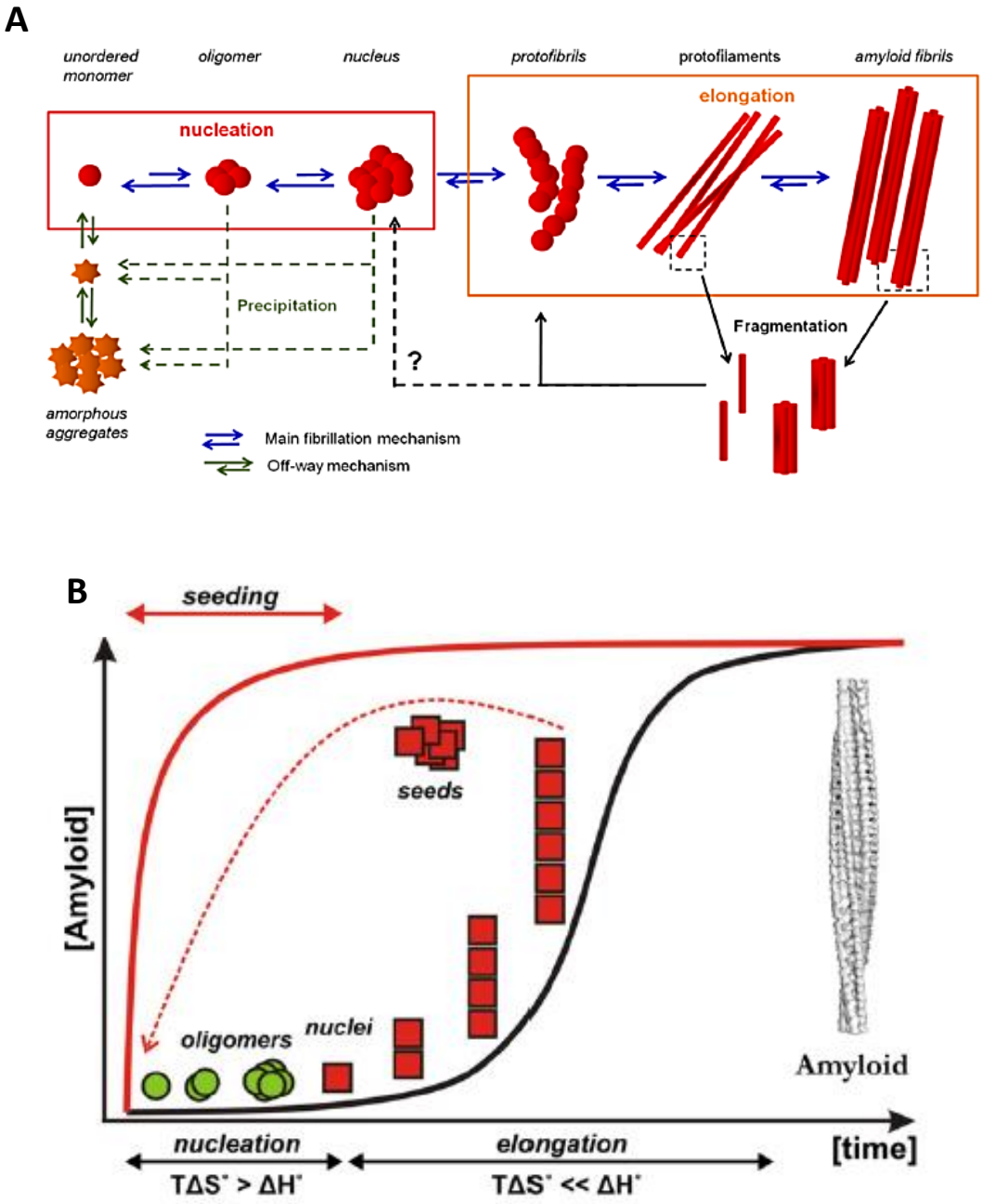

Figure 1.05 Aβ Aggregative Pathways.

(A) A representative schematic of amyloid-β aggregation, highlighting the alternative routes of amorphous aggregation, and fibrillogenesis, the second of which is thought essential to Alzheimer's disease pathology. Reprinted with permission from (Faller et al, 2013), copyright (2013) American Chemical Society. (B) Kinetics of amyloid fibrillogenesis. The entropic cost for nucleus formation that creates a kinetic barrier that may be overcome with addition of a seed. Reprinted from (Eichner & Radford, 2011), Copyright (2011), with permission from Elsevier.

1.4.3 Plaques

The characteristic Aβ “plaques” of AD, are composed partly of amorphous aggregates of the peptide; unordered precipitates of Aβ that arise from aberrant interactions following adoption of a β-sheet rich fold, and are comprised themselves of a diverse range of aggregates (Goncalves et al, 2010); and amyloid fibres, a much more orderly aggregative pathway proceeding the adoption of a β-sheet rich fold in Aβ. Though initially considered as a crucial mediator of AD pathology (Alzheimer et al, 1995), it is now generally considered that the plaques are a by-product of the disease, and though they may be in equilibrium with more toxic aggregate species, they are not the primary perpetuator. Evidence for this is provided by the clinical trial of an Aβ vaccine, which though it removed plaques did not prevent progressive neurodegeneration (Holmes et al, 2008). Additionally, it has been demonstrated that oligomers and protofibrils much better correlate with disease progression than plaques (Lue et al, 1999). The pathway towards generating oligomers and protofibrils involves the more ordered aggregative pathway of fibrillogenesis, and as such is of more relevance to disease aetiology than amorphous aggregation.

1.4.4 Amyloid Fibre Structure

It has been determined with X-ray fibre diffraction that Aβ may self-associate into fibres with a cross-β structure, in which β-sheets are orientated nearly perpendicular to the fibril axis, with intermolecular hydrogen bonding parallel to the axis (Eanes & Glenner, 1968; Geddes et al, 1968; Sikorski et al, 2003). This has been expanded upon with electron paramagnetic resonance (EPR), which has been used to identify the location and contacts of β-sheet strands within the fibre (Torok et al, 2002). This identified that though there are regions of mobility, such as in the N-terminus and between residues 23 – 26 (which likely contains a bend or turn region), the Aβ fibre structure is generally ordered and specific, forming in register parallel β-sheets within the fibre. This has

been supported with hydrogen/deuterium exchange, which shows that about half of the backbone amide protons are protected from exchange, indicative of their being within highly structured core regions of the fibre (Kheterpal et al, 2003).

Electron and atomic-force microscopy have been used to delineate the topological character of amyloid fibres, revealing that they are long, straight, non-branching structures, that themselves are composed of a number of protofilaments that entwine one another to form the complete fibre (Goldsbury et al, 1999; Jimenez et al, 2002; Serpell et al, 2000). Insights into the atomic organisation of the cross-β motif have also been advanced using X-ray crystallography (Nelson & Eisenberg, 2006; Sawaya et al, 2007). Small fragments from a variety of amyloidogenic proteins were used, revealing that for amyloid structures pairs of β-sheets join via a dry “steric zipper” configuration: an interdigitating of sidechains. It has been proposed that such an interaction may drive the association of β-sheets in early stages of amyloid fibre formation.

Interestingly, it is now known that more than 20 other proteins involved in disease can misfold and form these cross-β amyloid fibrils (Sunde et al, 1997). This observation, combined with the existence of functional amyloids in yeast (Wickner, 1994), bacteria (Chapman et al, 2002), and even humans (Fowler et al, 2006), supports the notion that amyloid assemblies were probably a prominent early fold in the evolution of life, that has since been retained (Chernoff, 2004; Eichner & Radford, 2011). However, the diversity of proteins that form pathological amyloid structures not only serves to further incentivise an elucidation of the process, but also demonstrates that amyloid fibrillogenesis is not the product of a specific native structure or sequence that has been conserved. Rather, it seems that it is a capacity of a protein to adopt erroneous conformations that underlies amyloid fibre formation. This has been demonstrated with transtheyretin, as inducing its partial misfolding with acidic conditions is seen to promote amyloid fibre formation (Colon & Kelly, 1992). Thus, proteins that are inherently unstructured, such as Aβ, are seen to readily form amyloid fibrils (Eichner et

al, 2011; Sgourakis et al, 2011; Yang & Teplow, 2008).

Despite the shared cross-β fold of amyloid fibrils, there is still a broad diversity of conformations available to be adopted at the macromolecular level. This has been shown extensively with such techniques as cryo-electron microscopy (cryo-EM) and solid-state NMR (ssNMR), which, as shown in figure 1.06, have demonstrated a great number of ways in which amyloid fibres may vary. These include the number of proto-filaments that may constitute a mature fibril (Jimenez et al, 2002), whether parallel or anti-parallel β-sheets comprise the cross-β fold (Iwata et al, 2006; Nielsen et al, 2009), the periodicity of twists along the fibril (Meinhardt et al, 2009), and a fibre's axial symmetry (Petkova et al, 2005). These variations in structure are significant as they may confer differences in a fibre's physical, chemical and biological properties. This is well demonstrated through consideration of the prion protein, for which the tertiary structure adopted by the misfolded protein determines the "strain" of prion disease, and its related pathology (Prusiner, 1998). Furthermore, it has more recently been shown that the conformational stability of a prion strain determines its incubation time (Colby et al, 2009).

Though fibril structure is sensitive to sequence, with a single point mutation in $A\beta_{(1-40)}$ (the Iowa mutation D23N) switching fibril structure from predominantly parallel to predominantly anti-parallel β-sheet, a change in structure which may underlie the enhanced pathogenicity of Aβ in those with the mutation (Tycko et al, 2009), environment is also an important determinant of fibril structure. It has been shown with $A\beta_{(1-40)}$ that a change from agitated to quiescent conditions causes a switch in the axial symmetry of fibres from 2-fold to 3-fold, which in turn influences fibres' potential to kill neuronal cell cultures, presumably as different side-chains are exposed, despite identical sequences (Paravastu et al, 2008; Petkova et al, 2005). Notably, as for prion strains, mature Aβ fibres impart their own structure upon daughter fibres. This explains why brain-derived Aβ fibres are not polymorphic, and also provides a potential

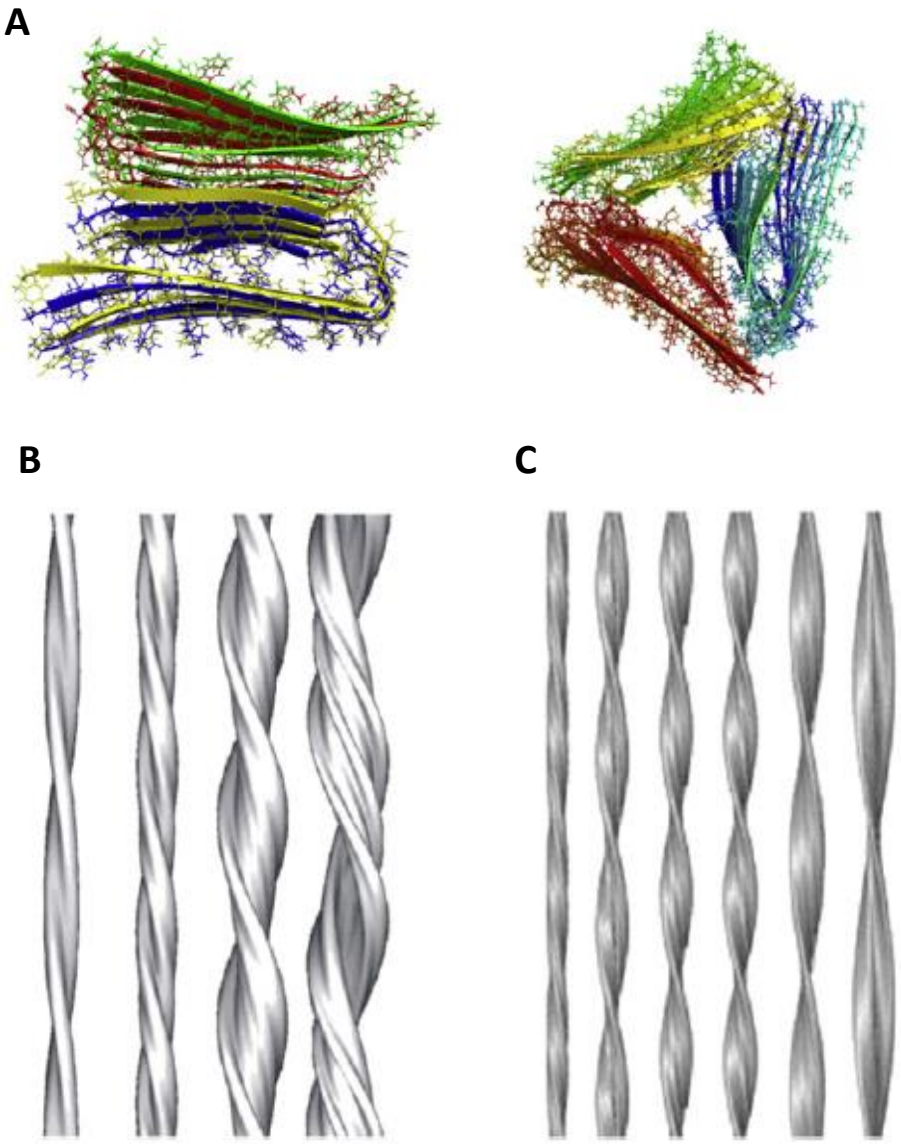

Figure 1.06 Diversity of Amyloid Fibres.

(A) It has been shown with ssNMR that growing $A\beta_{(1\text{-}40)}$ quiescently results in a 3-fold symmetry rather than 2-fold (Paravastu et al, 2008; Petkova et al, 2005). (B) Cryo-EM showing amyloid fibrils of insulin containing 2 – 6 proto-fibrils (Jimenez et al, 2002). (C) Cryo-EM showing diversity of twist frequency for $A\beta_{(1\text{-}40)}$ fibres (Meinhardt et al, 2009). Reprinted from (Eichner & Radford, 2011), Copyright (2011), with permission from Elsevier.

explanation for the variations in disease development observed between patients, as it has been identified that AD patients with distinct clinical histories possess distinct predominant Aβ fibril structures (Lu et al, 2013). The potential for prion-like propagation of AD strains has recently been explored through transmission studies, in which transgenic mice were inoculated with brain homogenates of patients with sporadic and heritable (Arctic and Swedish) forms of AD (Watts et al, 2014). Mice treated with the three samples presented two distinct sets of disease behaviours, with Arctic AD causing one set of symptoms, and both sporadic and Swedish AD causing the second set. This divergent pathology was retained during second passage to mice, establishing that Aβ strains have the potential to be serially transmissible. The high-fidelity preservation of Aβ fibre strains is likely due to the crystal-like seeding through which they are formed, in which parent morphology determines daughter morphology.

1.4.5 Amyloid Fibre Formation

A general agreement of the fundamental kinetics for fibre formation has been reached in recent years. Fibre growth undergoes a characteristic sigmoidal growth curve, as shown in figure 1.05b, in which the rate-limiting step is the nucleation phase. This is a stochastic process, in which nuclei consisting of several monomeric units transiently form and dissociate, due to the resultant molecular interactions not exceeding the entropic cost of association (Schnabel, 2011). This creates a kinetic barrier to the commencement of fibre formation, leading to a lag-time analogous to that observed in crystallisation; indeed, as for crystallisation, the addition of a seed (in this case preformed fibrils) overcomes this barrier and no lag-time is observed (Come et al, 1993). Following the nucleation phase is the elongation phase.

During the elongation phase, stabilised nuclei act as templates for the further addition of monomers, generating nascent fibrils. Mature fibrils are then formed from the continuous addition of monomers to the growing fibril ends (Lomakin et al, 1996; Walsh

et al, 1999). This gives rise to the exponential period of growth shown in figure 1.05b, which ultimately plateaus once a dynamic equilibrium is reached (Wetzel, 2006). It has been suggested that the nucleation-elongation model is insufficient, as inclusion of both fragmentation and secondary nucleation events have been seen to provide a better agreement between computational models and observed data (Knowles et al, 2009; Xue et al, 2008). Such steps lead to a greater acceleration of fibril formation during the elongation phase, as they increase the number of fibril ends available to which monomers may be added. However, now thought to be more significant to disease pathology than fibres are small Aβ aggregates, oligomers. Oligomers may serve as precursors to fibres, form from fibril fragmentation, or perhaps even compete with fibre formation.

1.4.6 Soluble Oligomers

As well as soluble aggregates better correlating with disease progression than larger insoluble aggregates (Lue et al, 1999), several studies have directly implicated them in disease pathology. For instance, when fibril growth is inhibited with low levels of clusterin, Aβ-derived diffusible ligands (ADDLs) form instead, a spectrum of globular oligomeric assemblies of 17 – 42 kDa; these have been demonstrated to bind to specific cell-surface receptors in neuronal cultures and exhibit neurotoxic potential (Lambert et al, 1998). These observations are supported by *in vivo* research, which has shown that in rats, a heterogeneous population of Aβ oligomers, with neither fibres nor monomers present, is capable of inhibiting hippocampal long-term potentiation (Walsh et al, 2002). Similarly, in mouse models the formation of a 56 kDa oligomer (Aβ*56) has been identified as coinciding with onset of behavioural symptoms; this assembly has since been isolated and injected into wild type rats, which then also developed memory deficits (Lesne et al, 2006).

A greater ability to diffuse, differences in structure, and more substantial exposure of

hydrophobic regions have all been suggested to confer the enhanced pathogenicity of Aβ oligomers. However, despite there being support for each of these proposals, such as the structure of ADDLs enabling its interaction with Fyn, a tyrosine kinase linked with apoptosis (Lambert et al, 1998), or evidence that fragmentation of Aβ fibres increases cytotoxic potential through an increase in the number of exposed hydrophobic ends (Xue et al, 2009), a consensus as to their relative significance has not yet been reached. This is partly due to the heterogeneity of oligomeric assemblies, which vary dramatically in size, from 8 – 56 kDa (Lesne et al, 2006; Walsh et al, 1999), as well as structure, forming annular pore-like assemblies, flexible curved protofibrils, or the perfect spheres of the "amylospheroids" (Lasagna-Reeves & Kayed, 2011; Matsumura et al, 2011; Walsh et al, 1999). The diversity of oligomers partly arises from differences in assembly pathways between Aβ alloforms, the two most notable being $A\beta_{(1-40)}$ and $A\beta_{(1-42)}$.

1.4.5 $A\beta_{(1-42)}$ vs. $A\beta_{(1-40)}$ Aggregation

$A\beta_{(1-40)}$ and $A\beta_{(1-42)}$ are of most interest as they respectively represent both the most prevalent and most pathological forms of the peptide (Burdick et al, 1992; Lambert et al, 1998). The particular significance of $A\beta_{(1-42)}$ in AD has been cemented through observation of certain familial forms of the disease, for which the ratio of $A\beta_{(1-40)}$ to $A\beta_{(1-42)}$ is seen to shift from 9:1 to 7:3 (Citron et al, 1997; Duff et al, 1996; Scheuner et al, 1996). These familial forms of AD have mutations in either *APP* itself, or in two proteins thought to comprise the γ-secretase complex, presenilin 1 and presenilin 2. These mutations all increase production of $A\beta_{(1-42)}$ relative to $A\beta_{(1-40)}$, and lead to early-onset forms of the disease.

It has been suggested that the reason $A\beta_{(1-42)}$ is more greatly associated with AD than $A\beta_{(1-40)}$ is due to its enhanced capacity to form oligomers, as evidenced by the demonstration that $A\beta_{(1-42)}$ may form stable trimers/tetramers, a quality not thought to

be shared by $A\beta_{(1-40)}$ (Chen & Glabe, 2006). In addition to this, $A\beta_{(1-42)}$ aggregates more readily than $A\beta_{(1-40)}$, with oligomers forming at a much earlier time-point (Burdick et al, 1992; Chen & Glabe, 2006). This difference in the kinetics of self-association is partly due to $A\beta_{(1-42)}$ having an additional alanine and isoleucine; the resultant increase in hydrophobicity would certainly be expected to lead to a concomitant rise in rates of self-association. However, there are also thought to be significant differences in the fundamental structures of $A\beta_{(1-42)}$ and $A\beta_{(1-40)}$.

A comparison between the structures of $A\beta_{(1-42)}$ and $A\beta_{(1-40)}$ peptides is difficult, as they both populate a broad ensemble of conformations. However, a combination of molecular dynamic simulations and NMR data sampling provided us early insights (Sgourakis et al, 2007; Yang & Teplow, 2008). Initial simulations demonstrated the C-terminus of $A\beta_{(1-42)}$ to be more stable than that of $A\beta_{(1-40)}$, with it being able to adopt a β-hairpin structure that may facilitate formation of amyloid aggregates (Sgourakis et al, 2007). This was corroborated by *ab initio* simulations that incorporated a modular organisation of $A\beta_{(1-42)}$ and $A\beta_{(1-40)}$ peptides to simplify the folding dynamics, with residues 1 – 5, 10 – 13, 17 – 22, 28 – 37, and 39 – 40/42 comprising relatively independent folding units that are connected by four turn structures (Yang & Teplow, 2008). As previously, $A\beta_{(1-42)}$ was observed to form a more stable β-structure than that of $A\beta_{(1-40)}$, with the two additional amino acids increasing contacts within the C-terminus, as well as between the C-terminus and the central hydrophobic cluster, enabling $A\beta_{(1-42)}$ to more readily adopt an amyloid conformation. Differences in fibril structure have since been confirmed with ssNMR, revealing $A\beta_{(1-42)}$ to have a triple β-sheet motif, incompatible with $A\beta_{(1-40)}$ monomers (Xiao et al, 2015); furthermore, a recent cryo-EM derived model has demonstrated that the $A\beta_{(1-42)}$ dimers comprising $A\beta_{(1-42)}$ fibres possess a kinked c-termini interface, leading to an increase in the number of peptide-peptide interactions than in $A\beta_{(1-40)}$ fibres (Schmidt et al, 2015).

These differences in underlying structure are thought to lead to different routes of

aggregation for these two peptides. A variety of techniques, including size exclusion chromatography, photo-induced crosslinking of unmodified proteins, electron microscopy, and dynamic light scattering, have provided evidence that $A\beta_{(1-42)}$ fibrillogenesis is preceded by the formation of on-pathway spheroidal pentamer/ hexamer oligomeric units, which ultimately rearrange to form fibres, as illustrated in figure 1.07. However, for $A\beta_{(1-40)}$ no such oligomeric species were observed (Bitan et al, 2003). Support for a fundamental disparity in aggregative mechanism has been provided through investigations into mixtures of these peptides. For instance, the addition of $A\beta_{(1-40)}$ to $A\beta_{(1-42)}$ demonstrably prevents formation of $A\beta_{(1-42)}$ fibres (Jan et al, 2008), instead stabilising $A\beta_{(1-42)}$ intermediates (Kuperstein et al, 2010). Likewise, the presence of $A\beta_{(1-42)}$ is able to significantly frustrate formation of $A\beta_{(1-40)}$ fibres (Chang et al, 2013; Jan et al, 2008; Kuperstein et al, 2010). Thus, a diverse population of oligomers may form due to variations in the misfolding landscape between different Aβ alloforms, but also as different alloforms may influence each other's aggregative pathways. Unfortunately, the exact pathogenic mechanism of these amyloid aggregates is still a subject of intense debate. Below I shall discuss several of the most well established hypotheses.

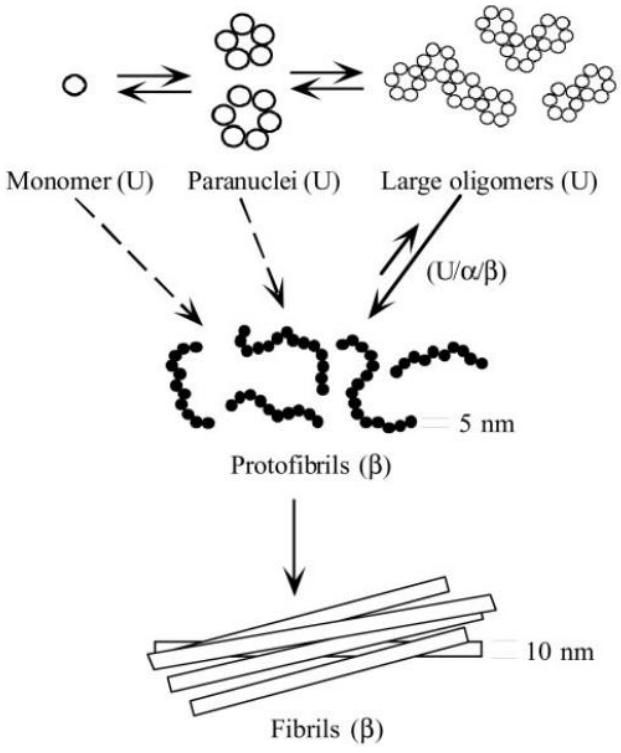

Figure 1.07 $A\beta_{(1-42)}$ Fibre Formation.

A simple model of $A\beta_{(1-42)}$ aggregation. Adapted from (Bitan et al, 2003). Copyright © 2003, The National Academy of Sciences.

1.5 MECHANISMS OF AMYLOID-β PATHOGENICITY

1.5.1 Oxidative Damage

The brain is particularly vulnerable to oxidative stress, due to its great oxygen demand, elevated levels of polyunsaturated fats, and high levels of redox transition metals (Bazinet & Laye, 2014; Masamoto & Tanishita, 2009; Viles, 2012); thus, oxidative damage is a potential mechanism of toxicity in neurodegenerative disease. This is underscored by the fact that several markers of oxidative stress are found to be present in AD, including protein oxidation, oxidation of DNA, and lipid peroxidation (Butterfield et al, 2002; Mecocci et al, 1994; Pamplona et al, 2005). Interestingly, an amino acid suggested to be crucial for Aβ neurotoxicity, Met35, is found to be oxidised in the brains of AD patients (Dong et al, 2003). The resultant methionine sulfoxide has been implicated in the generation of free-radicals in the brain of AD patients (Butterfield & Boyd-Kimball, 2005; Hensley et al, 1994), a situation which may be exacerbated as the enzyme capable of converting methionine sulfoxide back to methionine, methionine sulfoxide reductase, is observed to be diminished in the AD brain (Gabbita et al, 1999; Lovell et al, 2000)**.**

Despite it being previously suggested that the generation of radicals by Aβ is oxygen dependent but metal independent (Hensley et al, 1994), the current consensus is that binding to a redox active metal, such as copper or iron, facilitates the generation of hydrogen peroxide and free radicals through Fenton/Haber-Weiss reactions (Huang et al, 1999; Liu et al, 2006; Nadal et al, 2008; Opazo et al, 2002). The resultant oxidative stress may impact neuronal health in a number of ways, as shown in figure 1.08. Of particular significance is the disruption of Ca^{2+} homeostasis, which causes excitotoxicity, disrupts neuronal plasticity, and ultimately leads to cell death. The function of mitochondria are also greatly perturbed, as the consequent lipid peroxidation disrupts the function of membrane proteins, such as ion-motive ATPases

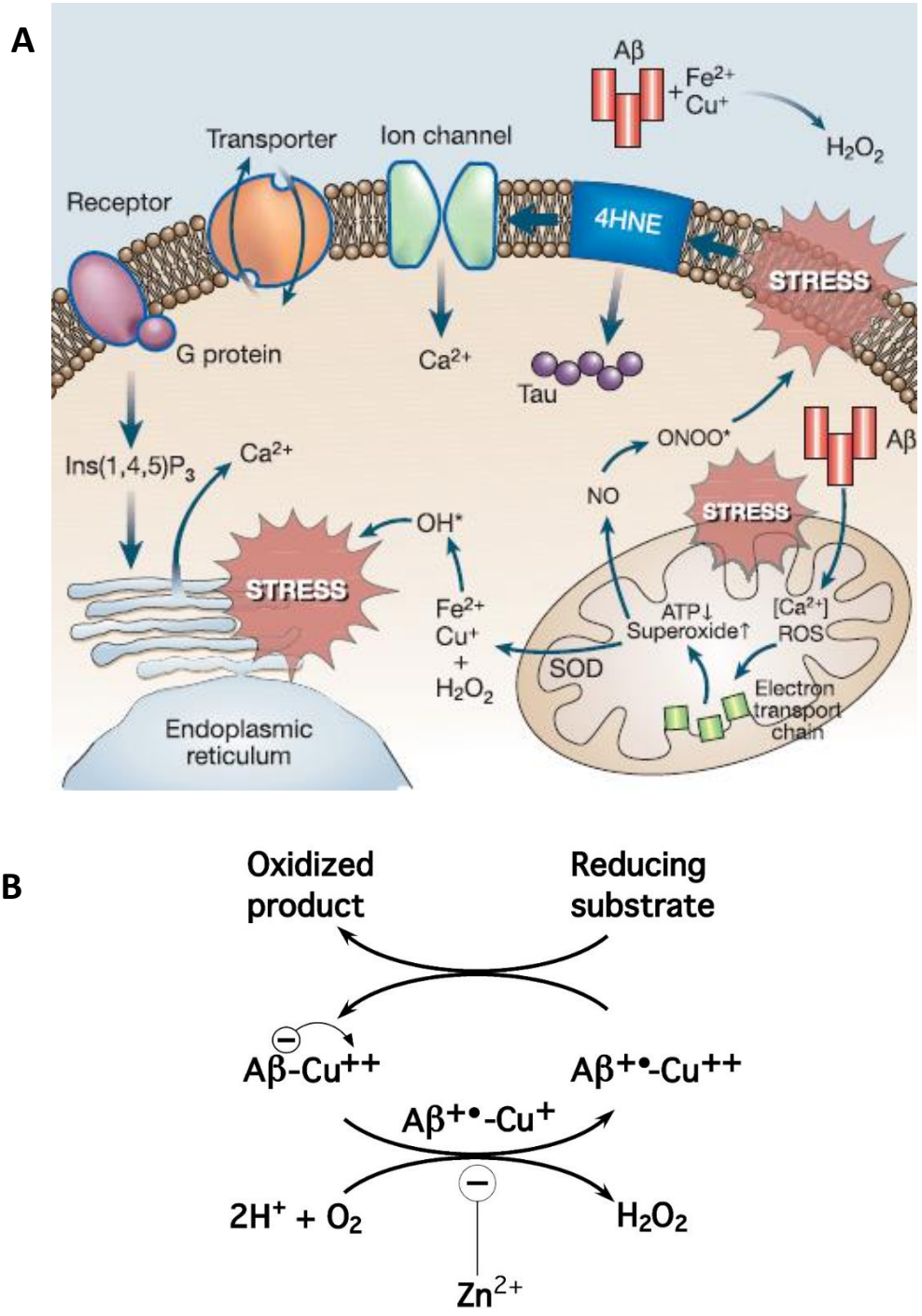

Figure 1.08 Aβ Induced Oxidative Stress.

(A) Reactive oxygen species generated by Aβ may impact cell health in a great many ways; for instance, lipid peroxidation impacts the function of cell membrane transporters, energy metabolism of mitochondria is perturbed, Ca^{2+} reserves in the endoplasmic reticulum are released, and the generation of the neurotoxic aldehyde, 4HNE, may oxidise tau and promote its aggregation. Reprinted by permission from Macmillan Publishers Ltd: Nature, (Mattson, 2004), copyright (2004). (B) A model for H_2O_2 production from Aβ-Cu^{2+}. Aβ-Cu^{2+} may be restored by a number of biological reducing agents, such as dopamine and vitamin C, the products of which may themselves by toxic. Reprinted from (Opazo et al, 2002).

and the electron transport chain (Mattson, 1997).

Though Aβ exerts oxidative stress *in vivo*, it is not clear whether this is the primary mechanism of Aβ neurotoxicity in AD. However, both oxidative stress and impaired energy metabolism have been associated with an increase in the amyloidogenic processing of APP (Gabuzda et al, 1994); thus, Aβ's oxidative potential may lead to an accumulation of Aβ, and a positive feedback loop of disease progression, regardless as to whether oxidation is the crucial factor in AD aetiology.

1.5.2 Aberrant Signalling

Aβ may perturb brain function through interfering with the signalling pathway of *N*-methyl-D-aspartate receptors (NMDARs), a glutamate receptor, and in this way reduce synaptic transmission, disrupt LTP, and ultimately result in cell death (Haass & Selkoe, 2007). It has been observed that exposure of NMDARs to Aβ promotes endocytosis of some NMDARs through a mechanism that is dependent on α7 nicotinic-receptors (Snyder et al, 2005). This is significant, as NMDAR activation promotes the phosphorylation and activation of a transcription factor, cAMP response element binding protein (CREB), that activates a number of genes involved in learning, synapse formation, and neuronal survival (Riccio et al, 1999; Taubenfeld et al, 2001). Thus, Aβ induced uptake of NMDA could inhibit learning, synapse integrity, and neuron survival, and in this way contribute towards AD pathology. Conversely, it has also been reported that Aβ is capable of elevating NMDAR activity, inducing steady-state NMDAR currents (You et al, 2012), supporting the heightened NMDAR activity previously seen in rat neurons (Wu et al, 1995). Such a potentiation of NMDAR activity is correspondingly harmful to neurons, as the subsequent chronic Ca^{2+} overload would induce synaptic loss (You et al, 2012), also contributing towards AD pathology, though through an alternate route.

The inconsistency of Aβ action upon NMDARs may in part be due to the α7 nicotinic-receptors that are required for NMDAR reuptake being non-uniformly distributed throughout the brain (Fabian-Fine et al, 2001; Zarei et al, 1999). However, the primary reason seems likely to arise from the nature of the NMDAR-Aβ interaction varying with subunit composition (Kessels et al, 2013; Li et al, 2011).

With transgenic mouse hippocampal slice cultures, it has been shown that inhibition of Aβ's interaction with NR2B-containing NMDARs prevents tau phosphorylation but does not attenuate dendritic spine loss or the elevated levels of caspase-3, whereas inhibition of the interaction with NR2A-containing NMDARs prevents loss of dendritic spines, down regulates caspase-3, and has no impact on tau phosphorylation (Tackenberg et al, 2013). This suggests two pathogenic pathways may originate from the interaction of NMDARs and Aβ independently of each other: caspase-3 induced apoptosis via NR2A-containing NMDARs, and tau mediated neurodegeneration through the NR2B-containing NMDARs. This also highlights the multifaceted nature of AD that has made it difficult to determine which mechanism of toxicity, if any, is the principal contributor towards AD pathology.

1.5.3 Cell Membranes Disruption

There is substantial support for Aβ exerting its neurotoxicity through a disruption of neuronal cell membrane integrity. This has been suggested to occur either through an insertion of ion-channel like assemblies of Aβ into the cell membrane (Arispe, 1993; Arispe et al, 1996; Jang et al, 2008; Quist et al, 2005), or through lowering the dielectric barrier of the membrane itself, through thinning and even puncturing the membrane (Kayed et al, 2004; Sokolov et al, 2006; Williams et al, 2010; Xue et al, 2009), presumably via the hydrophobic ends of fibrillar aggregates, as seen in figure 1.09 (Milanesi et al, 2012). For both scenarios, the subsequent loss in regulation of

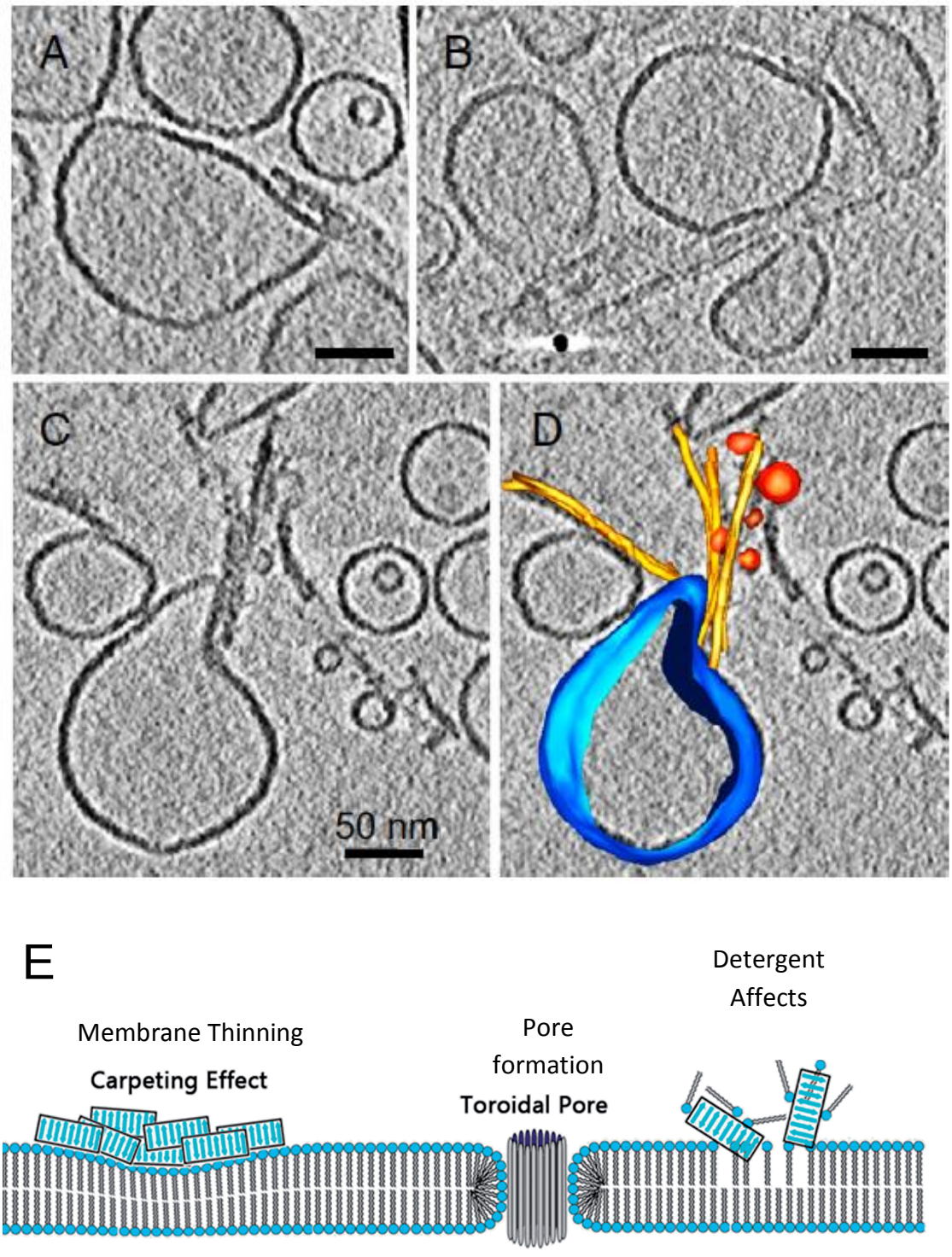

Figure 1.09 Aβ Induced Membrane Distortion.

Cryoelectron tomograms of amyloid fibrils (of β_2-microglobulin) clearly disrupting the membranes of unilamellar vesicles (A-C), and a rendered 3D model of this interaction (D). Reprinted from (Milanesi et al, 2012), Copyright © 2015 National Academy of Sciences. Scale bar 50 nm. (E) Schematic of three mechanisms through which Aβ is thought to disrupt cell membrane integrity. Reproduced from (Zhang et al, 2014), with permission of The Royal Society of Chemistry.

intracellular ions, particularly Ca^{2+}, would cause synaptic dysfunction and neuronal loss (Khachaturian, 1987; Mattson et al, 1992), thus contributing towards AD pathology.

The occurrence of pathological interactions between Aβ and cell membranes is physiologically feasible; as Aβ is cleaved from APP at the cell membrane it may retain an affinity to the membrane, especially as the amphipathic phospholipids provide an extensive surface for Aβ binding (Williams & Serpell, 2011). This interaction has been studied extensively, using a range of biophysical techniques, including atomic-force microscopy, ssNMR, cryo-EM/tomography, and fluorescence spectroscopy, with biomimetic vesicles providing a simplified system that may be stringently regulated. Preliminary studies used only single-lipid vesicles, consisting entirely of phosphatidylcholine (PC), a neutral lipid that is a major constituent of the outer leaflet of the cell membrane (Andrick et al, 1991; Wirtz, 1991). Even in such a simplified model, a relationship between the membranes and Aβ is evident, with the vesicles dramatically influencing the aggregative properties of Aβ, through an increase in the lag time of fibre formation (Sabate et al, 2005). Additionally, early studies established that Aβ has the capacity to penetrate the membranes of these minimal models, and that vesicles comprised of a single acidic lipid, particularly the highly acidic phosphatidylinositol, could induce Aβ to adopt a β-structure in a pH dependent manner, as shown with circular dichroism (McLaurin & Chakrabartty, 1997).

The success of these early studies in establishing the importance of the interaction between Aβ and cell membranes is particularly striking, as *in vivo* it is now understood that there are additional components that may aid the interaction between membranes and Aβ. One such component is cholesterol, an essential constituent of the membrane *in vivo*, but that has also been found to be an important risk factor for AD (Breteler et al, 1998; Kivipelto & Solomon, 2006). The role of cholesterol in a healthy brain is to regulate the fluidity of the cell membrane (Ohvo-Rekila et al, 2002), while also decreasing permeability to small solutes (Haines, 2001; Yeagle, 1991). However,

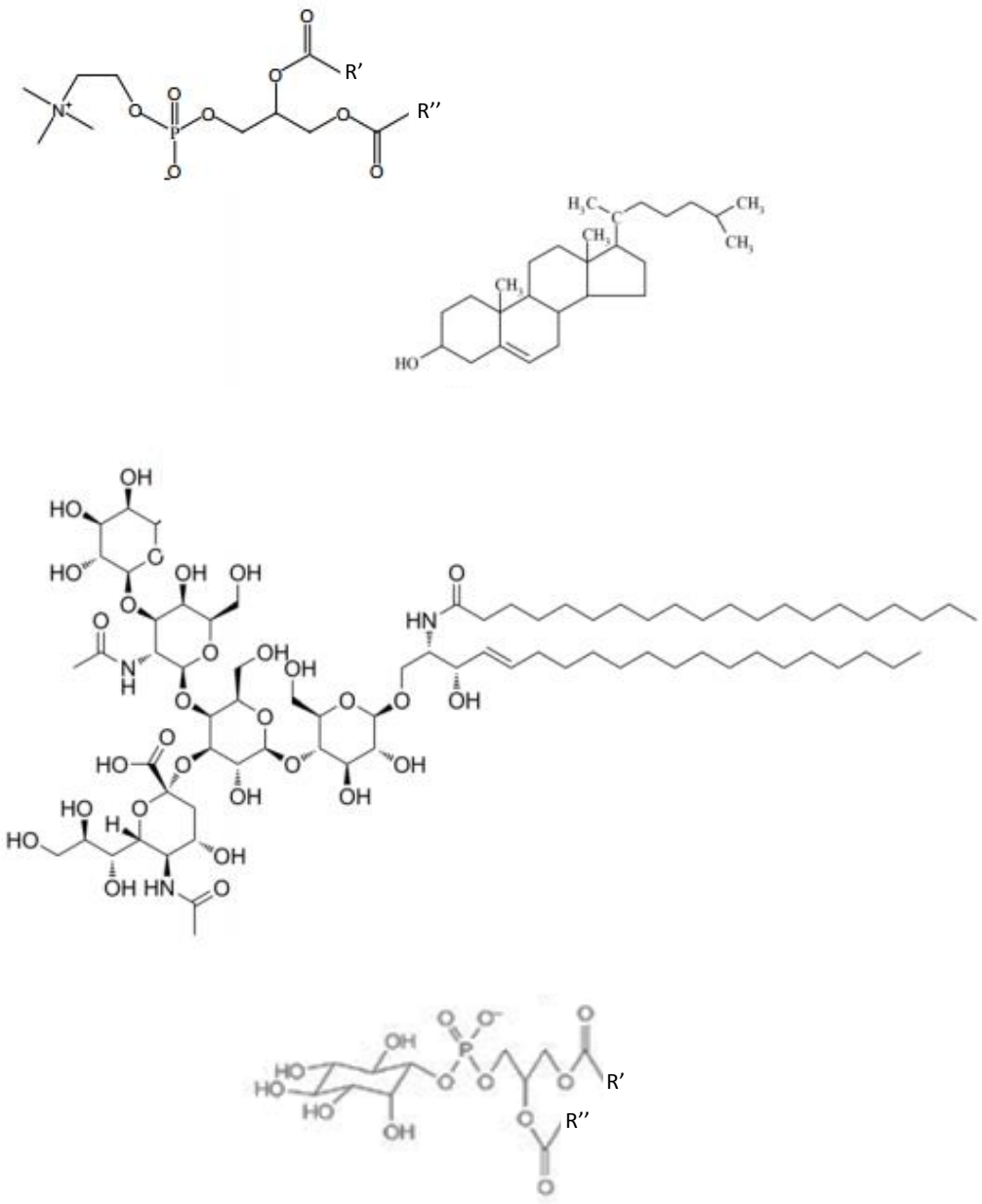

Figure 1.10 Lipid Structures.

From the top to the bottom, structures of phosphatidylcholine, cholesterol, GM1, and phosphatidylinositol. Adapted from (Becucci et al, 2014).

cholesterol has also been seen to aid in the insertion of Aβ into small unilamellar vesicles and lipid monolayers, while also promoting the adoption of an α-helical structure, presumably inhibiting Aβ aggregation (Ji et al, 2002). This has made it somewhat unclear as to whether membrane cholesterol may prevent or augment AD pathogenicity.

Evidence that membrane cholesterol is diminished in those with AD (Mason et al, 1992; Roth et al, 1995), and the observation that membrane cholesterol inversely correlates with $A\beta_{(1-40)}$ induced cell death, of both PC-12 and SH-SY5Y cells (Yip et al, 2001), seemingly suggests a protective role. However, it has also been shown that membrane cholesterol facilitates the insertion of $A\beta_{(1-42)}$ oligomers into neuronal cell membranes, which subsequently induces a rearrangement of the lipid membrane that the authors suggest may have an important role in AD, through a disruption of intercellular signalling at the synapse (Ashley et al, 2006). Additionally, with both synthetic lipid mixtures and vascular smooth muscle cell membranes, Aβ toxicity is observed to be proportional to membrane binding, which in turn is dependent on the presence of membrane cholesterol; the implied relationship between cholesterol and Aβ toxicity was confirmed when a reduction of cholesterol was demonstrated to significantly ameliorate the toxic effects of both $A\beta_{(1-40)}$ and $A\beta_{(1-42)}$ (Subasinghe et al, 2003). Thus, the relationship between membrane cholesterol and Aβ is highly contentious, and though discrepancies may potentially arise in part from differences in cells, Aβ alloforms, or the aggregated states of Aβ, this does not resolve all disputes in the literature. However, it is clear that cholesterol is a significant factor in determining the relationship between Aβ and cell membranes *in vivo*, so to develop an accurate model of Aβ at the cell membrane, it is a necessary constituent to include.

Gangliosides are another important component of the cell membrane in AD aetiology. They are a family of glycosphingolipids (consisting of hydrophilic sialic acid moieties on a terminal oligosaccharide, and a hydrophobic ceramide tail) that are abundant in the

brain, where they comprise 5 – 10 % of neuronal outer membrane leaflets, and are important for neuronal plasticity, differentiation and cell adhesion (Fishman & Brady, 1976; Hakomori, 2003; Mocchetti, 2005). The first ganglioside discovered, and that with the highest affinity for $A\beta_{(1-42)}$, is GM1 (Valdes-Gonzalez et al, 2001). Despite initial suggestions that GM1 may sequester Aβ and prevent fibre formation (McLaurin & Chakrabartty, 1996), it has since been demonstrated that the inclusion of GM1 in lipid vesicles increases Aβ fibrillogenesis (Choo-Smith et al, 1997), and may facilitate insertion of Aβ into the membrane, potentiating Aβ induced distortion of vesicles, and the subsequent increase in permeability (Williams et al, 2010). Thus, GM1 likely has an important role in mediating Aβ toxicity, at least at the cell membrane. This is supported by the coincident decline of glucosylceramide synthase activity with age (Marks et al, 2008), which may lead to an increase in the number of gangliosides at the cell membrane, as has been shown for transgenic mouse models of AD (Barrier et al, 2007), and consequently providing more sites for Aβ membrane insertion.

1.6 THE SYNAPSE

1.6.1 During Alzheimer's Disease

Though in AD we are able to observe dramatic changes in brain anatomy, such as extensive neuronal loss, shrinkage of the brain, and expansion of ventricles, it is generally accepted that looking at earlier more subtle effects provides a greater understanding of disease aetiology; in AD, that means studying synaptic loss is a priority (Klyubin et al, 2012; Selkoe, 2002; Selkoe, 2008). Synapses are essential to neuronal function, as they enable "communication" between neurons, be it via an electrical or chemical signal (Daniel L. Schacter, 2011). This occurs at the synaptic cleft, a junction between the synapses of two neurons that is 20 – 30 nm wide, and is described in Figure 1.11 (Christopher Moyes, 2008). The widely accepted Hebbian theory postulates that it is at the synaptic level that learning occurs, as repeated

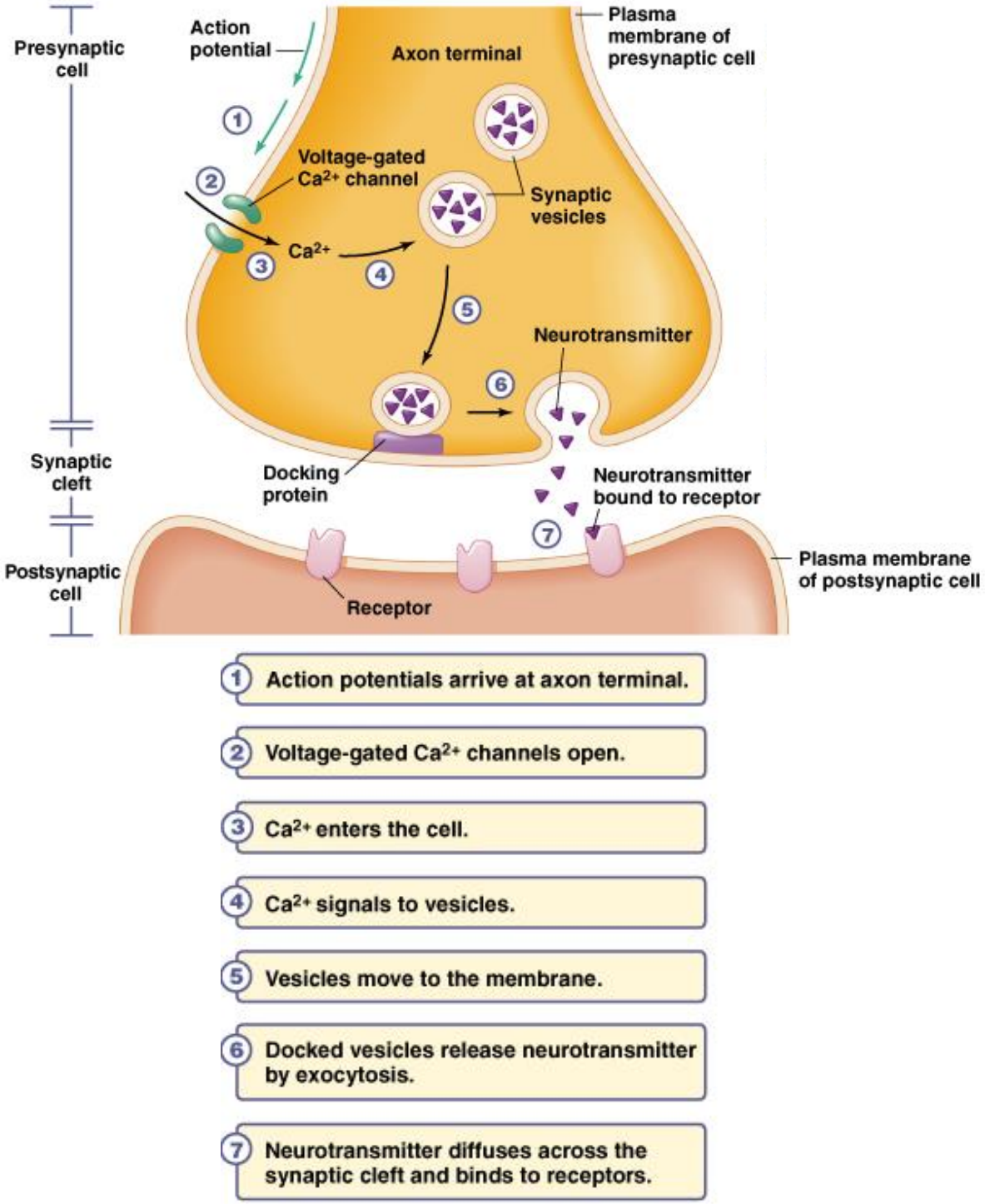

Figure 1.11 Synaptic Transmission.

A schematic of synaptic transmission between neurons. Reproduced from (Christopher Moyes, 2008), copyright © 2015, Pearson Education Inc.

signalling across a synaptic cleft strengthens the inter-neuron connection, and it is this strengthening of connection, LTP, that likely facilitates information storage (Lynch, 2004).

At early stages of AD there is extensive synaptic loss, with an ~25 – 35 % loss of synapses in the cortex 2 – 4 years after diagnosis (Davies et al, 1987). This is not simply the result of neuronal loss, as individual cortical neurons are also observed to have an ~15 – 35 % reduction in their number of synapses. The importance of synaptic loss in AD aetiology is underscored by the observation that it is the best correlate of cognitive decline for all stages of AD (Terry et al, 1991). As such, there is much interest in the relationship between Aβ and the synapse.

1.6.2 Aβ and the Synapse

Levels of Aβ are estimated to be 0.5 nM at the synapse (Seubert et al, 1992); however, it is well established that Aβ monomers do not perturb synaptic function (Klyubin et al, 2012), and may Instead actually support LTP and learning (Puzzo et al, 2011; Puzzo et al, 2008). This has been supported in a range of experiments, that have demonstrated the necessity of Aβ to first aggregate for it to be capable of disrupting the synapse (Cleary et al, 2005; Klyubin et al, 2008; Klyubin et al, 2005; Shankar et al, 2008).

In several pioneering studies it was clearly shown that Aβ aggregates have the capacity to perturb LTP independently of neurodegeneration, using mouse brain slices (Lambert et al, 1998), rat brain slices (Wang et al, 2002), and rats (Walsh et al, 2002). Subsequent experiments have suggested that Aβ dimers are sufficient to mediate this synaptotoxicity (Barry et al, 2011; Li et al, 2009; Li et al, 2011; Shankar et al, 2008), and are more potent neurotoxins than larger oligomeric species, such as Aβ*56 (Lesne et al, 2006; Shankar et al, 2008). However, more recent evidence has shown that these dimers need to assemble themselves into large protofibril-like oligomers before they

are able to disrupt LTP (Hartley et al, 2008; O'Nuallain et al, 2010). This highlights the difficulty in determining the precise aggregate species responsible for mediating synaptic disruption *in vivo*, as the heterogeneity of Aβ populations and the dynamic equilibrium between different aggregate species can lead us to erroneous conclusions. Consequently, the relative significance of different aggregative species is still uncertain (Klyubin et al, 2012). A more effective route for elucidating how the vast range of Aβ aggregates fit into AD aetiology may be to first delineate the role of Aβ ligands that are able to influence Aβ's aggregative landscape. Metal ions, particularly Zn^{2+} and Cu^{2+}, are thought to be particularly important in directing Aβ aggregation *in vivo* (Faller et al, 2013; Viles, 2012).

1.6.3 Cu^{2+} at the Synapse

At the synaptic cleft, Cu^{2+} has been reported to reach concentrations of 15 – 250 μM during depolarisation (Hartter & Barnea, 1988; Kardos et al, 1989). These high fluxes in Cu^{2+} ions are now understood to be indicative of an important role for Cu^{2+} in regulating neuronal transmission (Gaier et al, 2013). It has been shown with rat cortical neurons that Cu^{2+} may inhibit NMDAR induced depolarisation, as well as that of α-amino-3-hydroxyl-5-methyl-4-isoxazolepropionic acid receptors (AMPARs), another glutamate receptor which is upregulated in response to heightened NMDAR activity (Weiser & Wienrich, 1996). Notably, the effect of Cu^{2+} on AMPARs was significantly inhibited by the addition of a reducing agent, diothiothreitol, whereas the effect of Cu^{2+} on NMDARs was not influenced by diothiothreitol. This suggests that the mechanism of Cu^{2+} mediated inhibition is different for these two glutamate receptors, being oxidation dependent for AMPARs, but oxidation independent for NMDARs. Later studies have shown that Cu^{2+} inhibits NMDAR activity non-competitively, with Cu^{2+} preferably binding agonist-bound receptors, and nullifying excitotoxicity (Schlief et al, 2006; Vlachova et al, 1996). A role for Cu^{2+} in preventing glutamate induced excitotoxicity is corroborated by the disease aetiology of Menkes disease, for which Cu^{2+} deficiency

causes seizures and extensive neurodegeneration (Barnes et al, 2005; Donsante et al, 2011; Kodama et al, 1999).

Menkes disease is also associated with developmental delay (Donsante et al, 2007; Kaler, 2011), which may be related to Cu^{2+} induced inhibition of a second class of neurotransmitter receptors: γ-aminobutyric acid (GABA) receptors, specifically the $GABA_A$ subtype (Sharonova et al, 1998; Trombley & Shepherd, 1996). $GABA_A$ receptors are Cl^- channels, and as such are generally inhibitory; however, they may be excitatory when intracellular levels of Cl^- are elevated, as is seen in development (Ben-Ari et al, 1997; Taketo & Yoshioka, 2000). It is at these neurons for which the action of Cu^{2+} on $GABA_A$ receptors is thought to be important for developmental onset.

Despite being crucial for proper neuronal functioning, Cu^{2+} requires tight regulation, partly due to the risk of reactive oxygen species generation (Uriu-Adams & Keen, 2005). However, disruption of the aforementioned neuronal signalling pathways through unregulated Cu^{2+} is also pathogenic, as demonstrated in Wilson's disease, a disease in which Cu^{2+} levels are elevated, and that leads to extensive neurodegeneration, motor impairment, and psychiatric symptoms (Das & Ray, 2006; Kodama et al, 2011).

1.6.4 Zn^{2+} at the Synapse

Zn^{2+} is another metal ion that has been reported to reach high concentrations at the synaptic cleft during depolarisation, typically as much as 100 – 300 μM (Kardos et al, 1989; Vogt et al, 2000). It is now understood to be an important signalling molecule within the nervous system; indeed, glutamatergic neurons, at which the greatest reserves of Zn^{2+} in the brain are co-released with glutamate, are frequently now referred to as "zincergic" neurons (Brown & Dyck, 2004; Takeda et al, 2013). However, Zn^{2+} is not limited to influencing glutamate receptors. It has been established that Zn^{2+}

may modulate the activity of almost all known ligand gated ion channels involved in neuronal transmission, though with a high degree of specificity for subunit composition (Marger et al, 2014; Yuan et al, 2014).

The receptors which are most sensitive to Zn^{2+} are NMDARs comprised of NR2A subunits, which are inhibited by Zn^{2+} at the nanomolar range in a voltage-independent manner (Yuan et al, 2014; Zheng et al, 2001) , demonstrating that Zn^{2+} binding occurs externally from the pore. However, there is also evidence that Zn^{2+} at micromolar concentrations may inhibit a broader range of NMDARs in a voltage-dependent manner (Christine & Choi, 1990; Hansen et al, 2014); suggesting that there is a second Zn^{2+} binding site within the pore itself. It is not yet clear the significance of there being two sites, though it is clear that Zn^{2+} is an important modulator of NMDAR activity, and by extension, neuronal plasticity (Marger et al, 2014; Vergnano et al, 2014), as well as likely being protective against excitotoxicity (Koh & Choi, 1988).

Zn^{2+} also regulates the family of pentameric four transmembrane receptors which nicotinic acetylcholine receptors (nACHR), $GABA_A$ receptors, serotonin receptors, and glycine receptors are members (Marger et al, 2014). Modulation by Zn^{2+} of these receptors can be highly subtype specific and complex; for instance, α2β2 nACHR activity is potentiated by Zn^{2+} at lower micromolar levels but inhibited at higher concentrations, whereas a slightly different subunit composition, α3β2, may only bind and be inhibited by Zn^{2+} (Hsiao et al, 2001). As for NMDARs, it is thought that there are two Zn^{2+} binding sites, one at the interface between subunit extracellular domains, and a second site within the pore, which has been supported by the site directed mutagenesis of $GABA_A$ receptors (Horenstein & Akabas, 1998).

The broad range of neuronal receptors that Zn^{2+} modulates, including NMDARs and glycine receptors, the brain's major excitatory and inhibitory receptors respectively, highlights the significant role of Zn^{2+} in a diversity of brain functions. This becomes

clearer still when one considers the impact of deregulated Zn^{2+}, with elevated levels of Zn^{2+} conferring epilepsy, ischemia and depression to mice (Lee et al, 2000), and Zn^{2+} deficiency causing such effects as depression, odour disorder, and learning impairment in humans (Adamo & Oteiza, 2010; Takeda, 2011). However, the complexity of Zn^{2+} regulated neuronal signalling has prevented us from yet completely delineating the more subtle effects of Zn^{2+} dyshomeostasis (Marger et al, 2014).

1.7 METAL IONS AND ALZHEIMER'S DISEASE

1.7.1 Metal Dyshomeostasis and Alzheimer's Disease

A network of metal binding proteins and transporters regulate the levels of Zn^{2+} and Cu^{2+} *in vivo*, which is especially important in the brain, where the levels of these ions are particularly high (Que et al, 2008). Within the cell there is almost no free zinc or copper, with these ions being carefully regulated through metal binding proteins, such as the metallothioneins, low molecular weight cysteine-rich proteins that buffer against harmful ion fluxes (Sigel et al, 2009). However, metal ion release and retrieval is also crucial for regulating ion levels. For Cu^{2+}, CTR1 mediates reuptake, and release is primarily facilitated by the P-type ATPase, ATP7A (Gaier et al, 2013); alternatively, for Zn^{2+}, fluxes are largely controlled by ZnT3 transporters, which deliver Zn^{2+} into synaptic vesicles that release Zn^{2+} into the synaptic cleft upon depolarisation, and ZIP transporters, that deliver Zn^{2+} from the extracellular space into the cytosol (Szewczyk, 2013).

Despite the many measures controlling metal ion levels in the brain, in patients with AD a disruption of Cu^{2+} and Zn^{2+} levels is observed. It has been reported that in the neuropil there is a 4-fold and 2-fold increase in Cu^{2+} and Zn^{2+} respectively, and that in the Aβ plaques there are high concentrations of these ions present (Lovell et al, 1998; Miller et al, 2006). There are several possible reasons for the diminished integrity of

Zn^{2+}/Cu^{2+} homeostasis. For instance cellular uptake of these metal ions, which is energy dependent, may become fatigued with age. Additionally, there is recent evidence to implicate the presenilins in Cu^{2+}/Zn^{2+} transport, providing a direct connection between Aβ processing and metal homeostasis (Greenough et al, 2011). A further potential factor is that those with AD have reduced levels of metal ion binding metallothioneins (Yu et al, 2001). However, despite several possible explanations, it cannot yet be said that the mechanism of metal ion dyshomeostasis in AD is fully delineated, as the components of Cu^{2+} and Zn^{2+} homeostasis, and the interactions of these components, is still being clarified (Banci et al, 2010; Kim et al, 2010; Sensi et al, 2011).

1.7.2 Metal ions and Aβ

It has been well characterised that Cu^{2+} and Zn^{2+} may influence Aβ metabolism. For instance, Zn^{2+} has been shown to bind APP, and block Aβ cleavage, as well as inhibit γ-secretase activity (Ayton et al, 2013; Stelmashook et al, 2014). The amyloidogenic processing of APP is also inhibited by Cu^{2+} (Bayer et al, 2003), with APP also being implicated in Cu^{2+} homeostasis, promoting the efflux of Cu^{2+} from the cell (Bayer et al, 2003; White et al, 1999). Thus, the disrupted reuptake of Cu^{2+}/Zn^{2+} into neurons, and their subsequent accumulation in the synaptic cleft may lead to overproduction of Aβ. It has also found that in the synaptic cleft, Zn^{2+} and Cu^{2+} may directly bind to Aβ (Adlard et al, 2010; Dong et al, 2003), which may in turn further inhibit the reuptake of Cu^{2+} and Zn^{2+}, and lead to even greater Aβ production. Notably, the loss of intracellular Cu^{+} could also lead to neuronal oxidative stress, as superoxide dismutase 1 activity would be much reduced (Bayer et al, 2003).

The affinities of Aβ for Zn^{2+} and Cu^{2+} at physiological pH are micromolar and picomolar respectively (Faller & Hureau, 2009; Sarell et al, 2009; Syme & Viles, 2006), which is high enough to be physiologically relevant, due to the high concentrations of these ions

during depolarisation and the reported concentration for Aβ of 0.5 nM (Seubert et al, 1992). Cu^{2+} binds to Aβ at a 1:1 ratio, with both monomeric and fibrillar Aβ having identical coordination geometries (Karr & Szalai, 2008; Sarell et al, 2009). SsNMR and pulsed EPR have suggested that Cu^{2+} coordination does not disrupt amyloid fibril structure (Gunderson et al, 2012; Parthasarathy et al, 2011), perhaps as the ligands involved in Cu^{2+} coordination fall just outside the region that constitutes the β-pleated core of Aβ fibres (between residues 14 – 40). A great number of studies have been carried out to elucidate the binding geometry of Cu^{2+} to Aβ, and it is now generally accepted that Cu^{2+} forms a tetragonal complex with Aβ involving the three histidines (His6, His13, His14), oxygen coordination from Asp1 and Asp7, and the amino group of the N-terminus (Damante et al, 2008; Dorlet et al, 2009; Karr & Szalai, 2008; Minicozzi et al, 2008; Sarell et al, 2009; Viles et al, 1999). Though some details of coordination are still unresolved, there has been increasing evidence to support there being a number of interchangeable Cu^{2+}-Aβ complexes, the relative distribution of which is influenced by pH (Dorlet et al, 2009; Drew et al, 2009; Sarell et al, 2009; Shin & Saxena, 2011). Two complexes that coexist at pH 7.4, typically noted I and II and shown in figure 1.11, differ due to a deprotonation at the Asp1-Ala2 amide bond; this deprotonation leads to formation of complex II rather than I (Faller et al, 2013).

Unlike Cu^{2+}, Zn^{2+} typically forms a tetrahedral complex with Aβ, although 5 and 6 coordinate complexes are also possible. The three histidine residues along with the carboxylate group of Glu11 or Asp1 (possibly with the N-terminal amino group) have been identified as the coordination ligands (Danielsson et al, 2007 ; Dorlet et al, 2009; Faller, 2009; Sarell et al, 2009; Syme & Viles, 2006). However, as for Cu^{2+}-Aβ, the Zn^{2+}-Aβ complex is not a fixed structure, with the model in figure 1.12 representing only one possibility. Indeed, the complex has been demonstrated to be in rapid exchange (on NMR timescales), suggesting that the ligands may dynamically exchange (Syme & Viles, 2006). Notably, the histidine residues that complex Zn^{2+} may come from different Aβ peptides, producing cross-linked Aβ that may disrupt fibre assembly (Minicozzi et

al, 2008; Syme & Viles, 2006).

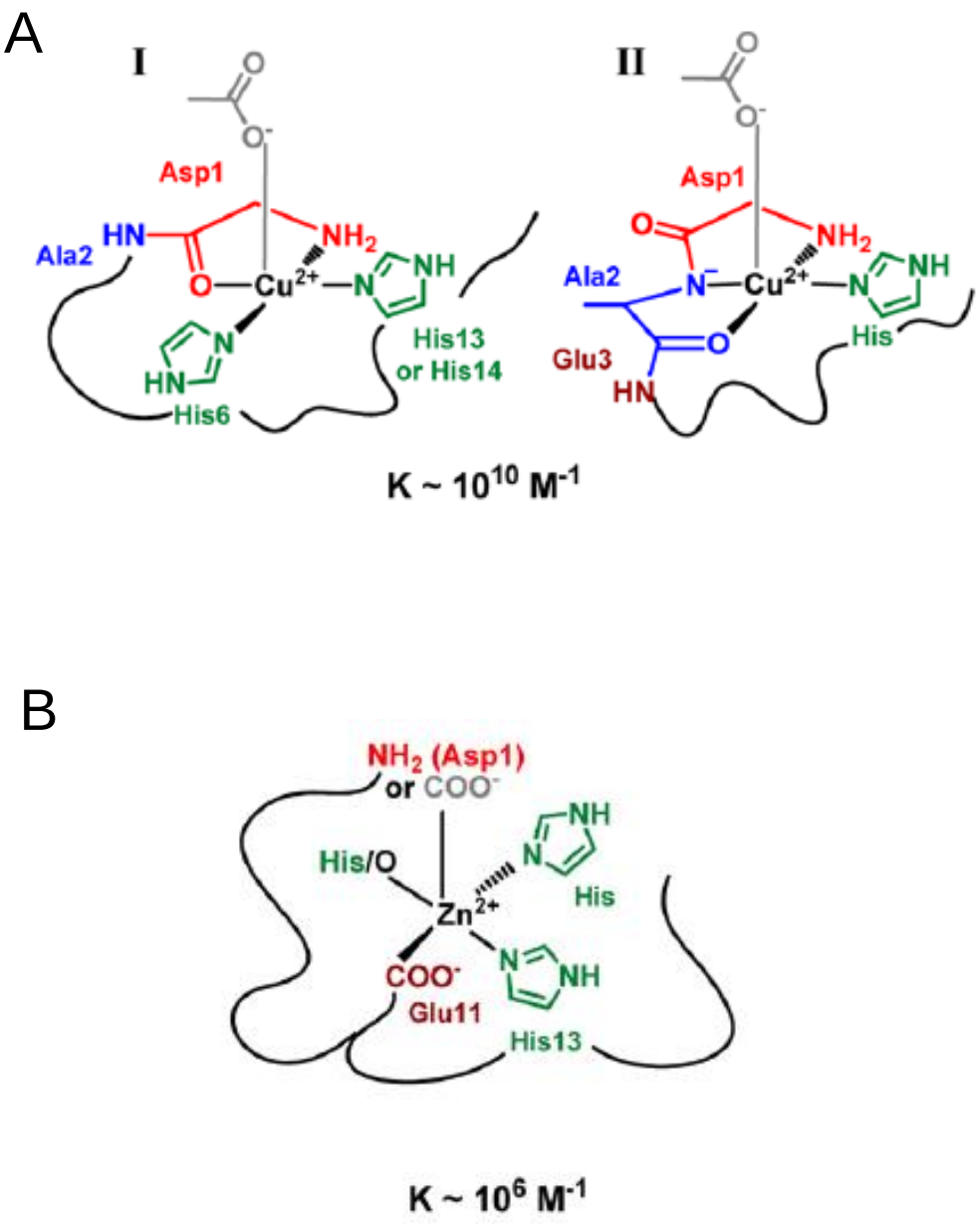

Figure 1.12 Metal Coordination.

Coordination of Cu^{2+} (A) and Zn^{2+} (B) by Aβ. Reproduced with permission from (Faller et al, 2013) copyright (2013) American Chemical Society.

1.8 AIMS OF THIS THESIS

There has been a number of investigations into the effect of Cu^{2+} and Zn^{2+} on Aβ misfolding; however, there has been little consensus in what has been reported. This may in part be due to differences in the Aβ alloform used (1-40/1-42), a lack of accounting for which aggregate species were formed, and differences in Aβ to metal ion ratios. Throughout this PhD, the aim has been to clarify the influence of Cu^{2+} and Zn^{2+} on the self-assembly of Aβ, while also providing physiological context. Specific aims include:

I. Observe how a range of Cu^{2+} and Zn^{2+} concentrations effects $Aβ_{(1-42)}$ and $Aβ_{(1-40)}$ self-association, in terms of fibre growth kinetics and assembly structure. Chapters 3 and 4.
II. Establish how Cu^{2+} influences the kinetics and morphology of aggregation when $Aβ_{(1-42)}$ and $Aβ_{(1-40)}$ are mixed together, both at a ratio found in healthy individuals, and at a ratio found in those with early-onset AD. Chapter 3.
III. Identify whether Cu^{2+} generated $Aβ_{(1-42)}$ aggregates have an enhanced capacity to disrupt membrane integrity, a mechanism through which Aβ is thought to cause synaptotoxicity *in vivo*. Chapter 3.
IV. Discern the mechanism through which trace levels of Zn^{2+} influence Aβ misfolding, and whether glutamate or Cu^{2+} inhibits Zn^{2+}'s effect upon Aβ, as all three are found at the synapse with Aβ. Chapter 4.
V. Investigate whether the effect of substoichiometric Cu^{2+} on $Aβ_{(1-40)}$ fibre growth is dependent on fibril growth conditions (quiescent vs agitated), due to the significant effect growth conditions have upon fibre structure. Chapter 5.
VI. Determine whether Cu^{2+} influences the stability of $Aβ_{(1-40)}$ fibres, to ascertain whether a reduction in stability may be the mechanism through which Cu^{2+} enhances the toxicity of $Aβ_{(1-40)}$ fibres. Chapter 5.

CHAPTER 2: Materials, Methods, and Theory

2.1 MATERIALS

2.1.1 Peptide Synthesis and Purification

Lyophilised $A\beta_{(1-40)}$ was purchased commercially from Cambridge Research Biochemicals, and Zinser, and lyophilised $A\beta_{(1-42)}$ was purchased from Imperial College of London and Zinser. The peptides were synthesised using solid phase F-moc chemistry, and HPLC indicated a single peak at the expected molecular mass. The peptides were also characterised using ^{1}H NMR which confirmed that Met^{35} was un-oxidised. Lyophilised $A\beta_{(1-40)}$ and $A\beta_{(1-42)}$ were stored in the freezer at -20 ^{o}C..

2.1.2 Aβ Peptide Sequences

Peptides used were synthesised from human sequences of $A\beta_{(1-40)}$ and $A\beta_{(1-42)}$, for which the N-terminus and C-terminus were left as native amino and carboxyl groups respectively. The sequences were as follows:

$A\beta_{(1-40)}$: DAEFRHDSGYEVHHQKLVFFAEDVGSNKGAIIGLMVGGVV

$A\beta_{(1-42)}$: DAEFRHDSGYEVHHQKLVFFAEDVGSNKGAIIGLMVGGVVIA

2.1.3 General Chemicals and Consumables

The chemicals I have used during my PhD have been presented in the table below.

Table 2.01 Chemicals used Throughout PhD

Chemicals	Supplier	Molecular Weight (g/mol)	Purity (%) / Grade
Chloroform	BDH - Biocehmical	119.38	≥ 99
Cholesterol	Sigma - Aldrich	386.65	≥ 99
Copper(II)Chloride Dihydrate	Sigma – Aldrich	170.48	≥ 99.99
Etylenediaminetetraacetic acis	Sigma - Aldrich	292.24	≥ 99.995
Guanidinium chloride	Sigma – Aldrich	95.53	≥ 99
(Brain, Ovine) Ganglioside GM1	Avanti Lipids	1,568.81	≥ 99
HEPES (4-(2-hydroxyethyl)-1-piperazineethanesulfonic acid)	Sigma – Aldrich	238.3	≥ 99.5
L-Histidine	Sigma – Aldrich	155.5	≥ 99
Hydrochloric acid (35 %)	BDH - Biochemical	36.46	Spectroscopy grade
Methanol	Sigma – Aldrich	32.04	≥ 99.93
(Egg, chicken) Phosphatidylcholine (chloroform 25 mg/ml)	Avanti Lipids	770.12	≥ 99
Phosphotungstic acid hydrate	Sigma – Aldrich	2880.05 (anhydrous basis)	Reagent grade
Potassium Chloride	Sigma – Aldrich	70.45	≥ 99
Sodium Hydroxide	Sigma – Aldrich	40	≥ 99
Thioflavin T	Sigma – Aldrich	318.87	-
Zinc chloride	Sigma – Aldrich	136.315	≥ 98

Consumables used during my PhD are displayed in the table below.

Table 2.02 Consumables used Throughout PhD

Consumables	Supplier	Specification
1 cm Path-length Cuvette	Hellma	1 ml Volume, made from Quartz Supersil
1 cm Path-length Cuvette	Hellma	3 ml Volume, made from Quartz Supersil
0.1 cm Path-length Cuvette	Hellma	0.1 ml Volume, made from Quartz Supersil
Falcon® 96 Well Plates	Corning Inc.	Flat Bottomed, clear Polystyrene
Mini Extruder	Avanti Lipids	Made from stainless steel and Teflon, comes with 100 nm filters
Transmission Electron Microscopy Grids	SPI supplies	Copper coated, square mesh

2.1.4 Software and Equipment

Software and equipment used to generate data presented in the table below.

Table 2.03 Consumables used Throughout PhD

Equipment	Manufaturer	Model	Software
96 Well plate fluorescence reader	BMG	Fluostar Galaxy	Fluostar Galaxy Ver:4.31.0
96 Well plate fluorescence reader	BMG	Fluostar Omega	Mars Data Analysis Software Ver: 2.10 R3
Circular Dichroism Spectrometer	Applied Photophysics	Chirascan	Applied Photophysics Ver:4.2.0
Single-cell Fluorescence Spectrometer	Hitachi	F-2500	FL Solutions Application Software
Transmission Electron Microscope	JEOL	JEM-2010	Olympus iTEM TEM Imaging Software
Ultraviolet-Visible Spectrometer	Hitachi	U-3010	UV Solution Ver: 2.0
(Data Analysis and Presentation Software)	Synergy Software	-	KaleidaGraph Ver: 4.0.1
(Spreadsheets, Presentations, and Writing)	Microsoft	-	Microsoft Office 2010
(Referencing Software)	Endnote	-	Endnote x7

2.2 THEORY

2.2.1 Absorbance (UV-VIS) Spectroscopy

This technique, UV-Vis spectroscopy, monitors absorbance within both the ultraviolet (UV) region, 180 – 400 nm, and visible region, 400 – 800 nm. UV-Vis absorption spectroscopy typically depends on the presence of either d-orbital electrons within transition metals or π-electrons within the molecule, as these electrons are more readily excited from the ground state to a higher energy level. The electronic states of particular systems are well defined, such that excitation of a particular electron in a given molecule requires a quantised amount of light at a certain wavelength. Thus, it follows that absorbance is proportional to molar concentration. It is from this understanding that the Beer-Lambert equation is derived:

$$A_\lambda = \varepsilon_\lambda . c . l \qquad \text{(Eq. 2.01)}$$

The equation shows that absorbance at a specific wavelength (A_λ) is equal to the product of concentration (c), path-length (l), and an extinction coefficient (ε). Path-length is dependent on the cuvette used, whereas extinction coefficient is dependent on the electronic states present in the molecule for which concentration is being determined.

The linear relationship between a molecule's absorbance and concentration has proven particularly useful for determining concentrations of proteins. An extinction coefficient at 280 nm for a particular protein can be determined using the following equation:

$$\varepsilon_{280} = {\varepsilon_{280}}^{Tyr} . N_{Tyr} + N_{Trp} . {\varepsilon_{280}}^{Trp} + N_{S-S} . {\varepsilon_{280}}^{S-S} \qquad \text{(Eq. 2.02)}$$

In this equation, number of chromophores (N_x) are multiplied by their respective extinction coefficients (ε^x), and summed, to give the extinction coefficient of the entire protein. The chromophores that contribute to absorbance at 280 nm in proteins are tyrosine, tryptophan and disulphide bonds, for which the extinction coefficients are 1280 $M^{-1}cm^{-1}$, 5690 $M^{-1}cm^{-1}$, and 120 $M^{-1}cm^{-1}$ respectively. As both $A\beta_{(1\text{-}40)}$ and $A\beta_{(1\text{-}42)}$ have only a single tyrosine, they each have an extinction coefficient of 1280 $M^{-1}cm^{-1}$.

For accurate estimation of protein concentration, it is necessary also to account for light scatter that may arise from the presence of aggregates in solution. The amount of absorbance at 280 nm that is attributable to light scatter is calculated from the following equation:

$$A_{scatter,280} = 10^{(2.5logA_{320} - 1.5logA_{250})} \quad \text{(Eq. 2.03)}$$

Consequently, a 1 cm path-length cuvette was consistently used, the following equation was used to determine Aβ concentration (M):

$$c = \frac{A_{280} - 10^{(2.5logA_{320} - 1.5logA_{250})}}{1280} \quad \text{(Eq. 2.04)}$$

For optimal accuracy, only absorbance values between 0.1 – 1 were used, as the theoretical optimal absorbance value is 0.864. Additionally, Quartz cuvettes were used, as they do not absorb light in the UV-Vis region. For further reading on absorbance spectroscopy, I suggest chapters 13 and 14 by Alex Drake, in volume 22 of “Methods in Molecular Biology” (Drake, 1994b).

2.2.2 Fluorescence Spectroscopy

Whereas absorption spectroscopy, discussed in the previous section, measures the light absorption that occurs in elevating an electron from the ground state to an excited state, fluorescence spectroscopy measures light that is released when electrons in an excited state return to their ground state. Excited electrons always emit energy when returning to the ground state; however, this energy is generally dissipated as heat, with only a minority of molecules, fluorophores, releasing this energy as light radiation. These fluorophores typically have electrons that are delocalised across conjugated double bonds.

As for absorbance spectroscopy, in fluorescence spectroscopy the sample's electrons are excited from a ground state to one of several possible vibrational excited states, as shown in figure 2.01. In fluorescence spectroscopy, the light source that is used to excite the sample is referred to as the excitation beam. The detector is set perpendicular to the excitation beam, so that one may enrich for photons that are a product of fluorescence (emission), rather than the excitation beam. The emission wavelength is longer than that of excitation and thus of lower energy; this is referred to as the Stokes shift, and occurs because an electron loses energy as heat and through collisions with other molecules, until it reaches the lowest energy vibrational level of the excited state.

Despite fluorescence signal intensity being approximately proportional to fluorophore concentration it is difficult to gain machine-independent values between fluorescence spectrophotometers. This is because the percentage of fluorescence received by the detector is dependent upon the system, which is subject to such variables as detector used, the time interval between excitation and detection, and the excitation by the light source. Consequently, the units used in fluorescence are generally described as

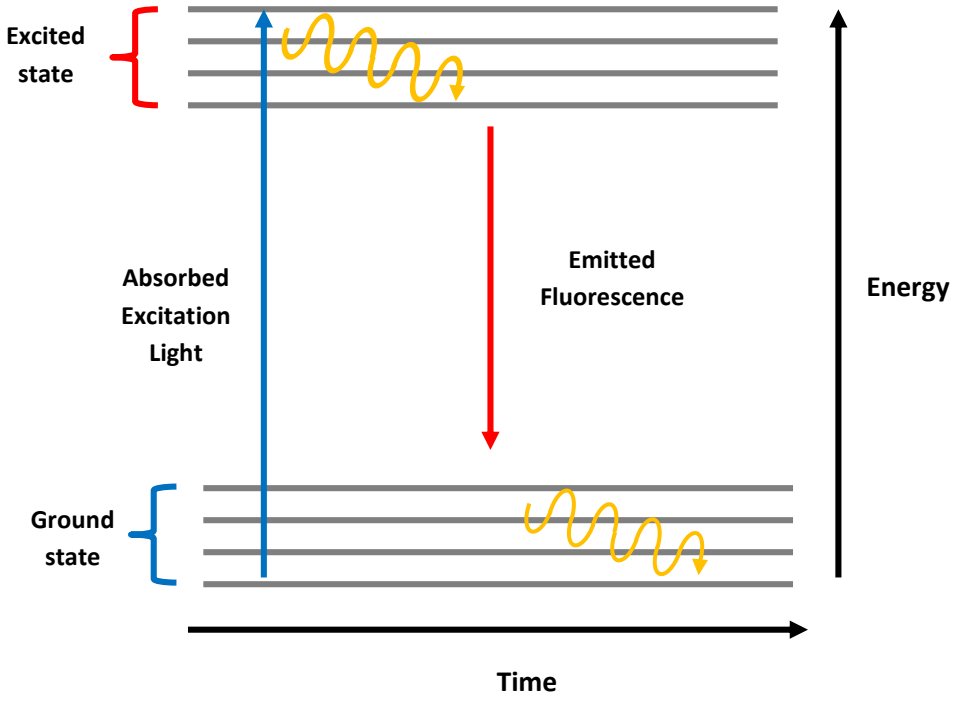

Figure 2.01 Schematic of Fluorescence.

In fluorescence, electrons are first excited from a ground state to an excited state. Energy is lost as heat, as the electron descends from one vibrational level to the next. Light radiation occurs as the electron passes from the excited state to the ground state; however, this light is of a longer wavelength to that absorbed, due to energy lost.

arbitrary fluorescence units, or AFU. Fluorescence techniques may be used with fluorophores that naturally occur within the molecule; such fluorophores are referred to as “intrinsic”, and include tyrosine and tryptophan. Intrinsic fluorophores may be used to follow processes that affect their electronic state, and, incidentally, fluorescence. Alternatively, fluorescence assays may use “extrinsic” fluorophores; those that are added to a sample to provide information.

For a more comprehensive review on the principles of fluorescence spectroscopy, I suggest chapter 15 by Paul G. Varley, in volume 22 of “Methods in Molecular Biology” (Drake, 1994a), and “The Principles of Fluorescence Spectroscopy” (Lakowicz, 2006).

2.2.3 Fluorophores

Extrinsic fluorescence was relied on in the present investigations, with two different fluorescent probes employed to follow two distinct processes. The first of these is Thioflavin T (ThT). ThT was used to follow the kinetics of Aβ fibre growth, as in interacting with the cross-β structure of amyloid fibres the fluorescence of ThT gains intensity and is red-shifted, with the peaks for excitation and emission moving from 385 nm and 445 nm to approximately 450 nm and 482 nm, respectively (LeVine, 1993). This is thought to be mediated via the repeating arrangement of the amyloid fibre side chains, which generates long grooves parallel to the fibre axis, into which ThT molecules may bind (Biancalana & Koide, 2010; Groenning, 2010; Krebs et al, 2005). When not bound to amyloid fibres, the benzylamine and the benzathiole rings of ThT will readily rotate about a central C-C bond. As this rotation is low energy, it may quench the excited state of the adjacent aromatic rings, resulting in a minimal florescence signal. However, upon ThT binding to the grooves of amyloid fibres, movement of the aromatic rings becomes fixed, which reduces quenching, and leads to a marked increase in florescence (Biancalana & Koide, 2010; Stsiapura et al, 2007).

Though there are other hydrophobic patches capable of influencing ThT fluorescence, such as the hydrophobic pockets of human serum albumin (Sen et al, 2009), the general dependence of this change in fluorescence on the presence of amyloid fibres means that ThT is a useful tool for following the kinetics of fibre formation, especially as ThT binds amyloid fibres at a physiologically relevant pH (5 – 9), and that this interaction is not disrupted by the presence of salts (LeVine, 1993).

The second fluorescent dye used was calcein, which has excitation and emission peaks of 495 nm and 515 nm respectively. At concentrations over 70 mM, calcein is self-quenching, a property that makes it valuable as an indicator of lipid vesicle leakage (Allen & Cleland, 1980; Patel et al, 2009). In these investigations, high concentrations of calcein are encapsulated in vesicles, leading to quenching of calcein fluorescence; consequently, calcein leakage may be monitored through increases in fluorescence, as once the calcein leaves the interior of the vesicle it is diluted and dequenched. It has been previously established that the use of calcein to assess lipid vesicle leakage is an effective biomimetic approach for discerning the effects Aβ may have on cell membranes *in vivo* (Pillot et al, 1996; Williams et al, 2010; Williams & Serpell, 2011). It was used here to elucidate how Cu^{2+} ions may modulate the effect of Aβ on lipid-bilayer permeability.

2.2.4 Transmission Electron Microscopy

Traditional optical microscopy relies on visible light to view objects with the naked eye, passing visible light through a series of lenses to grant a magnified view of the sample. However, there is a defined limit to the resolution of any microscopy technique. This limit is referred to as the diffraction limit (*d*), and is a function of the source of illumination's wavelength, the numerical aperture of the objective lens (*NA*), and optical aberrations present in the lens. If optical aberrations are considered to be negligible

compared to the other variables, as is commonly the case, the following equation may be used to determine *d* (Ariel Lipson et al, 2010):

$$d = \frac{\lambda}{2NA} \quad \text{(Eq 2.05)}$$

In turn, *NA* is related to both the refractive index of the medium in which the lens is working (*n*), and the half-angle of the maximal cone of light that may enter/exit the lens (*θ*), through the following equation:

$$NA = n.sin\theta \quad \text{(Eq 2.06)}$$

This makes it apparent that resolving power is inversely proportional to wavelength, and directly proportional to the refractive index of the medium being used. The reason that shorter wavelengths improve resolution is that objects that are smaller than a given wavelength exert little interference on the source of illumination, and are thus less detectable. In turn, higher refractive indexes yield better resolution simply because refraction shortens wavelength. Practically, *NA* cannot exceed 1.4 – 1.6, and, as for visible light λ may be approximated to 550 nm, it is clear the resolution of light microscopy is limited to ~200 nm; much too large to observe protein structures and individual amyloid fibres. To achieve greater resolutions, sources of illumination with shorter wavelengths must be used.

As for all matter, electrons have the properties of both waves and particles. This quality is referred to as wave-particle duality, and can be demonstrated using the famous double-slit experiment, as the wave-like nature of an electron enables it to be influenced by both slits (Falkenberg, 2007). The wave properties of electrons are of particular interest to the field of microscopy, as not only do electrons have a shorter

wavelength than photons, but they may also be accelerated to an appreciable fraction of the speed of light to shorten their wavelength even further. Consequently, using an accelerated beam of electrons as a source of illumination, electron microscopy has much greater resolution than an optical microscope, enabling the visualisation of protein structures, with resolutions as high as 50 pm being reported for transmission electron microscopy (TEM) (Erni et al, 2009).

For TEM, either a tungsten filament or LaB_6 source is connected to a high-voltage "electron gun", under vacuum, which induces electrons to be released through either thermionic or field electron emission (Egerton, 2005). The "lenses" which focus the electrons into an appropriate beam are provided by electromagnet generated electrostatic fields. There are generally three stages of lensing: condenser lenses are responsible for primary beam formation, objective lenses focus the beam as it passes through the sample, and finally projector lenses expand the beam onto an imaging device, be it film or a fluorescent phosphor screen, so as to visualise how the electron beam interacted with the sample.

To increase contrast, an electron opaque material is often used as a negative stain. Such stains should have a sufficiently high electron density to disperse the electron beam, and also readily adsorb to biological material. Negative staining also has the additional benefit of preserving structural details if the electron beam were to damage the biological material. Phosphotungstic acid (PTA) was chosen as its not radioactive, as is uranyl acetate, and its adsorption to biological matter is well established (Quintarelli et al, 1971).

For further reading into the theory of TEM and the other methods of electron microscopy, I recommend Egerton's "Physical Principles of Electron Microscopy" (Egerton, 2005).

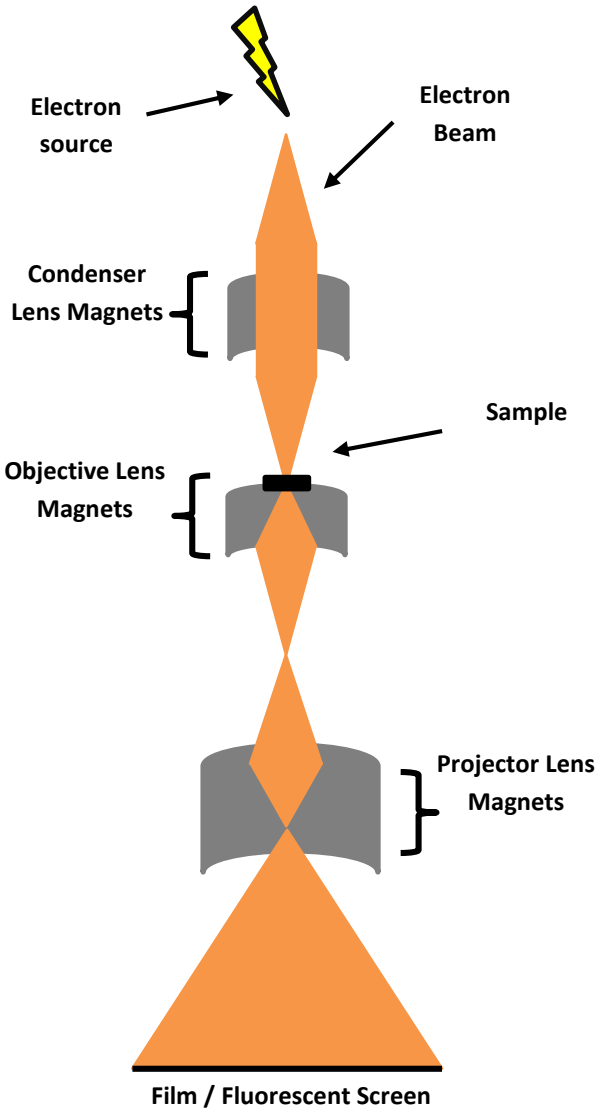

Figure 2.02 Schematic of Transmission Electron Microscopy.

In TEM, electrons are emitted from an electron gun, and then focused through a series of “lenses”, each being an electromagnetically generated magnetic field. The condenser lens is involved in initial beam formation, the objective lens in focusing the beam as it passes through the specimen, and the projector lens enlarges the image for capturing on a detector.

2.2.5 Circular Dichroism

Circular dichroism (CD) utilises the fact that plane polarised light may be split into both left (*L*) and right (*R*) polarised light, of equal intensity, as shown in figure 2.03, with *R* polarised light rotating in a clockwise direction, and *L* polarised light rotating counter-clockwise direction. CD is a form of absorption spectroscopy specifically for chiral chromophores, as chiral molecules, such as most amino acids (and incidentally proteins), differ in their absorbance spectrum for *R* and *L* polarised light, with greater degrees of asymmetry accentuating this discrepancy. Plotting the difference in absorption for *R* and *L* polarised light yields a CD spectrum; such spectra have a broad range of applications, including determining the secondary structure of proteins (Nakanishi et al, 1994).

It is well established that important characteristics of a protein's secondary structure may be investigated using CD, as it readily determines the fraction that is α-helical, in a β-sheet conformation, present in a β-turn, or forming a random coil structure (Greenfield, 2006; Whitmore & Wallace, 2008). To do so, the Far-UV region is used, where absorbance is dominated by transition of the polypeptide backbone's amide groups' *n* and π electrons to the π^* excited state. These transitions are influenced by the conformation of the polypeptide backbone; thus, CD spectra produced are indicative of secondary structure present, with each secondary structure being associated with a particular spectrum, as shown in figure 2.04.

CD gives much less information than X-ray crystallography and NMR. Unlike these methods, which both may provide atomic resolution data, CD cannot say which amino acids are involved with particular structural motifs, or how the secondary structures are organised. However, CD is a much quicker technique which requires much less protein and data processing. It can also be carried out at a range of conditions making it

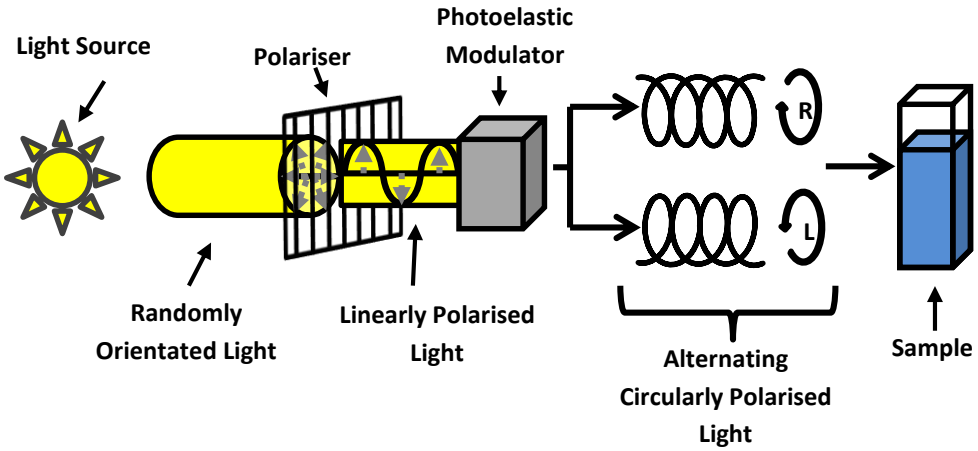

Figure 2.03 Schematic for the Generation of Circularly Polarised Light.

The basic components used to generate circularly polarised light in a CD spectrometer. The circularly polarised light is then alternately passed through a sample, and the difference in absorbance is detected using a photomultiplier.

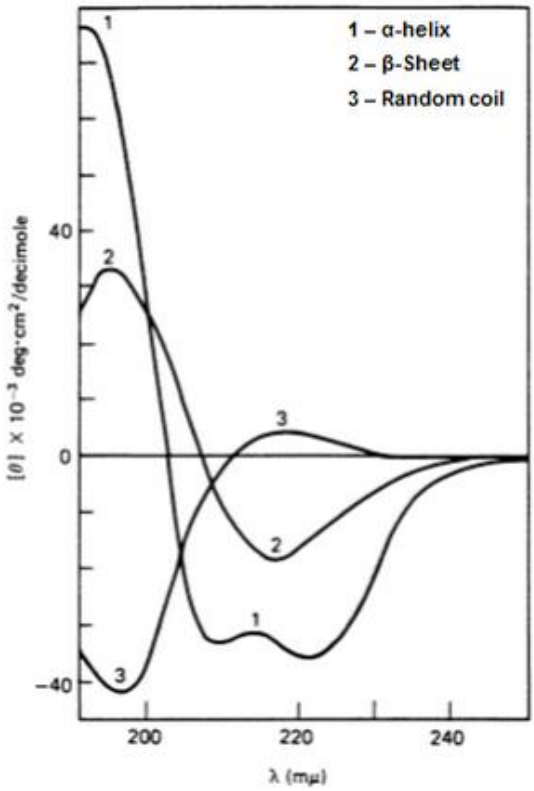

Figure 2.04 Representative CD Spectra for Protein Secondary Structures.

This figure shows ellipticity (differential absorbance of circularly polarised light) for different secondary structures at a range of wavelengths. Reprinted from (Greenfield & Fasman, 1969). Copyright (1969) American Chemical Society.

invaluable for assessing how protein structure changes as a function of temperature, pH, salinity, or with the addition of denaturants, such as guanidinium chloride. For a review on CD, refer to chapter 16 of “Methods in Molecular Biology”, volume 22 (Drake, 1994c).

2.3 GENERAL EXPERIMENTAL METHODS

2.3.1 Buffer and pH Measurements

UHQ water ($10^{-18}\ \Omega^{-1}\ cm^{-1}$ resistivity) was used for all solutions. HEPEs was used, for its low affinity to metal ions, and its physiological effective pH range (6.8 – 8.2) (Dawson, 1986). The pH was adjusted using small aliquots of 10-100 mM NaOH or HCl. It was found that with HEPEs buffer a stable pH was maintained throughout the course of the experiments.

2.3.2 Aβ Solubilisation and Concentration Determination

Background

For these investigations, it is important that in solubilising Aβ a homogenous population of monomers is ensured. The propensity for Aβ to self-associate via hydrophobic interactions makes this difficult, particularly when the pH approaches the isoelectric point of Aβ, 5.3. Unfortunately, Aβ produced via F-moc (*N*-(9-fluorenyl) methoxycarbonyl) chemistry removes the *tert*-butyloxycarbonyl protecting group with trifluoroacetate (Englund et al, 2004). The difficulty this presents is that the trifluoracetate remains bound to the peptide, meaning that when Aβ is solubilised it will generate an acidic environment. Consequently, when Aβ is later added to a buffer of physiological pH (7.4), the solution would pass through the isolelectric point,

temporarily maximising Aβ aggregation and precipitation. This in turn has been shown to yield Aβ solutions which present highly variable kinetic behaviours and fibril morphologies (Wood et al, 1996). One method to avoid this is to use NaOH to create basic conditions (~10.5) for solubilising Aβ, effectively preventing the problems that would occur if Aβ were to pass through its isoelectric point (Fezoui et al, 2000; Teplow et al, 2006).

Using NaOH has been found to be as effective at reducing aggregates and variability as both hexaflouroisopropanol (HFIP), an organic cosolvent, and dimethylsulfoxide (DMSO), a chaotropic agent (Hortschansky et al, 2005; Lashuel et al, 2003). Both HFIP and DMSO are also common approaches to Aβ solubilisation found in the literature (Chen & Hung, 2001; Stine et al, 2003; Zagorski & Barrow, 1992); however, the presence of these solvents may influence fibrillogenesis, exacerbating the variability common to fibre growth studies (Faller et al, 2013; Shen & Murphy, 1995), and compromising the physiological relevance of *in vitro* studies. Additionally, they may disrupt the lipid membranes that used. For these reasons, the NaOH method was chosen as most appropriate to solubilise Aβ.

Protocol

$A\beta_{(1-40)}$ and $A\beta_{(1-42)}$ were solubilised at a concentration of 0.7 mg/ml in water at pH 10.5, and then left at 5 ^{o}C over 48 – 72 hours. Samples were then centrifuged for 10 minutes at 16,000 x g at 5 ^{o}C, to remove any precipitates that may seed aggregation. It is clear that solubilised preparations of Aβ were essentially seed-free as at pH 7.4 solubilised Aβ preparations typically have a lag-phase of at least 70 hours when agitated, and several weeks in the absence of shaking. Final Aβ concentration was determined using the Tyrosine absorbance at 280 nm, ε_{280} = 1280 M^{-1} cm^{-1}, and correcting for any light scatter with absorbance values at 320 nm and 350 nm. A 1 cm path-length cuvette and

UV-spectrometer was used to determine these values, and the Beer-Lambert law (Eq 2.03) used to calculate the concentration.

2.3.3 Fibril Growth Assay

The kinetics of amyloid formation were monitored using binding of ThT to amyloid fibres, which induces ThT to fluoresce at 482 nm; this signal is typically directly proportional to the amount of amyloid fibrils present. BMG-Galaxy and BMG-Omega FLUOstar fluorescence 96-well plate readers were used for the measuring of ThT fluorescence. Fluorescence readings were typically taken every 30 mins, following 30 seconds of orbital agitation. Fluorescence excitation and emission detection were at 440 nm and 490 nm respectively.

Fibre growth kinetics are sensitive to a number of factors, including pH, concentration, agitation, ionic strength and temperature; consequently, measures were taken to reduce variance in these parameters. All fibre growth experiments were incubated at 30 ^{0}C, in 30 mM HEPEs buffer, typically in 160 mM NaCl. The pH, a critical factor in rate of fibre growth, was adjusted to pH 7.4, and variation between samples was measured to be 0.05 pH units or less. Two molar equivalents of ThT was added to samples at the start of the experiment.

2.3.4 Curve Fitting

Growth Curve Analysis

Conversion of essentially monomeric Aβ to Aβ fibres follows a characteristic growth curve, consisting of first a lag-phase (nucleation) and then a growth phase (elongation). A growth curve can be fitted to the data, to obtain a number of empirical parameters,

using the following equation (Uversky et al, 2001):

$$Y = (\upsilon_i + m_i x) + \frac{\upsilon_{f+m_f x}}{1+exp^{-(x-x_{0/\tau})}} \quad \text{(Eq 2.07)}$$

Y represents fluorescent intensity, and x represents time. Initial fluorescence intensity is represented by υ_I, υ_f represents the final fluorescence intensity. A number of kinetic parameters may be extracted with this equation; for instance, x_0 is the time at which half maximal fluorescence is reached (t_{50}), the apparent fibre growth rate (k_{app}) is obtained by $1/\tau$ and the lag-time (t_{lag}) may be determined by x_0-2τ. This equation allows for a slope in the initial and final parts of the growth curve, ($\upsilon_i + m_i x$), ($\upsilon_f + m_f x$), rather than forcing these to be horizontal.

Unfolding Curve Analysis

GdnCl denaturation curves were fitted using a modified Hill equation, shown below:

$$y = y_{min} + \frac{y_{diff}[D]^n}{[D^{50\%}]^n + [D]^n} \quad \text{(Eq 2.08)}$$

In this equation, Y represents signal intensity, $Y_{diff} = Y_{max} - Y_{min}$, D is the concentration of GdnCl, $D^{50\%}$ is the concentration of GdnCl at which half of the protein is unfolded, and n represents the Hill coefficient (Crowhurst et al, 2002).

2.3.5 Large Unilamellar Vesicle Preparation

Large unilamellar vesicles (LUVs) were created as has been previously described (Williams et al, 2010). A lipid mixture of phophatidylcholine (PC), cholesterol, and

monosialotetrahexosylganglioside (GM1), at a ratio of 68:30:2 by weight in a glass phial, solubilised to 5 mg/ml in a 2:1 mixture of chloroform and methanol. The mixture was then left overnight, to enable solvent to evaporate, leaving behind a lipid film. Lipid films were rehydrated to a concentration of 10 mg/ml, with 200 mM calcein, aqueous buffer at pH 7.4 with 50 mM HEPES; this mixture was left for 2 hours, with vortexing every 15 minutes. Next, the lipid mixture was passed through an extruder once, with a 100 nm polycarbonate filter, so as to generate vesicles with a uniform range of diameters. To remove non-encapsulated calcein from the LUVs the samples were centrifuged for 4 mins (at 16,000 g), the supernatant discarded, and resuspended in aqueous buffer (30 mM HEPES, 160 mM NaCl, pH 7.4). This centrifugation was repeated four times. After the final centrifugation, LUVs were resuspended to 5 mg/ml, in buffer.

2.3.6 Vesicle Dye Release Assay

The effect of Aβ samples on membrane integrity was assessed through release of calcein from large unilamellar vesicles (LUVs) using a 96-well plate readers, to facilitate statisitical quantification of dye release. Calcein is largely self-quenching when encapsulated within the vesicles, giving a strong fluorescent signal upon release. Readings were taken every 30 minutes following 30 seconds of mild agitation, and temperature maintained at 30 ^{o}C. Final readings were taken after 12 days. Samples were excited at 485 nm, and fluorescent emission was recorded at 520 nm, with 10 μM EDTA being added before final fluorescence readings were taken, to tightly chelate any Cu^{2+} ions, which have been shown to be capable of quenching calcein fluorescence. LUVs were diluted to 1 mg/ml for this experiment, while, concentration of $A\beta_{(1\text{-}42)}$ was 10 μM, and concentration of Cu^{2+} was 4 μM. Each fluorescence measurement is presented as a percentage of maximum possible calcein release, determined by the addition of the detergent triton, to a final triton concentration of 10 ml/l.

2.3.7 Circular Dichroism

CD spectra were recorded at 25° C on a circular dichroism spectrometer instrument between 180 and 260 nm, with sampling points every 0.5 nm, using a 1 cm or 0.1 cm path-length cuvette. Three scans were recorded and averaged, and zeroed at 260 nm. An averaged baseline spectrum subtracted from each spectrum. This was followed by a 2 nm window smoothing.

2.3.8 Visualising Aβ Aggregate Species with Transmission Electron Microscopy

Aliquots of Aβ samples from the fibre growth assays, or aliquots of LUV samples, were added to flow-discharged carbon-coated 300-mesh using the droplet method, with UHQ H_2O washes before and after addition of stain. Phosophotungstic acid (2 % w/v), adjusted to pH 7.4, was used to negatively stain the sample. Typically selected images shown are representative of ~ 30 images that were taken over 30 – 60 minutes, across at least 10 fields. Images were recorded using a JEOL JEM-1230 electron microscope operated at 80 kV.

The TEM images of LUVs and Aβ aggregates were not discernibly different to images recorded with cryoelectro-tomography (Milanesi et al, 2012), suggesting that the stain did not disrupt their respective morphologies. This was confirmed using the calcein dye release assay which showed no difference in dye release in the presence or absence phosphotungstic acid.

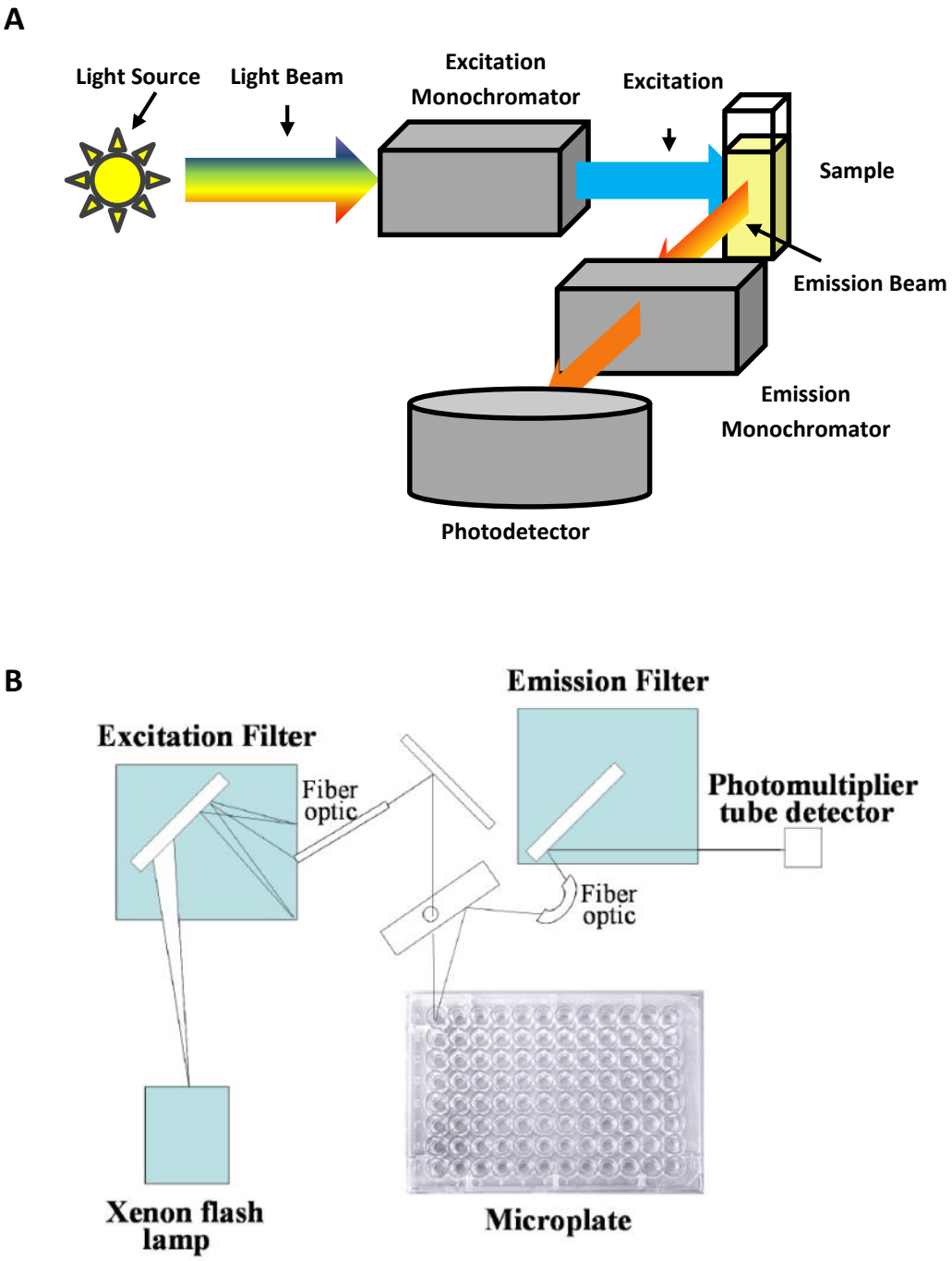

Figure 2.05 Optical Path in Fluorescence Spectroscopy.

Single-cell fluorescence (A) and multi-well fluorescence (B) are largely the same, other than the fact that the former uses monochromators rather than filters, and the latter detects the emission above the plate, rather than at 90°, as in single-cell fluorescence (adapted from (Lakowicz, 2006)).

2.3.8 Single Cell Fluorescence

A single cell fluorescent spectrophotometer was used to monitor ThT fluorescent spectrum. Samples were excited at 440 nm, and emission readings taken from 420 nm to 600 nm. The spectrometer used was temperature controlled, and maintained the temperature at 30 ^{0}C unless stated otherwise. A 1 cm path-length cuvette was used, and for each sample three readings were taken, which were then averaged. From this a baseline was subtracted; the baseline was an aqueous solution of 30 mM HEPEs, 20 μM ThT, and 160 μM NaCl. For these experiments, preformed $A\beta_{(1\text{-}40)}$ fibre samples were used, which were prepared as described in 2.3.3.

2.3.9 Statistical Analyses

When directly comparing two samples, statistical significance ($p < 0.05$) was determined using a two-tailed student's *t*-test, for which the null hypothesis is rejected when difference between means is several fold greater than the standard error (depending on degrees of freedom) (Abramowitz, 1965; Student, 1908). However, when comparing whether there were differences in the means of more than two samples, ANOVA was used. ANOVA was developed by R. A. Fischer (Fisher, 1921), and essentially generalises the *t*-test to a group, without the associated increase in false positives that would occur if one were to use multiple *t*-tests. As ANOVA just states whether there is a significant difference within the total set, it is necessary to carry out a follow up test to determine which specific samples are different from each other, typically a post-hoc-test. Fisher's Least Significant Difference (LSD) was used, which though similar to carrying out a series of *t*-tests, has greater power, as it computes the collated standard deviation from all groups, rather than just the two being compared at that moment. Additionally, because an ANOVA test is required to be significant to carry out Fisher's LSD, false positives are also reduced.

CHAPTER 3: Cu^{2+} Accentuates Distinct Misfolding of $Aβ_{(1-40)}$ and $Aβ_{(1-42)}$ Peptides, and Potentiates Membrane Disruption

3.1 ABSTRACT

Metal ion homeostasis is disrupted in the brains of sufferers of Alzheimer's disease and causes heightened AD phenotype in animal models. Here it is illustrated that substoichiometric Cu^{2+} effects the misfolding pathway of $A\beta_{(1-40)}$, and the more toxic $A\beta_{(1-42)}$, in markedly different ways. Cu^{2+} accelerates $A\beta_{(1-40)}$ fibre formation, in contrast, for $A\beta_{(1-42)}$ substoichiometric levels of Cu^{2+} almost exclusively promote the formation of oligomeric and protofibrillar assemblies. Indeed, mature $A\beta_{(1-42)}$ fibres are disassembled into oligomers when Cu^{2+} is added. These Cu^{2+} stabilised oligomers of $A\beta_{(1-42)}$ interact with the lipid-bilayer, disrupting the membrane and increasing permeability. The investigation of $A\beta_{(1-40)}$/$A\beta_{(1-42)}$ mixtures with Cu^{2+} revealed that $A\beta_{(1-40)}$ neither contributed nor perturbed formation of $A\beta_{(1-42)}$ oligomers, though Cu^{2+}-$A\beta_{(1-42)}$ will frustrate Cu^{2+}-$A\beta_{(1-40)}$ fibre growth. Small amounts of Cu^{2+} accentuates differences in the propensity of $A\beta_{(1-40)}$ and $A\beta_{(1-42)}$ to form synaptotoxic oligomers, providing an explanation for the connection between disrupted Cu^{2+} homeostasis and elevated $A\beta_{(1-42)}$ neurotoxicity in AD.

3.2 INTRODUCTION

It is generally accepted that Aβ aggregation mediates AD neurotoxicity; specifically, there is considerable evidence to suggest that small diffusible oligomers of $A\beta_{(1-42)}$, rather than fibres are the dominant toxic form (Lambert et al, 1998; Lesné et al, 2006; Walsh et al, 2002; Yankner & Lu, 2009). A major unanswered question remains the precise mechanism by which oligomeric Aβ exerts its toxic effect. Although controversial, one popular hypothesis involves the disruption of cell membranes at the synapse. Ultimately, Aβ might lead to thinning, puncture the lipid-bilayer, or form ion channels or pores (Demuro et al, 2005; McLaurin & Chakrabartty, 1996; Milanesi et al, 2012; Quist et al, 2005; Williams & Serpell, 2011), all of which could cause synaptic dysfunction, membrane leakage and, finally, loss of cellular ion homeostasis.

AD is a multifactorial disease; however, the central question of what induces Aβ to enter into an amyloidogenic cascade remains unclear (Ballard et al, 2011; Hardy & Selkoe, 2002). A possible determinant of Aβ self-association *in vivo* are metal ions (Viles, 2012). Indeed metal ion homeostasis is disrupted in AD patients, with the levels of Cu^{2+} in the neuropil increased 4-fold, where Cu^{2+} ions are found concentrated in plaques, directly bound to Aβ (Dong et al, 2003; Lovell et al, 1998; Miller et al, 2006). Disrupted Cu^{2+} homeostasis has been demonstrated to potentiate disease pathology in drosophila (Sanokawa-Akakura et al, 2010; Singh et al, 2013) and rabbit models (Sparks & Schreurs, 2003) of AD. Likewise, clioquinol, a Cu^{2+}/Zn^{2+} chelator, has been found to reduce Aβ deposition while improving the general health of mouse models (Cherny et al, 2001), although, unfortunately, these beneficial effects, have not been replicated in human trials (Prana, 2014). In humans, a recently identified mutation (D7H) for early-onset Alzheimer's disease has been found to grant Aβ a greater affinity for Cu^{2+}/Zn^{2+}, and exaggerate the effects of Zn^{2+}/Cu^{2+} on Aβ aggregation (Chen et al, 2012). AD pathology is also influenced by prion protein interactions (Laurén et al, 2009; Younan et al, 2013), which have recently been linked to Aβ binding Cu^{2+} (You et al, 2012), further emphasising a potential significance of Cu^{2+} in AD.

A significant role for Cu^{2+} ions in AD is supported by the observation that Aβ has a picomolar affinity for Cu^{2+} (Sarell et al, 2009). As Aβ levels are estimated to be greater than 0.5 nM at the synapse (Seubert et al, 1992), Aβ would be expected to be able to compete with other metal chelators for the binding of Cu^{2+} ions, especially during depolarisation, when Cu^{2+} is reported to reach concentrations of 15 – 250 μM within the synaptic cleft (Hartter & Barnea, 1988; Kardos et al, 1989).

Cu^{2+} has been shown to bind with a full (1:1) stoichiometric complement with a similar affinity to both monomeric Aβ and mature Aβ fibres (Sarell et al, 2009). Potentially, metal ion coordination might influence the Aβ misfolding pathway and synaptic toxicity

in a number of ways, including altering the structure of oligomer and fibre assemblies, and the kinetics of formation, as well as generation of reactive oxygen species via a redox active Cu^{2+} or Fe^{3+} (Viles, 2012). It has been known for more than a decade that binding of Cu^{2+} and Zn^{2+} is able to promote aggregation of Aβ (Atwood et al, 1998; Bush et al, 1994). However, these initial studies did not make the distinction between amorphous aggregates and neurotoxic species, and subsequent studies using the amyloid fibre specific fluorophore ThT suggested that Cu^{2+} only promotes formation of amorphous aggregates, and inhibits both fibre formation and cytotoxicity (Raman et al, 2005; Yoshiike et al, 2001). These observations seemingly conflict with animal models which state the significance of Cu^{2+} in AD pathology (Cherny et al, 2001; Sanokawa-Akakura et al, 2010; Singh et al, 2013; Sparks & Schreurs, 2003). An explanation for this conflict has been proposed, as a study using both ThT and TEM has shown that at more physiologically relevant substoichiometric levels, Cu^{2+} accelerates $Aβ_{(1-40)}$ fibre growth, whereas suprastoichiometric levels promote amorphous aggregation and inhibit fibre growth (Sarell et al, 2010). It was observed that different stoichiometric levels of Cu^{2+} also affect the ability of $Aβ_{(1-42)}$ to form ThT binding aggregates (Smith et al, 2007). However, the relationship between Cu^{2+} ions and Aβ misfolding is still controversial, with reports of Cu^{2+} preventing $Aβ_{(1-42)}$ fibre formation at suprastoichiometric (Smith et al, 2007), but also, more recently, at substoichiometric levels (Sharma et al, 2013; Tougu et al, 2009). There are reports of Cu^{2+} promoting amorphous aggregates rather than $Aβ_{(1-42)}$ fibres (House et al, 2009; Jiang et al, 2012; Mold et al, 2013; Pedersen et al, 2011); however, others have reported elevated $Aβ_{(1-42)}$ cytotoxicity with substoiciometric Cu^{2+} (Sharma et al, 2013; Smith et al, 2007).

The aim of this investigation was to obtain a more complete picture of Cu^{2+}-$Aβ_{(1-40)}$/$Aβ_{(1-42)}$ interactions. This study demonstrates that many seemingly conflicting observations surrounding Aβ aggregation may be attributed to Cu^{2+} influencing $Aβ_{(1-40)}$ and $Aβ_{(1-42)}$ very differently, as well as the significant distinction between substoichiometric and suprastoichiometric Cu^{2+} exposure. It is shown that although Cu^{2+} accelerates $Aβ_{(1-40)}$

fibre formation, Cu^{2+} stabilises $A\beta_{(1-42)}$ oligomers and protofibrils to such an extent that fibres are largely absent. These two distinct Cu^{2+} promoted pathways are also present for mixtures of $A\beta_{(1-40)}$ plus $A\beta_{(1-42)}$ found *in vivo.* The TEM images, and a dye release assay with large unilamellar vesicles (LUVs) show marked disruption of membrane structure and permeability, compared to Cu^{2+} free fibres of $A\beta_{(1-42)}$, providing an explanation for increased Alzheimer's pathology in the presence of Cu^{2+} ions (Cherny et al, 2001; Sanokawa-Akakura et al, 2010; Singh et al, 2013; Sparks & Schreurs, 2003). It has been suggested that distinct pathways of fibre assembly occur for $A\beta_{(1-40)}$ and $A\beta_{(1-42)}$, and these may account for differences in their cytotoxicity (Bitan et al, 2003). It is demonstrated here that small substochiometric amounts of Cu^{2+} heighten the differences in assembly between $A\beta_{(1-40)}$ and $A\beta_{(1-42)}$, as for only $A\beta_{(1-42)}$, Cu^{2+} promotes almost exclusive generation of protofibrils and oligomers.

3.3 RESULTS

3.3.1 Copper and $A\beta_{(1-42)}$ Oligomer Assembly

The well-established amyloid-binding ThT fluorescence assay was used, as well as TEM, to examine the fibre formation kinetics and assembly of $A\beta_{(1-42)}$ over a range of Cu^{2+} concentrations. Aβ fibre growth progresses through a nucleation-dependent pathway; formation of an oligomeric nucleus precedes elongation into mature fibrils (Jarrett & Lansbury, 1993; Roychaudhuri et al, 2009). This classic pattern of fibre formation can be seen for $A\beta_{(1-42)}$ without Cu^{2+} present, with the lag time for nucleation being 58 ± 3 hours, and half maximal fluorescence being reached at 70 ± 3 hours (Fig. 3.01). Cu^{2+} was found to inhibit $A\beta_{(1-42)}$ fibre formation in a concentration dependent manner. With as little as 0.1 equivalents of Cu^{2+}, the lag time of fibre formation was increased to 89 ± 2 hours, and t_{50} was increased to 98 ± 2 hours (a two tailed unpaired *t* test confirms that these increases are significant with > 99 % confidence). For 0.4

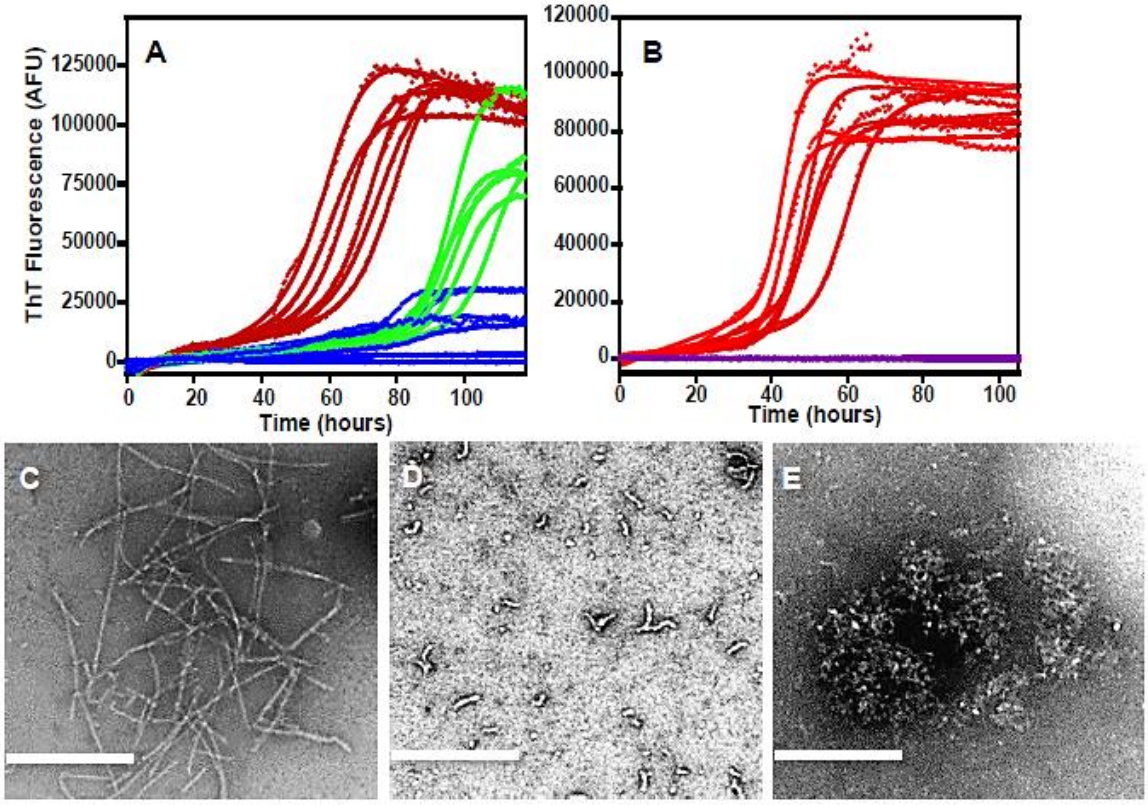

Figure 3.01 $A\beta_{(1-42)}$ Fibre Growth with Cu^{2+}.

(A) $A\beta_{(1-42)}$ fibre growth, monitored by Thioflavin T fluorescence, with no Cu^{2+} (red), 0.1 equivalence of Cu^{2+} (green) and 0.4 equivalence of Cu^{2+} (blue). (B) $A\beta_{42}$ fibre growth with no Cu^{2+}(red) and 10 equivalence of Cu^{2+} (purple). Fibre growth was carried out at pH 7.4, with 10 μM $A\beta_{(1-42)}$, 30 mM HEPES, 10 mM NaCl and agitation, at 30 ^{o}C. There where at least six individual wells for each condition. (C – D) Samples taken directly after 120 hrs of incubation for TEM, negatively stained with phosphotungsic acid. The images show that fibres formed without Cu^{2+} (C), oligomers formed with 0.4 equivalence of Cu^{2+} (D), and amorphous aggregates formed with 10 equivalence of Cu^{2+} (E). Scale bar is 200 nm.

mole equivalents of Cu^{2+}, fibre growth was largely prevented, and for 10 equivalents of Cu^{2+}, fibre growth was completely abolished. This experiment has been repeated a number of times, at a range of $A\beta_{(1-42)}$ concentrations (5 – 20 μM) and NaCl concentrations (5 – 160 mM), with similar results. Thus, preliminary data, showing ThT florescence in the presence of substoichiometric Cu^{2+} and $A\beta_{(1-42)}$, previously reported as supplemental information (Sarell et al, 2010), is not supported by this study.

The species of $A\beta_{(1-42)}$ aggregate formed was characterised with TEM (Fig. 3.01). TEM images showed that for $A\beta_{(1-42)}$, in the absence of Cu^{2+}, amyloid fibres dominate the TEM grids after 120 hours incubation, with a typical straight unbranched morphology of 10 – 20 nm thickness (depending on the number of filaments stacked together), and typically many microns in length. However, at 0.4 equivalents of Cu^{2+}, very few fibres were observed, with $A\beta_{(1-42)}$ chiefly existing as a variety of oligomeric species, ranging from 10 – 30 nm circular oligomers to “curly” protofibrillar oligomers of 10 – 20 nm thickness, and 30 – 100 nm length.

Different species of aggregate is observed for 10 equivalents of Cu^{2+}, with $A\beta_{(1-42)}$ primarily forming amorphous aggregates, of 100 – 1000 nm, dense staining, and no repeating structure. Thus, the results show that substoichiometric levels of Cu^{2+} promote $A\beta_{(1-42)}$ oligomer formation, whereas suprastochiometric levels favour formation of amorphous aggregates. These observations were made consistently, over numerous Cu-$A\beta_{(1-42)}$ preparations and TEM grids.

It is also notable that the influence of Cu^{2+} on $A\beta_{(1-42)}$ oligomer formation does not occur in a stoichiometric manner. Less than half a mole equivalents of Cu^{2+} relative to $A\beta_{(1-42)}$ is able to almost completely inhibit fibre formation, and even as little as 0.1 mole of Cu^{2+} causes substantial delays in fibre formation, extending the amount of time that $A\beta_{(1-42)}$ molecules exist as oligomers. Indeed, TEM indicates that even at just 0.1 molar equivalent of Cu^{2+} the majority of assemblies observed are protofibrils rather than

fibres. Thus, a single Cu^{2+} ion can influence the assembly of a number of $A\beta_{(1-42)}$ molecules, promoting and stabilising oligomer and protofibril populations over fibres.

The next question, was whether Cu^{2+} was able to influence preformed $A\beta_{(1-42)}$ fibres. For this, 0.4 molar equivalents of Cu^{2+} was added to $A\beta_{(1-42)}$ that had been incubated for 100 hours at 30 ^{o}C, and for which ThT fluorescence reported completed growth of amyloid fibrils. It was found that once Cu^{2+} was added, ThT signal rapidly dropped (within 60 mins) by ~ 40 % as shown in Fig. 3.02. TEM showed that when substoichiometric Cu^{2+} was added to fully formed $A\beta_{(1-42)}$ fibres, the predominant species of aggregate formed

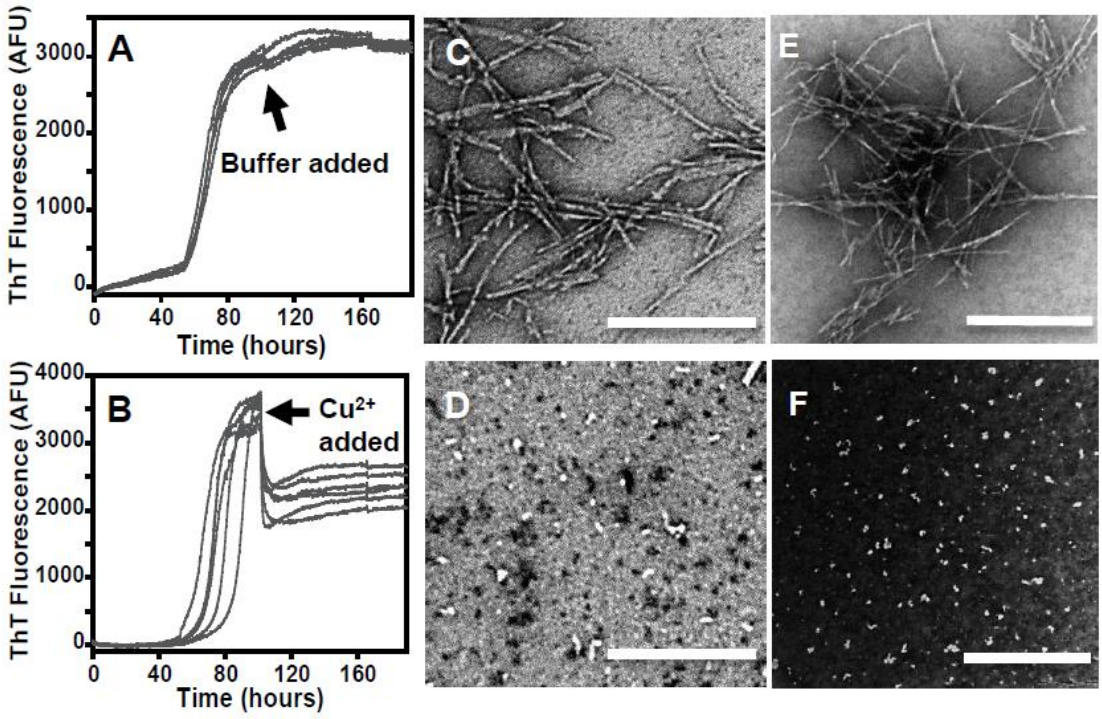

Figure 3.02 Addition of EDTA to Cu^{2+} Generated $A\beta_{(1-42)}$ Oligomers.

(A) $A\beta_{(1-42)}$ fibre growth (monitored by Thioflavin T fluorescence) with no Cu^{2+}. (B) $A\beta_{(1-42)}$ fibre growth with 0.4 mole equivalence of Cu^{2+} added after 100 hours. Fibre growth was carried out at pH 7.4, with 10 μM $A\beta_{(1-42)}$, 30 mM HEPES, 160 mM NaCl and agitation, at 30 ^{o}C. There were five individual wells for each condition. (C – F) samples observed by TEM, negatively stained with phosphotungsic acid. These images show 10 μM $A\beta_{(1-42)}$ incubated for 385 hours, without Cu^{2+} (C,E), and then for a further 15 hours after 3.2 μM Cu^{2+} was added (D, F), where fibres are observed to have disassembled into oligomers. Scale bar 400 nm (E, F) and scale bar 200 nm (C, D).

very much resembled the oligomers generated when monomeric $A\beta_{(1-42)}$ is incubated with Cu^{2+}; protofibril-like oligomers of 10 – 20 nm thickness, 30 – 100 nm length. The same observation was made when substoichiometric levels of Cu^{2+} was added to more "mature" $A\beta_{(1-42)}$ fibres; those that had been incubated a further 48 hours. In addition, different substoichiometric levels of Cu^{2+} were added; 0.4, 0.6, 0.8 mole equivalents. All ratios showed a similar reduction in ThT signal, of ~ 40 %. It is clear Cu^{2+} not only delays $A\beta_{(1-42)}$ from forming fibres, but maintains $A\beta_{(1-42)}$ in a protifibrillar form, and even reverts fibres back to oligomers.

To assess whether the protofibril-like oligomers formed by $A\beta_{(1-42)}$ in the presence of Cu^{2+} would persist following Cu^{2+} removal, they were exposed to EDTA, a very tight Cu^{2+} chelator. The results illustrate that upon removal of Cu^{2+} with EDTA, $A\beta_{(1-42)}$ resumes typical amyloidogenecity, rapidly forming fibres with no lag time, as determined by ThT fluorescence, shown in Fig. 3.03. After the addition of EDTA, TEM images indicate the formation of the typical long unbranched fibres.

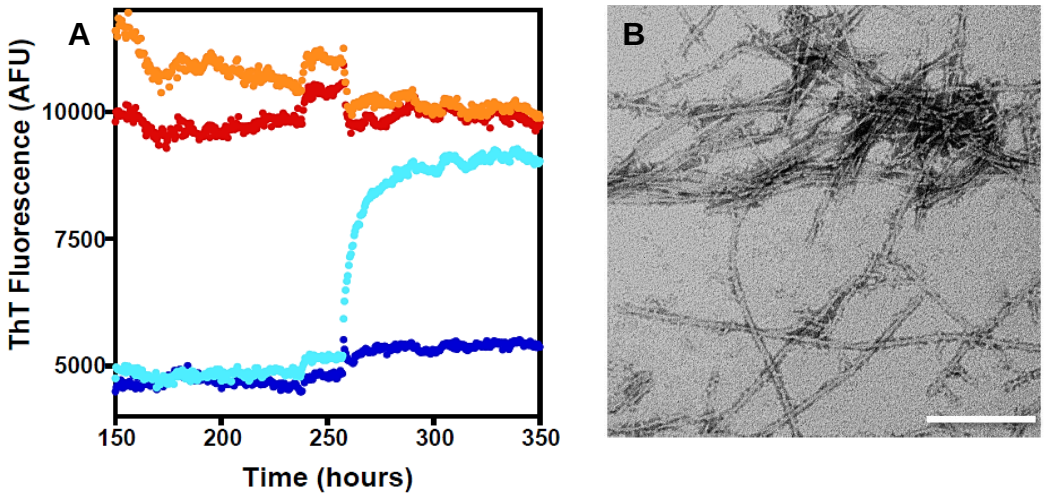

Figure 3.03 Addition of EDTA to Cu^{2+} Generated $A\beta_{(1-42)}$ Oligomers.

(A) This figure shows averaged $A\beta_{(1-42)}$ Thioflavin T fluorescence, for mature fibres grown with no Cu^{2+} (red and orange), and with 0.3 mole equivalents of Cu^{2+} (blue). At 250 hours, 10 μM EDTA was added to half the samples (orange and light blue). Once Cu^{2+} was stripped from $A\beta_{(1-42)}$, fibres were able to form. Fibre growth was carried out at pH 7.4, with 10 μM $A\beta_{(1-42)}$, 30 mM HEPES, 160 mM NaCl and agitation, at 30 ^{o}C. Traces shown are an average of four individual wells for each condition. (B) TEM image of $A\beta_{(1-42)}$ that has been incubated with 0.3 mole equivalents of Cu^{2+} for 250 hours, and then for 100 hours with EDTA. Scale bar is 200 nm.

3.3.2 Copper and $A\beta_{(1-40)}$ Fibre Assembly

The behaviour of $A\beta_{(1-40)}$ in the presence of substoichiometric amounts of Cu^{2+} significantly differs from $A\beta_{(1-42)}$. Rather than completely inhibiting fibre formation, 0.4 equivalents of Cu^{2+} markedly accelerates $A\beta_{(1-40)}$ fibre formation (Fig. 3.04). In the absence of Cu^{2+}, $A\beta_{(1-40)}$ fibre growth had a lag time of 84 ± 7 hours, and a t_{50} of 91 ± 7 hours, and addition of just 0.4 equivalents of Cu^{2+} halved both lag time and t_{50}, to 40 ± 1 hours and 45 ± 1 hours respectively. A two tailed unpaired *t*-test confirms that these increases are significant with > 95 % confidence. In contrast, 10 molar equivalents of Cu^{2+} ions prevents $A\beta_{(1-40)}$ prevented from forming fibres. This confirms the previous observation, that for $A\beta_{(1-40)}$, substoichiometric levels of Cu^{2+} accelerate fibre formation, while suprastoichiometric levels of Cu^{2+} prevent fibre formation (Sarell et al, 2010).

The striking differences in behaviour of $A\beta_{(1-40)}$ and $A\beta_{(1-42)}$ in the presence of Cu^{2+} is also apparent from the TEM images, see Fig. 3.04. It was observed that for $A\beta_{(1-40)}$ without Cu^{2+} and for $A\beta_{(1-40)}$ grown with 0.4 equivalents of Cu^{2+}, fibres predominate; there was no discernible difference in morphology for these two samples, both being 10 – 20 nm thick, typically > 1000 nm long, and with twists at regular intervals, with periodicity ranging from 30 – 300 nm. With 10 equivalents of Cu^{2+} it was found that amorphous aggregate formation is favoured, with no regular structure, and a greatly variable size, and dense staining. Many images supporting this behaviour were observed.

3.3.3 Effect of Cu^{2+} on fibre growth for mixtures of $A\beta_{(1-42)}$ and $A\beta_{(1-40)}$

Following the observation that Cu^{2+} influences the misfolding pathway of the two alloforms, $A\beta_{(1-42)}$ and $A\beta_{(1-40)}$, in strikingly differing ways, the question arose, as to how substoichiometric Cu^{2+} would influence mixtures of the two peptides, as is the case *in vivo*. When the total concentration of peptide was kept at 10 μM ($A\beta_{(1-42)}$ + $A\beta_{(1-40)}$),

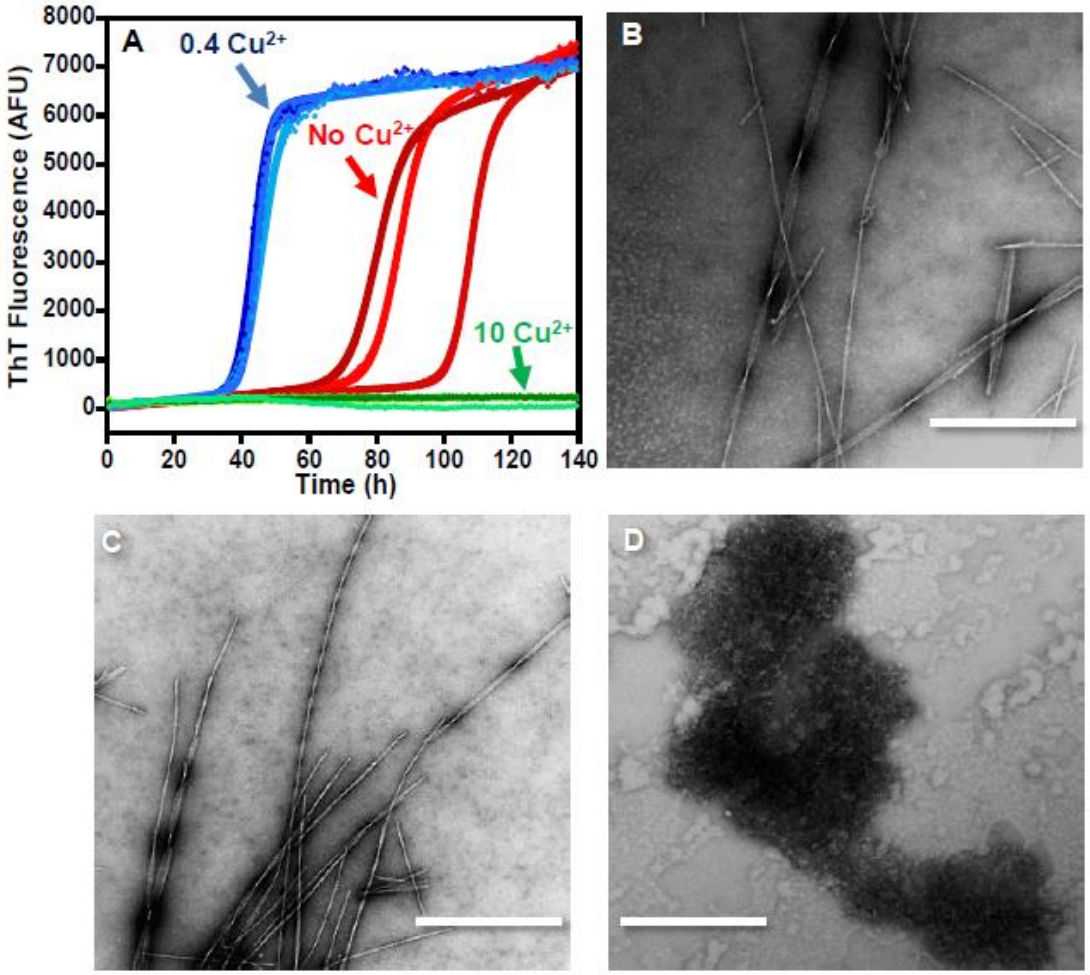

Figure 3.04 $A\beta_{(1-40)}$ Fibre Growth with Cu^{2+}.

(A) $A\beta_{(1-40)}$ fibre growth (monitored by Thioflavin T fluorescence) with no Cu^{2+} (red), 0.4 equivalence of Cu^{2+} blue) and 10 equivalence of Cu^{2+} (green). Fibre growth was carried out at pH 7.4, with 10 μM $A\beta_{(1-42)}$, 30 mM HEPES, 160 mM NaCl and agitation, at 30 ^{o}C. At least four individual wells for each condition. (B – D) samples observed by TEM, negatively stained with phosphotungsic acid, show that fibres formed without Cu^{2+} (B) and with 0.4 equivalence of Cu^{2+} (C), but amorphous aggregates formed with 10 equivalence of Cu^{2+} (D). Scale bar is 400 nm.

It was found that a higher ratio of $A\beta_{(1-42)}$ relative to $A\beta_{(1-40)}$ (in the presence of Cu^{2+}) caused decrease in the intensity of the final fluorescent signal, as seen in Fig. 3.05A. This reduction appeared to be due to a decrease in the total $A\beta_{(1-40)}$ concentration, rather than an interaction between the two peptides. This is strongly supported by the second experiment, in which concentration of $A\beta_{(1-40)}$ was kept constant, at 10 μM, as the concentration of $A\beta_{(1-42)}$ increased from 0 – 10 μM. As can be seen in Fig. 3.05B, addition of $A\beta_{(1-42)}$ to $A\beta_{(1-40),}$ in the presence of Cu^{2+}, did not decrease the final fluorescent signal, as would be expected if $A\beta_{(1-40)}$ formed oligomers with $A\beta_{(1-42),}$ nor did fluorescent signal increase, as would be expected if $A\beta_{(1-42)}$ formed mature fibres with $A\beta_{(1-40)}$. This data strongly suggests that at equilibrium (indicated by a plateau in the ThT signal) Cu^{2+}-$A\beta_{(1-40)}$ and Cu^{2+}-$A\beta_{(1-42)}$ are distinct, with essentially all $A\beta_{(1-40)}$ forming fibres and all $A\beta_{(1-42)}$ forming oligomers, in the presence of Cu^{2+}. This is supported by the TEM images; as can be seen in Fig. 3.06, in a mixture of $A\beta_{(1-42)}$ and $A\beta_{(1-40),}$ species representative of $A\beta_{(1-40)}$ fibres and species representative of Cu^{2+}-$A\beta_{(1-42)}$ oligomers are both observed.

However, although the two peptides appear to adopt two distinct final misfolded states in the presence of Cu^{2+}, with Cu^{2+}-$A\beta_{(1-40)}$ forming fibres and Cu^{2+}-$A\beta_{(1-42)}$ forming oligomers, there is clear interaction between the two misfolding pathways. As illustrated in Fig. 3.05C, the presence of $A\beta_{(1-42)}$ is able to dramatically frustrate growth of $A\beta_{(1-40)}$ fibres in the presence of Cu^{2+}. $A\beta_{(1-40)}$ fibre growth, with 0.4 equivalents of Cu^{2+}, had a t_{50} of 38 ± 4 hours, and a lag time of 27 ± 5 hours; addition of just 0.3 mole equivalents of $A\beta_{(1-42)}$ (which is the $A\beta_{(1-40)}$: $A\beta_{(1-42)}$ ratio found in those with familial Alzheimer's disease) almost doubled t_{50} and lag time, to 62 ± 2 hours and 50 ± 1 hours respectively. A two tailed unpaired *t*-test confirms that these increases are significant with > 99 % confidence.

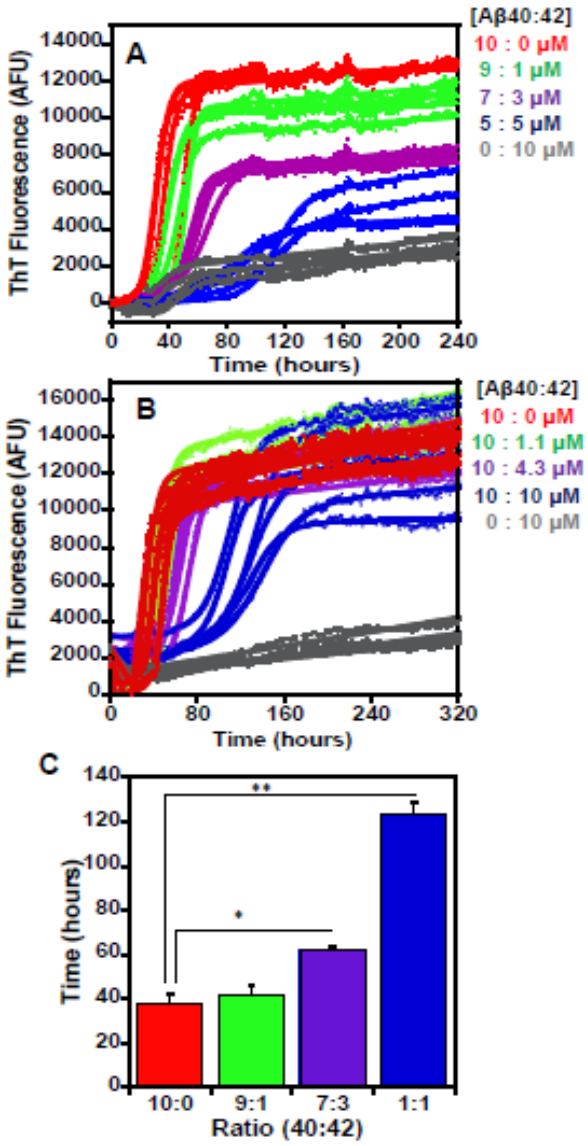

Figure 3.05 $A\beta_{(1-40)}$:$A\beta_{(1-42)}$ Fibre Growth with Cu^{2+}.

(A) Fibre growth for $A\beta_{(1-40)}$:$A\beta_{(1-42)}$ mixtures with 0.4 molar equivalents Cu^{2+}, monitored by Thioflavin T fluorescence. Total ($A\beta_{(1-40)}$ + $A\beta_{(1-42)}$) peptide concentration was kept at 10 μm. Fibre growth was monitored for an $A\beta_{(1-40)}$:$A\beta_{(1-42)}$ ratio of 10:0 (red), 9:1 (green), 7:3 (purple), 5:5 (blue), and 0:10 (grey) There were four individual wells for each condition (B) Fibre growth for $A\beta_{(1-40)}$:$A\beta_{(1-42)}$ mixtures with 0.4 mole equivalents Cu^{2+}, monitored by Thioflavin T fluorescence. $A\beta_{(1-40)}$ concentration was maintained at 10 μm, and $A\beta_{(1-42)}$ ranged from 0 – 10 μm. Fibre growth was monitored for an $A\beta_{(1-40)}$:$A\beta_{(1-42)}$ ratio of 10:0 (red), 9:1 (green), 7:3 (purple), 5:5 (blue), and 0:10 (grey), There were six individual wells for each condition. Fibre growth was carried out at pH 7.4, 30 Mm HEPES, 10 mM NaCl and agitation, at 30 ^{o}C. (C) t_{50} of fibre growth (time for 50 % of fluorescence to be reached), for mixtures where $A\beta_{(1-40)}$ concentration was maintained at 10 μm. $A\beta_{(1-42)}$ is observed to frustrate $A\beta_{(1-40)}$ fibre growth in the presence of 0.4 mole equivalents of Cu^{2+}. Error bars indicate S.E.M (n = 6). The statistical significance of differences from 100 % $A\beta_{(1-40)}$ was determined using a two-tailed unpaired *t*-test. * = P < 0.005 ** = P < 0.0005.

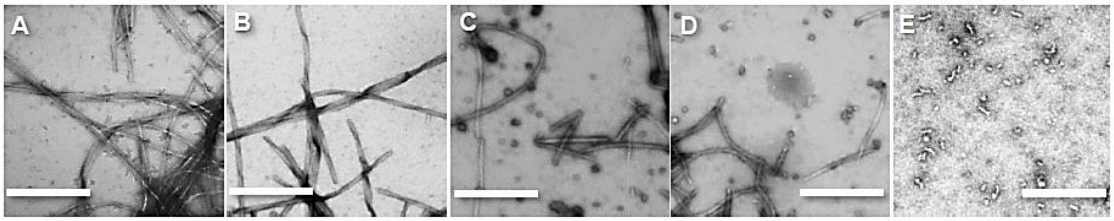

Figure 3.06 Images of $A\beta_{(1-40)}$:$A\beta_{(1-42)}$ Mixtures with Cu^{2+}.

(A – E). $A\beta_{(1-40)}$:$A\beta_{(1-42)}$ samples, incubated with 0.4 mole equivalence of Cu^{2+}, at a ratio of 1:0 (A), 9:1 (B), 7:3 (C), 1:1 (D), and 0:1 (E) . All samples were stained with phosphotungstic acid. Scale bar is 200 nm.

3.3.4 Effect of Cu^{2+} on $A\beta_{(1-42)}$ lipid membrane structure and permeability

A popular hypothesis suggests that Aβ synaptotoxicity is the result of cellular membrane interactions and disruption. The question was therefore asked as to how Cu^{2+} binding to $A\beta_{(1-42)}$ might influence the interaction between $A\beta_{(1-42)}$ and lipid membranes, as the presence of Cu^{2+} facilitates the study of an almost exclusively oligomeric/protofibrillar population, which are stable over long periods of time. Using TEM, the interaction of liposomes with $A\beta_{(1-42)}$ fibres was observed, and compared to the effects of Cu^{2+} generated oligomers on the lipid-bilayer, as shown in Fig. 3.07. In the absence of $A\beta_{(1-42),}$ smooth, spherical vesicles, of 50 – 250 nm in diameter were observed. It was found that in the presence of $A\beta_{(1-42)}$ fibres, some large unilamellar vesicles (LUVs) were distorted from their regular spherical appearance where they made contact with $A\beta_{(1-42)}$ fibres, particularly at their ends, as has recently been observed for amyloid fibres of β_2-microglobulin (Milanesi et al, 2012). TEM of LUVs in the presence of Cu^{2+} generated $A\beta_{(1-42)}$ oligomers and protofibrils show markedly more distortions of the vesicle membrane, shown in Fig. 3.07. Notably, the short curly morphology of the oligomers and protofibrils, penetrate the membrane and disrupt the membrane more readily, leading to much greater distortion of the LUVs than that typically observed with $A\beta_{(1-42)}$ fibres. In particular, there are complete breakages / discontinuations in the lipid-bilayer, highlighted in Figure 3.07, which were not observed

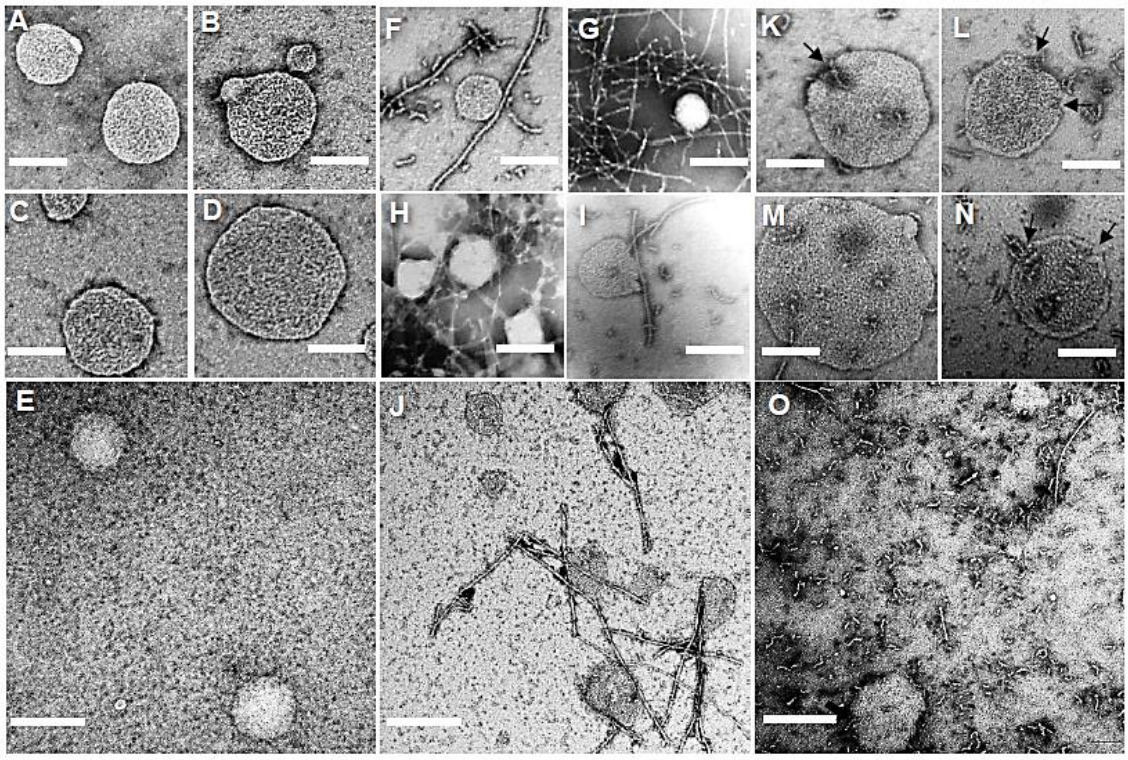

Figure 3.07 LUVs in the Presence of $A\beta_{(1-42)}$ Fibres and Cu^{2+} Generated oligomers.

LUVs, after ~120 hours of incubation, in the absence of $A\beta_{(1-42)}$ (A – E), in the presence of $A\beta_{(1-42)}$ fibres (F – J) and in the presence of Cu^{2+} generated $A\beta_{(1-42)}$ oligomers (K – O). Arrows indicate protofibril interactions with the lipid-bilayer that cause rupturing of the liposome. Samples were observed by TEM, using phosphotungstic acid negative staining. The scale bar is 100 nm, except for E, J & O, here the scale bar is 250 nm.

with $A\beta_{(1-42)}$ fibres. In addition, there are a greater number of oligomers observed relative to $A\beta_{(1-42)}$ fibres, from the same concentration of $A\beta_{(1-42)}$ monomers.

A dye release assay was used with LUVs to quantitatively measure the influence of $A\beta_{(1-42)}$ fibres and Cu^{2+} generated $A\beta_{(1-42)}$ oligomers on membrane permeability. Calcein dye release from LUVs was measured by monitoring fluorescence every 30 mins. Typically, in the absence of Aβ the LUVs remained stable for more than 300 hours with negligible dye release. It was found that incubation of LUVs with Cu^{2+} generated $A\beta_{(1-42)}$ oligomers results in significantly greater release of calcein than when LUVs are incubated with $A\beta_{(1-42)}$ fibres alone, Fig. 3.08. Furthermore, both samples of $A\beta_{(1-42)}$ induced significantly greater fluorescence release than control (LUVs in the absence of Aβ), as determined by a one-way analysis of variance (ANOVA) followed by Fisher's least significant difference (LSD) post-hoc test.

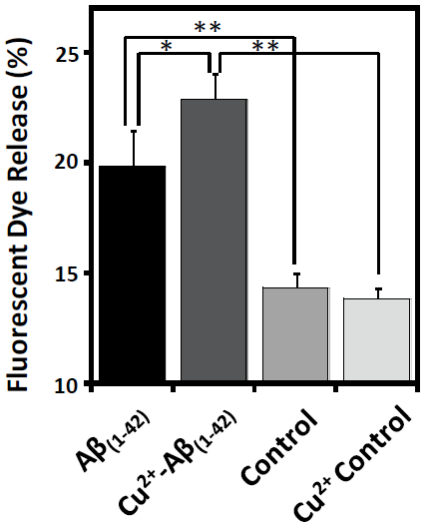

Figure 3.08 Liposome permeability in the presence of preformed $A\beta_{(1-42)}$ fibres and Cu^{2+} generated oligomers.

Both $A\beta_{(1-42)}$ fibres, and $A\beta_{(1-42)}$ oligomers generated with 0.4 molar equivalents of Cu^{2+}, disrupt liposome permeability significantly more than their respective controls, as shown through greater release of the fluorescent dye calcein. Cu^{2+} generated $A\beta_{(1-42)}$ oligomers significant more dye release than $A\beta_{(1-42)}$ fibres after 12 days. The concentration of LUVs and $A\beta_{(1-42)}$ were 1 mg/ml and 10 μM respectively. Fluorescence was measured after a 280 hour incubation, following addition of 10 μM EDTA. Results were presented as a percentage of maximum fluorescence after triton addition, 10 ml/l. Samples were incubated at pH 7.4, and 30 ^{o}C. Error bars indicate S.E.M (n = 5 – 6) * = $P < 0.05$, ** = $P < 0.0001$. Statistical significance was determined using ANOVA, followed by Fisher's LSD post-hoc test.

3.4 DISCUSSION

In these investigations, it was have found that substoichiometric levels of Cu^{2+} influence the misfolding pathways of $A\beta_{(1-40)}$ and $A\beta_{(1-42)}$ in markedly distinct ways. For $A\beta_{(1-40)}$, Cu^{2+} accelerates the rate of fibre formation, but had little influence on the morphology or amount of fibres generated. The mechanism by which Cu^{2+} increases rate of $A\beta_{(1-40)}$ fibre growth has been suggested to originate from the addition of the two positive charges making Aβ more neutral in overall net charge at pH 7.4, and consequently more prone to self-association (Sarell et al, 2010). However, for $A\beta_{(1-42)}$, Cu^{2+} greatly reduced fibre number, instead promoting formation of oligomers and short "curly" protofibrils. These typically transient forms of Aβ were surprisingly stable in the presence of substoichiometric Cu^{2+}, over a period of weeks at 30 ^{o}C. Furthermore, preformed mature fibres of $A\beta_{(1-42)}$ rapidly dissociated in the presence of Cu^{2+}, also generating oligomers and protofibrils, indicating that in the presence of substoichiometric Cu^{2+}, protofibrilar and oligomeric assemblies are the thermodynamically stable form of Cu^{2+} loaded $A\beta_{(1-42)}$.

It is significant that Cu^{2+} is able to promote formation of $A\beta_{(1-42)}$ oligomers over fibres, as studies suggest that Aβ oligomers are the primary mediator of synaptotoxicity in AD (Lambert et al, 1998; Lesné et al, 2006; Walsh et al, 2002; Yankner & Lu, 2009). This is supported by the observation that soluble, diffusible forms of Aβ monomers and small oligomers, better correlates with cognitive impairment and synaptic dysfunction than the number of larger aggregates (Lue et al, 1999; Wang et al, 1999). The differing structures of fibres and oligomers and the extent of exposed hydrophobic residues may be key to oligomer cytotoxicity.

Cu^{2+} could contribute to AD pathology through binding to $A\beta_{(1-42)}$ and promoting oligomer formation. This is supported by TEM images of the oligomer-liposome interaction and the vesicle permeability assay, which both indicate that Cu^{2+} generated

oligomers / protofibrils of $A\beta_{(1-42)}$ profoundly influence lipid membrane structure and integrity. Consequently, it appears that the increased AD phenotype in animal models for which copper homeostasis is disrupted (Cherny et al, 2001; Sanokawa-Akakura et al, 2010; Singh et al, 2013; Sparks & Schreurs, 2003) and in cell culture (Opazo et al, 2002; Sarell et al, 2010; Sharma et al, 2013; Smith et al, 2007) is at least in part due to Cu^{2+} dramatically altering the distribution between fibre and oligomer for $A\beta_{(1-42)}$, and these Cu^{2+} generated oligomers having a more marked effect on membrane integrity than $A\beta_{(1-42)}$ in the absence of Cu^{2+}. Additionally, as at neutral pH, the contribution of two positive charges upon Cu^{2+} binding to Aβ makes Aβ more neutrally charged overall, this may facilitate greater penetration of the hydrophobic lipid-bilayer.

It was surprising that just two amino acids at the C-terminus of Aβ (Ile, Ala) that are not directly involved in Cu^{2+} coordination (Dorlet et al, 2009; Drew et al, 2009; Sarell et al, 2009) have such a profound influence on the extent of oligomer formation. The marked difference in the effect Cu^{2+} has on the two Aβ alloforms may arise from distinct differences in the pathway to fibril assembly (Bitan et al, 2003; Chen & Glabe, 2006). Unlike $A\beta_{(1-40)}$, it is believed $A\beta_{(1-42)}$ fibre growth proceeds through an initial stage of oligomerisation, in which pentamer / hexamer units are formed that ultimately reassemble to form fibres (Bitan et al, 2003). It may be possible that Cu^{2+} binding stabilises these otherwise transient species that are more readily formed by $A\beta_{(1-42)}$, conceivably by cross-linked inter-molecular coordination (Hane et al, 2013), promoting a more thermodynamically stable oligomer rich population of $A\beta_{(1-42)}$. Substoichiometric levels of Cu^{2+} were sufficient to promote almost exclusive formation of oligomers and protofibrils; thus, the data suggests that a single Cu^{2+} ion is sufficient to alter the stability of a number of $A\beta_{(1-42)}$ molecules in an oligomeric form. Interestingly, recent studies using ssNMR suggest differences in secondary structure between fibres and oligomers occur in the N-terminus of $A\beta_{(1-42)}$ (residues 3 – 14) (Haupt et al, 2012). It is these residues that adopt a β-strand structure in the oligomer structure but not in fibres. This is significant, as it is these N-terminal residues that are directly involved in Cu^{2+}

coordination, via His 6, His 13, and His 14 (Sarell et al, 2009).

In vivo, there is a mixture of $A\beta_{(1-40)}$ and $A\beta_{(1-42)}$ present, the ratio of which increases from 9:1 to 7:3 in familial forms of Alzheimer's disease (Citron et al, 1997; Duff et al, 1996; Scheuner et al, 1996). How these two peptides influence the misfolding of the other is a subject of intense interest. It appears $A\beta_{(1-42)}$ is able to frustrate the fibre formation of $A\beta_{(1-40)}$ (Chang et al, 2013; Jan et al, 2008; Kuperstein et al, 2010; Pauwels et al, 2012). The observations for Cu^{2+} loaded mixtures of $A\beta_{(1-40)}$ and $A\beta_{(1-42)}$ provides a fascinating insight. The data suggests that in the presence of Cu^{2+}, $A\beta_{(1-42)}$ can frustrate $A\beta_{(1-40)}$ fibre formation, prolonging the time that $A\beta_{(1-40)}$ spends as prefibrillar oligomers, but ultimately only Cu^{2+}-$A\beta_{(1-40)}$ forms fibres, while $A\beta_{(1-42)}$ forms stable protofibrils and oligomers.

The present study illustrates that Cu^{2+} accentuates differences in the self-assembly pathways for $A\beta_{(1-42)}$ and $A\beta_{(1-40)}$. This suggests the significance of $A\beta_{(1-42)}$ in AD aetiology could be related to its very different aggregation properties in the presence of Cu^{2+} ions released at the synapse. Thus, the elevated levels of Cu^{2+} that occur with age (Barnham & Bush, 2008) may serve as an important factor in AD onset, through stabilising neurotoxic oligomeric species of $A\beta_{(1-42)}$. Supporting a role for Cu^{2+} in AD, a recent unbiased screen indicated that copper binding compounds, clioquinol in particular, ameliorated Aβ toxicity in a yeast model of Alzheimer's disease (Matlack et al, 2014). Indeed, the investigations show that chelation of Cu^{2+} from $A\beta_{(1-42)}$ results in the rapid conversion of $A\beta_{(1-42)}$ oligomers to the less neurotoxic amyloid fibres.

CHAPTER 4: Rapid Exchange of Zn(II) Enables Trace Levels to Influence Aβ Misfolding and Dominate Assembly Outcomes in Cu^{2+}/Zn^{2+} Mixtures

4.1 ABSTRACT

One factor that is thought to have a significant role in AD aetiology is Zn^{2+} homeostasis, which is disrupted in the brains of AD sufferers, and has been shown to modulate AD symptoms in animal models. In this study, itwas investigated how the kinetics of Aβ fibre growth are affected at a range of Zn^{2+} concentrations, and transmission electron microscopy was used to characterise the aggregate assemblies formed. It was demonstrated that for $Aβ_{(1-40)}$ and $Aβ_{(1-42)}$ as little as 0.01 mole equivalents of Zn^{2+} is sufficient to greatly perturb the formation of amyloid fibres irreversibly. Instead, $Aβ_{(1-40)}$ assembles into short rod-like fibrils that pack tightly together into ordered stacks, whereas $Aβ_{(1-42)}$ forms short crooked assemblies that knit together to form a mesh of disordered tangles. The data suggests that a small number of Zn^{2+} ions are able to influence a great many Aβ molecules through the rapid exchange of Zn^{2+} between Aβ peptides. As high levels of both Zn^{2+} and Aβ are found at glutamatergic neurons, it was demonstrated that glutamate does not modulate the effect of Zn^{2+} upon Aβ misfolding, indicating that observations are physiologically relevant. Surprisingly, although Cu^{2+} binds to Aβ ten-thousand times tighter than Zn^{2+}, the effect of Zn^{2+} on Aβ assembly dominates in Cu^{2+}/Zn^{2+} mixtures, suggesting trace levels of Zn^{2+} must have a profound effect on extracellular Aβ accumulation.

4.2 INTRODUCTION

The pathology of AD is characterised by the misfolding of amyloid-β, and its subsequent aggregation into oligomers, fibres and plaques (Ballard et al, 2011). However, it is not clear what promotes the initial misfolding of Aβ in sporadic AD, or what promotes aggregation of the neurotoxic oligomers and fibres over benign amorphous aggregates (Ballard et al, 2011; Hardy & Selkoe, 2002). One possibility is that aggregation is influenced through the elevated levels Zn^{2+} (Bush et al, 1994), for which levels in the neuropil are increased 2-fold in patients with AD (Lovell et al, 1998).

Zn^{2+} is an important intracellular signalling molecule that is thought to be crucial for synaptic plasticity, learning, and memory (Ceccom et al, 2014; Fukada et al, 2011; Lin et al, 2001). In the brain, large reserves of free Zn^{2+} are found to be stored in the presynaptic vesicles of glutamatergic neurons, transported there by Zinc transporter-3 (ZnT3) (Assaf & Chung, 1984; Howell et al, 1984; Nydegger et al, 2010; Qian & Noebels, 2006). These stores of Zn^{2+} exit the vesicles with glutamate following neuronal depolarisation, and are reported to bind and regulate the function of a range of neurotransmitter receptors, including NMDA-type glutamate receptors (Paoletti et al, 2009). A general consensus has been reached that the affinity of Zn^{2+} for Aβ at pH 7.4 is within the range 1 – 20 μM (Faller & Hureau, 2009); though this is a relatively moderate affinity, the high levels of Zn^{2+} at the synapse, especially during depolarisation, when Zn^{2+} is reported to reach concentrations of up to 100 – 300 μM (Frederickson, 1989; Vogt et al, 2000), would be expected to facilitate the binding of Zn^{2+} to Aβ *in vivo* (Noy et al, 2008).

There is much evidence to support Zn^{2+} homeostasis being associated with AD pathology. It has been found that a Cu^{2+}/Zn^{2+} chelator, PBT2, decreases soluble Aβ levels and improves cognition in a transgenic mouse model of AD (Adlard et al, 2008), and in another study, it has been found that for two transgenic mouse models of AD (Tg2576 and TgCRND8), a Zn^{2+} enriched diet is associated with potentiated Alzheimer's-like spatial memory impairment, as well as a reduction in Aβ plaque deposition, potentially increasing soluble Aβ levels (Linkous et al, 2009). Conversely, others have reported that Zn^{2+} supplementation for 3 x TG-AD transgenic mice actually attenuated disease pathology, delaying hippocampal-dependent memory deficits and preventing the mitochondrial dysfunction observed in untreated 3 x TG-AD transgenic mice (Corona et al, 2010). Likewise, mice depleted of synaptic Zn^{2+} through a ZnT3 knockout mutation present age-dependent memory impairments similar to those observed in AD models (Lee et al, 2002); this is particularly significant as the authors

found that ZnT3 levels also decline in humans with aging, particularly those with AD (Adlard et al, 2010). Similarly, in drosophila models of AD, tight control of copper and zinc availability ameliorates disease phenotype (Hua et al, 2011). It is thought that Zn^{2+} influences AD pathology through direct binding to the Aβ peptide.

Metal ions binding to Aβ may alter the kinetics of on-pathway amyloid fibre formation, or alternatively, promote formation of off-pathway aggregates (House et al, 2004; Viles, 2012). Initially, it was thought that Zn^{2+} promoted formation of off-pathway, amorphous aggregates (Ha et al, 2007; Raman et al, 2005; Yoshiike et al, 2001); however, it has subsequently been reported that Zn^{2+} can cause Aβ to form annular protofibrils (Chen et al, 2012; Chen et al, 2011). A comprehensive study has shown that Zn^{2+} induces $Aβ_{(1-40)}$ to rapidly form disc shaped oligomers that are highly toxic to primary cell culture, but may then further aggregate to form non-toxic assemblies (Solomonov et al, 2012); while others have suggested that Zn^{2+} induced amorphous aggregation destabilises oligomers entirely (Garai et al, 2007). Conversely, it was recently reported that trace levels of Zn^{2+} are able to slow $Aβ_{(1-40)}$ fibre growth without affecting the number of fibres ultimately formed (Abelein et al, 2015). Consequently, though many studies agree that Zn^{2+} has a profound effect on Aβ misfolding, which aggregate species develop from the Aβ-Zn^{2+} interaction is still controversial and not fully understood.

A great amount of research has highlighted the importance of controlling Zn^{2+} levels in the brains of AD sufferers and those at risk of developing the disease, while emphasising that both an excess of Zn^{2+} and Zn^{2+} deficiency may be pathogenic (Adlard et al, 2008; Adlard et al, 2010; Corona et al, 2010; Garai et al, 2007; Linkous et al, 2009; Solomonov et al, 2012). Thus, it is of great importance to understand how Aβ is influenced by Zn^{2+} at a full range of concentrations, and whether glutamate may affect the Aβ-Zn^{2+} interaction, particularly as Zn^{2+} is released at the synapse with glutamate (Assaf & Chung, 1984; Howell et al, 1984; Nydegger et al, 2010; Qian &

Noebels, 2006). In this study, both ThT fluorescence and TEM have been use to clarify the influence of Zn^{2+} on Aβ self-association, for both $Aβ_{(1-42)}$ and $Aβ_{(1-40)}$ alloforms, at a range of physiologically relevant conditions, including very low substoichiometric levels of Zn^{2+}.

The interaction of a second divalent metal ion, Cu^{2+}, with Aβ has also generated a lot of attention (Viles, 2012). Cu^{2+} is also released at the synapse during depolarisation (Kardos et al, 1989), and has a 50 pM affinity for Aβ (Sarell et al, 2009). It has been previously shown that while substoichiometric Cu^{2+} accelerates $Aβ_{(1-40)}$ fibre formation (Sarell et al, 2010), Cu^{2+} stabilises protofibrillar/oligomeric assemblies of $Aβ_{(1-42)}$, and can even rapidly convert $Aβ_{(1-42)}$ fibres to protofibrillar/oligomeric assemblies (Matheou et al, 2015). Here, the effect of a range of Cu^{2+} and Zn^{2+} mixtures on Aβ assemblies were investigated, as both are present extracellularly at the synapse, and share histidine coordinating ligands (Alies et al, 2013; Silva & Saxena, 2013). It was demonstrated that trace levels of Zn^{2+} (0.01 mole equivalents) profoundly influences the misfolding pathways of both $Aβ_{(1-42)}$ and $Aβ_{(1-40)}$. The data suggests this may occur through a rapid exchange mechanism, or potentially through Zn^{2+} exerting longer-range intermolecular influence, that enables Zn^{2+} to exert more influence over Aβ assembly than Cu^{2+} in Zn^{2+}/Cu^{2+} mixtures, despite the latter having a much higher affinity for Aβ.

4.3 RESULTS

4.3.1 Zn^{2+} and $Aβ_{(1-42)}$ Aggregation

The ThT fluorescence assay was used to examine the fibre formation kinetics of $Aβ_{(1-42)}$ at a range of Zn^{2+} concentrations, with TEM being used to examine the species of aggregates formed. The fibre growth of Aβ progresses through a nucleation-dependent pathway, for which formation of an oligomeric nucleus precedes elongation of Aβ into mature fibrils (Jarrett & Lansbury, 1993; Roychaudhuri et al, 2009). This classic

pattern of fibre formation is observed for $A\beta_{(1-42)}$ in the absence of Zn^{2+}, while at 2 mole equivalents, Zn^{2+} is found to abolish ThT binding amyloid assembly (Fig 4.01A), as has been observed by others (Chen et al, 2012; Chen et al, 2011; Garai et al, 2007; House et al, 2004; Raman et al, 2005; Sarell et al, 2010; Solomonov et al, 2012; Viles, 2012; Yoshiike et al, 2001). The next aim, was to determine whether much lower levels of Zn^{2+} are also capable of influencing $A\beta_{(1-42)}$ misfolding. The effect of substoichiometric levels of Zn^{2+} on $A\beta_{(1-42)}$ fibre growth was investigated, and it was found that as little as 0.01 mole equivalents of Zn^{2+} is sufficient to greatly perturb $A\beta_{(1-42)}$ fibre growth (Fig 4.01B), even though at any one time ~ 99 % of Aβ molecules will not be bound to Zn^{2+}.

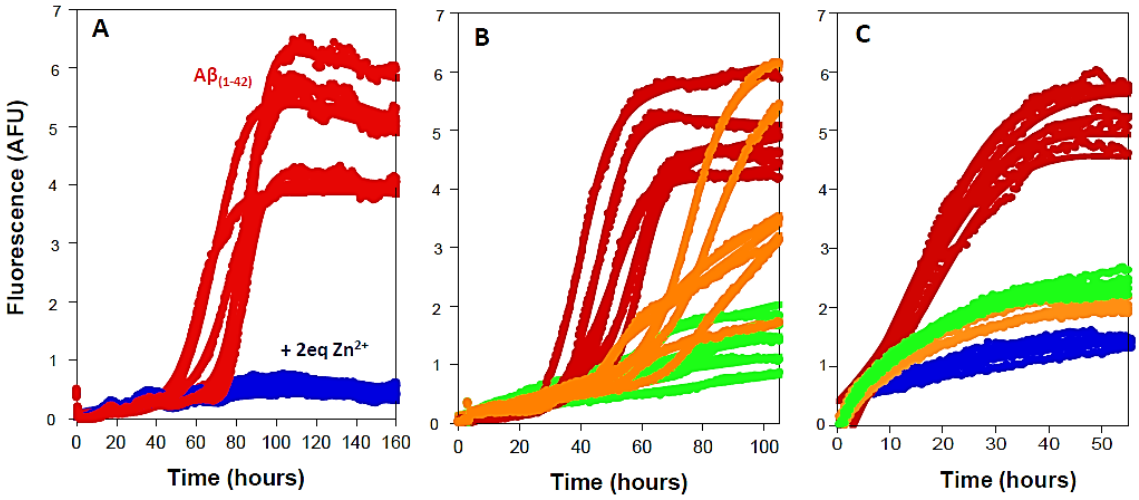

Figure 4.01 $A\beta_{(1-42)}$ Fibre Growth with Zn^{2+}.

A. $A\beta_{(1-42)}$ fibre growth, monitored by Thioflavin T fluorescence, with no Zn^{2+} (red) and 2 equivalents of Zn^{2+} (blue). *B.* $A\beta_{(1-42)}$ fibre growth with no Zn^{2+} (red), 0.01 equivalents of Zn^{2+} (orange), and 0.05 equivalents (green). *C.* $A\beta_{(1-42)}$ fibre growth with glutamate and Zn^{2+}. No Zn^{2+} (red); 0.01 equivalents of Zn^{2+} (orange); 0.05 equivalents of Zn^{2+} (green), and 2 equivalents of Zn^{2+} (blue). Ratio of Zn^{2+}:glutamate; 1:2. As little as 0.01 equivalents of Zn^{2+} strongly inhibited ThT fluorescent fibre formation. Fibre growth was carried out at pH 7.4, with 10 μM $A\beta_{(1-42)}$, 30 mM HEPES, 160 mM NaCl and mild agitation, at 30 ^{o}C. (N = 6 traces).

In vivo, Zn^{2+} is co-released with glutamate, thus, whether glutamate may modulate the effect of Zn^{2+} upon $A\beta_{(1-42)}$ self-association was an important question. The ThT data shows that in the presence of two-fold as much glutamate as Zn^{2+}, 0.01 mole equivalents of Zn^{2+} is still sufficient to greatly impede $A\beta_{(1-42)}$ fibre growth (Fig 4.01C).

The morphology of the $A\beta_{(1-42)}$ assemblies formed were characterised using TEM, figure 4.02. The images show that in the absence of Zn^{2+}, $A\beta_{(1-42)}$ predominantly formed amyloid fibres, with a typical straight unbranched morphology of 10 – 20 nm thickness (depending on the number of filaments stacked together), and many microns in length. However, as little as 0.05 equivalents of Zn^{2+} visibly influences the population of aggregates that develop, with $A\beta_{(1-42)}$ generally forming very disjointed crooked fibril-like assemblies, 10 nm thick and 50 – 200 nm long, that are non-ThT binding. These short fibrous aggregates self-associate to form large disorderly tangles which are not observed in the absence of Zn^{2+}. These tangles were 100 – 1000 nm, densely stained, and had no repeating structure. At 2 equivalents of Zn^{2+} large disorderly tangles, resembling those observed for 0.05 equivalents of Zn^{2+}, predominated. The TEM images also demonstrate that the influence of Zn^{2+} on $A\beta_{(1-42)}$ aggregation is not altered by the presence of glutamate (Fig. 4.02E-H). Thus, the results show that both substoichiometric and suprastoichiometric levels of Zn^{2+} promote $A\beta_{(1-42)}$ to form disorderly tangles, rather than growth of amyloid fibrils, and that this may be relevant *in vivo*, as it was found that glutamate does not prevent this affect. These observations were made consistently, over numerous Zn^{2+}-$A\beta_{(1-42)}$ preparations and TEM grids.

4.3.2 Zn^{2+} and $A\beta_{(1-40)}$ Aggregation

It has previously been observed that the effect of Cu^{2+} on $A\beta_{(1-42)}$ and $A\beta_{(1-40)}$ differs substantially (Matheou et al, 2015). Consequently, ThT fluorescence was used to investigate how $A\beta_{(1-40)}$ amyloid fibre growth is influenced by Zn^{2+}, at a range of Zn^{2+}

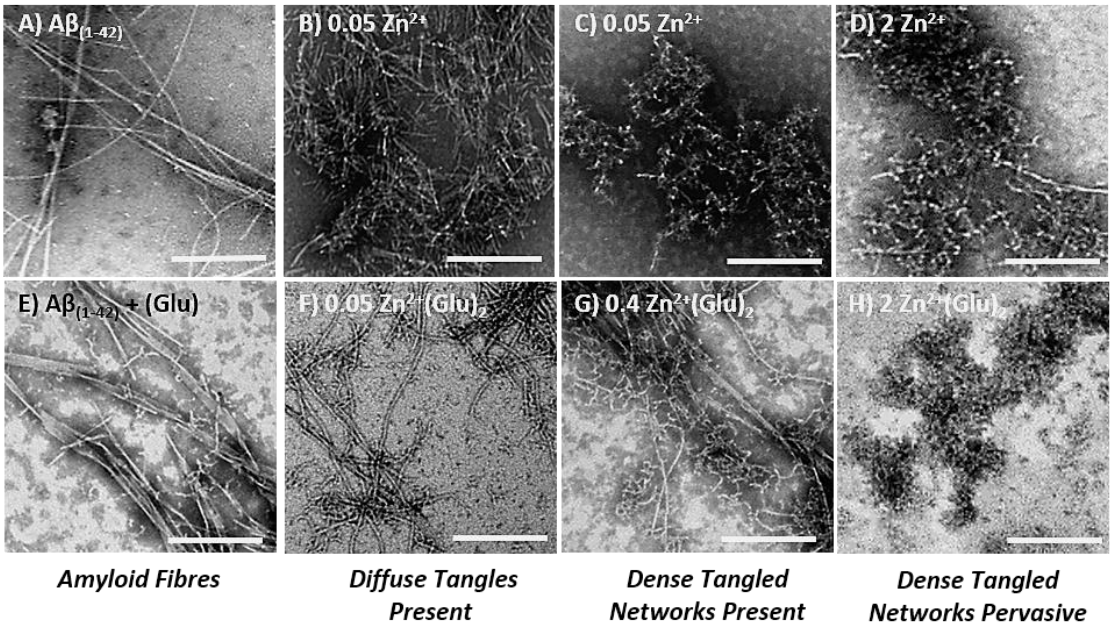

Figure 4.02 TEM Images of $A\beta_{(1-42)}$ with Zn^{2+} and Glutamate.

A-H. Representative TEM images of $A\beta_{(1-42)}$ samples, incubated with no Zn^{2+} (A), 0.05 equivalents of Zn^{2+} (B-C), 2 equivalents of Zn^{2+} (D), 4 equivalents of glutamate (E), 0.05 equivalents of Zn^{2+} (F), 0.4 equivalents of Zn^{2+} (G), and 2 equivalents of Zn^{2+} (H). E – H also have glutamate present; ratio Zn^{2+}:glutamate is 1:2. All samples were stained with phosphotungstic acid. Scale bars are 250 nm.

concentrations (Fig. 4.03). It was observed that for $A\beta_{(1-40)}$, as for $A\beta_{(1-42)}$, 2 equivalents of Zn^{2+} essentially abolished ThT signal, suggesting that it greatly inhibits amyloid fibre growth. Additionally, as for $A\beta_{(1-42)}$, as little as 0.01 equivalents of Zn^{2+} was able to inhibit growth of $A\beta_{(1-40)}$ fibres, according to ThT fluorescence. It was also demonstrated that these low levels of Zn^{2+} were able to perturb $A\beta_{(1-40)}$ fibre growth even in the presence of glutamate (Fig. 4.03B).

Using TEM, the species of $A\beta_{(1-40)}$ aggregates formed in the presence of varying levels of Zn^{2+} was characterised. It was found that there are apparent differences between $A\beta_{(1-40)}$ and $A\beta_{(1-42)}$ assembly in the presence of low levels of Zn^{2+}, but not for suprastoichiometric levels (Fig. 4.04). The images show that in the absence of Zn^{2+}, $A\beta_{(1-40)}$ forms typical straight unbranched amyloid fibres, 10 – 20 nm thick and many microns in length. The presence of 0.05 equivalents of Zn^{2+} greatly reduces the number

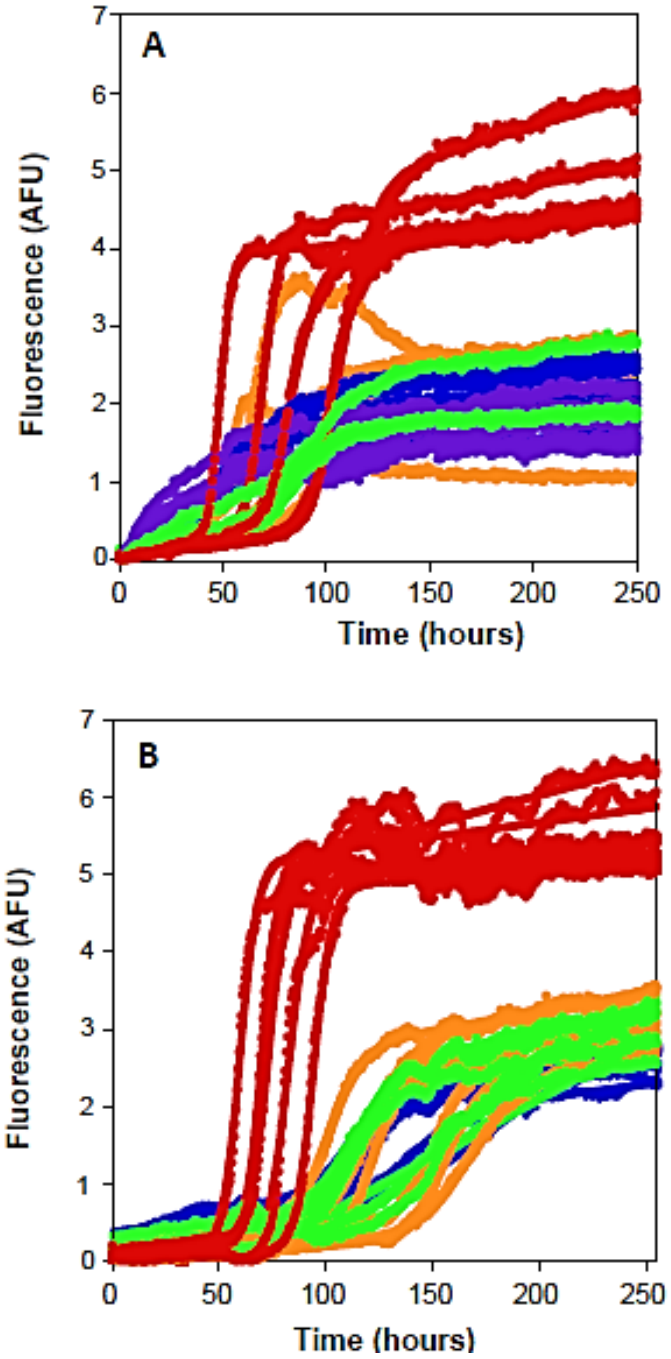

Figure 4.03 $A\beta_{(1-40)}$ Fibre Growth with Zn^{2+}.

A. $A\beta_{(1-40)}$ fibre growth, monitored by Thioflavin T fluorescence, with no Zn^{2+} (red), 0.05 equivalents of Zn^{2+} (orange), 0.2 equivalents of Zn^{2+} (green), 0.4 equivalents of Zn^{2+} (blue) and 2 equivalents of Zn^{2+} with (purple). *B.* $A\beta_{(1-40)}$ fibre growth with Zn^{2+} and glutamate, where the Zn^{2+}:glutamate ratio is 1:2. No Zn^{2+} (red), 0.01 equivalents of Zn^{2+} with (orange), 0.05 equivalents of Zn^{2+} (green), and 0.4 equivalents of Zn^{2+} (blue). Fibre growth was carried out at pH 7.4, with 10 μM $A\beta_{(1-40)}$, 30 mM HEPES, 10 mM NaCl and agitation, at 30 ^{o}C. (N = 4 – 6 traces).

of mature amyloid fibres that form, and, unlike for $A\beta_{(1-42)}$, promotes the formation of short rod-like fibres, which are 10 – 20 nm thick, 50 – 200 nm long, and pack closely together, to form stacks 50 – 300 nm thick (Fig. 4.04B). These stacks were observed at greater number for 0.2 equivalents of Zn^{2+} (Fig. 4.04C). For 2 equivalents of Zn^{2+}, a similar effect as for $A\beta_{(1-42)}$ was observed, as large disordered tangles predominate. These tangles were found to be 100 – 1000 nm, densely stained, and to have no repeating structure (Fig. 4.04D).

Notably, it was found that the presence of glutamate did not influence the morphology of Zn^{2+} induced $A\beta_{(1-40)}$ aggregates (Fig 4.04E-H). Thus the differences in behaviour between $A\beta_{(1-40)}$ and $A\beta_{(1-42)}$ at low levels of Zn^{2+} could potentially be relevant *in vivo*. These observations were made consistently, over numerous Zn^{2+}-$A\beta_{(1-42)}$ preparations and TEM grids.

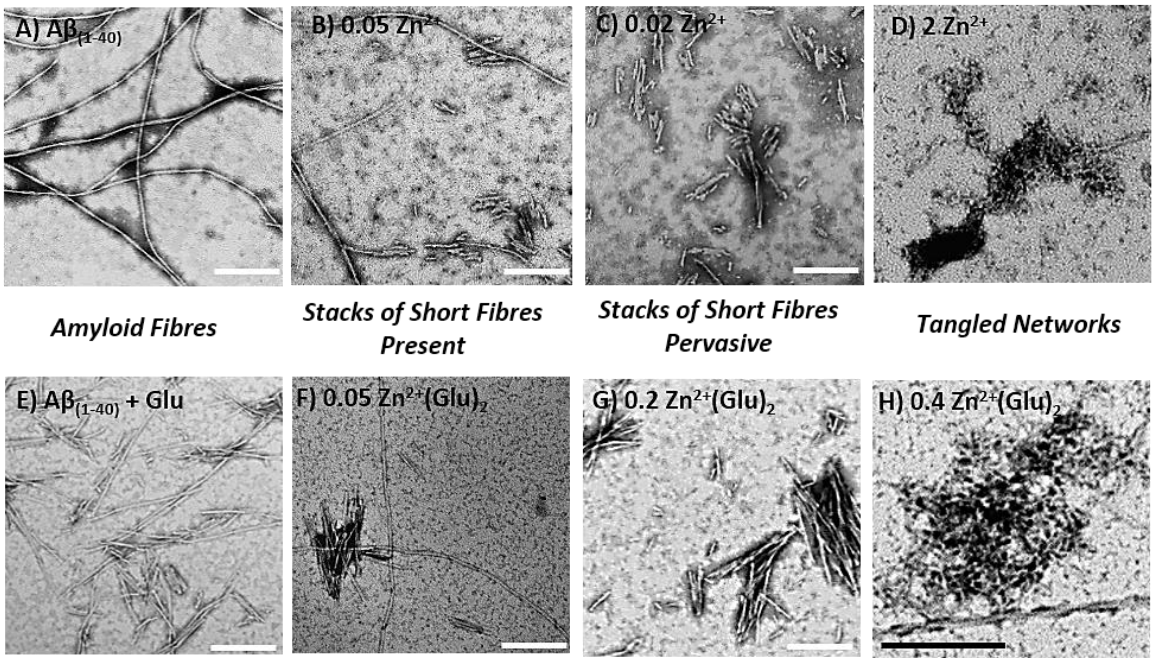

Figure 4.04 TEM Images of $A\beta_{(1-40)}$ with Zn^{2+} and Glutamate.

A-H. Representative TEM images of $A\beta_{(1-40)}$ samples, incubated with no Zn^{2+} (A), 0.05 equivalents of Zn^{2+} (B), 0.2 equivalents of Zn^{2+}(C), 2 equivalents of Zn^{2+} (D), 4 equivalents of glutamate (E), 0.05 equivalents of Zn^{2+} (F), 0.2 equivalents of Zn^{2+} (G), and 0.4 equivalents of Zn^{2+} of glutamate and 0.8 equivalents of glutamate (H). All samples were stained with phosphotungstic acid. Scale bars are 250 nm.

4.3.3 Adding and Removing Zn^{2+} from Aβ Assemblies at Equilibrium

The effect of adding Zn^{2+} to mature, preformed $Aβ_{(1-40)}$ fibres was investigated. Using a ThT assay (Fig. 4.05A), it was found that after adding 0.4 mole equivalents of Zn^{2+} to the preformed fibres, ThT fluorescence stayed constant following a further 100 hours of incubation, suggesting that Zn^{2+} does not readily dissociate fully formed amyloid fibres. This was corroborated by TEM data, figure 4.05B, which showed that the mature $Aβ_{(1-40)}$ fibres to which Zn^{2+} was added retained a typical amyloid fibre structure, and did not adopt the structural features characteristic of monomeric $Aβ_{(1-40)}$ incubated with Zn^{2+}, of short rod-like assemblies.

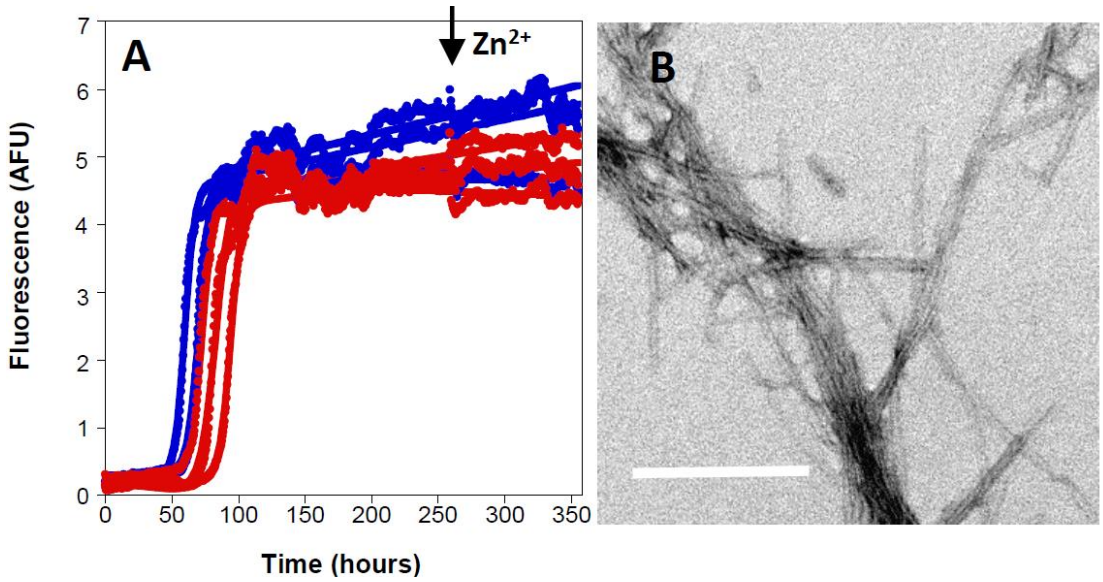

Figure 4.05 Zn^{2+} Added to Mature $Aβ_{(1-40)}$ Fibres.

A. $Aβ_{(1-40)}$ fibre growth, monitored by Thioflavin T fluorescence, to which buffer (red) and 0.4 equivalents of Zn^{2+} (blue) was added at 250 hours. Fibre growth was carried out at pH 7.4, with 10 μM Aβ(1-42), 30 mM HEPES, 10 mM NaCl and agitation, at 30 ^{o}C. (N = 3 Traces).
B. Representative TEM image of mature $Aβ_{(1-40)}$ fibres, which after fibre growth were incubated with 0.4 equivalents of Zn^{2+} for 100 hours. The addition of Zn^{2+} to mature fibres has no effect on morphology. Samples were stained with phosphotungstic acid. Scale bar is 250 nm.

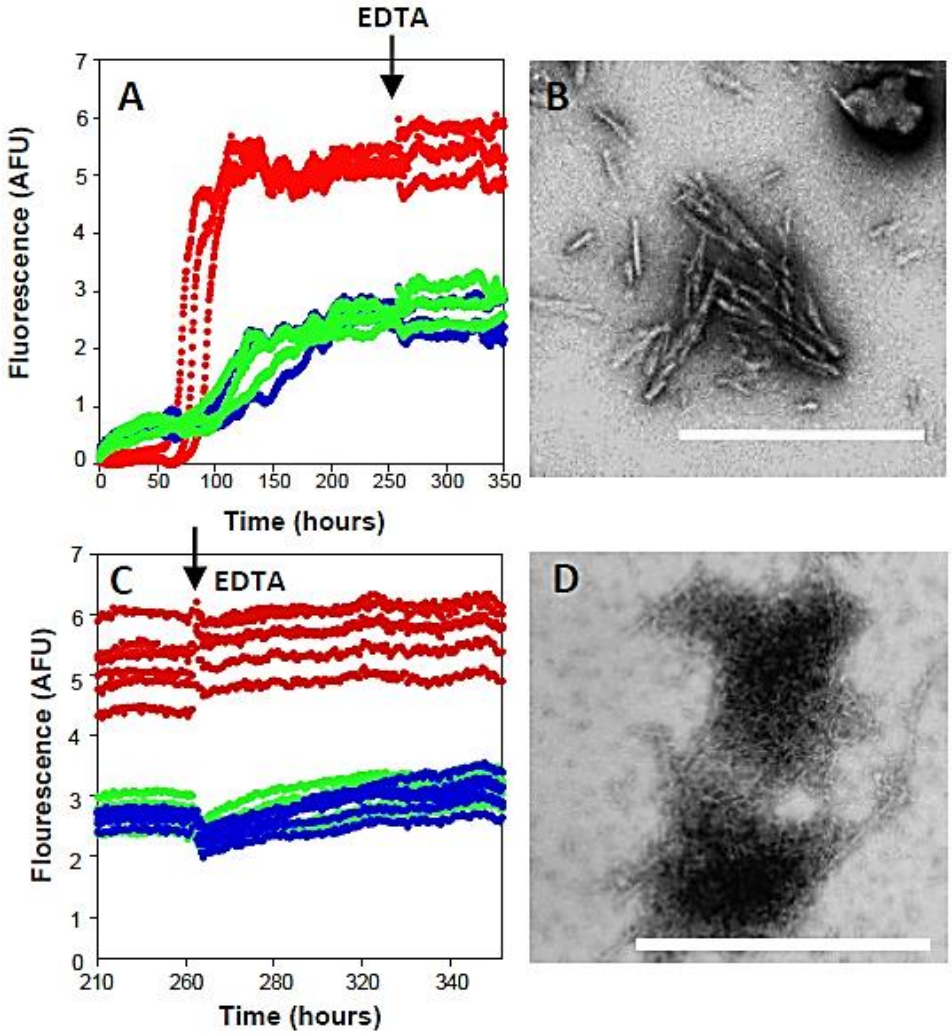

Figure 4.06 EDTA Added to Aβ Fibres Incubated with Zn^{2+}.

A. $A\beta_{(1\text{-}40)}$ fibre growth, monitored by Thioflavin T fluorescence, for samples with no Zn^{2+} (red), 0.05 equivalents of Zn^{2} (green), and 0.4 equivalents of Zn^{2+} (blue), to which 50 μM EDTA was added at 250 hours. (n = 3). *B.* Representative TEM image of $A\beta_{(1\text{-}40)}$ incubated with 0.4 equivalents Zn^{2+}, to which 50 μM EDTA was added after 250 hours, and incubated for a further 100 hours. *C.* ThT fluorescence for $A\beta_{(1\text{-}42)}$ with no Zn^{2+} (red), 1 equivalents of Zn^{2+} (green), and 2 equivalents of Zn^{2+} (blue), to which 50 μM EDTA was added at 265 hours. (n = 6) *D.* Representative TEM image of $A\beta_{(1\text{-}42)}$ incubated with 2 equivalents Zn^{2+}, to which 50 μM EDTA was added after, and incubated for a further 70 hours. fibre growth was carried out at pH 7.4, with 10 μM Aβ, 30 mM HEPES, 10 mM NaCl and agitation, at 30 ^{o}C. Samples also contained glutamate, at a Zn^{2+}: glutamate ratio of 1:2. Samples were stained with phosphotungstic acid. Scale bar is 500 nm. Once $A\beta_{(1\text{-}40)}$ or $A\beta_{(1\text{-}42)}$ form Zn^{2+} induced aggregates EDTA has little effect.

In addition to this, the question was asked as to whether aggregates formed in the presence of Zn^{2+} would persist in the absence of Zn^{2+}. For this investigation, EDTA (a strong Zn^{2+} chelator) was added to both $Aβ_{(1-42)}$ and $Aβ_{(1-40)}$ samples which had previously been incubated with Zn^{2+} (Fig. 4.06). The data suggest that removal of Zn^{2+} from Aβ does not enable resumption of amyloid fibre formation, as ThT signal did not increase following EDTA addition. The TEM confirmed that the aggregate species formed when monomeric Aβ is incubated with Zn^{2+} persist once Zn^{2+} is removed with EDTA. This data suggests that Zn^{2+} promotes formation of aggregates that are off-pathway to amyloid fibre formation. Interestingly, even the short rod structures (formed with $Aβ_{(1-40)}$ + Zn^{2+}), whose gross morphology is reminiscent of amyloid fibres, do not seed the formation of ThT binding fibres once Zn^{2+} is removed by EDTA (Fig. 4.06B). Notably, regardless of Zn^{2+} inducing off-pathway Aβ aggregates, Zn^{2+} induced assemblies have similarly high β-sheet content to Aβ incubated in the absence of Zn^{2+} (Fig. 4.07).

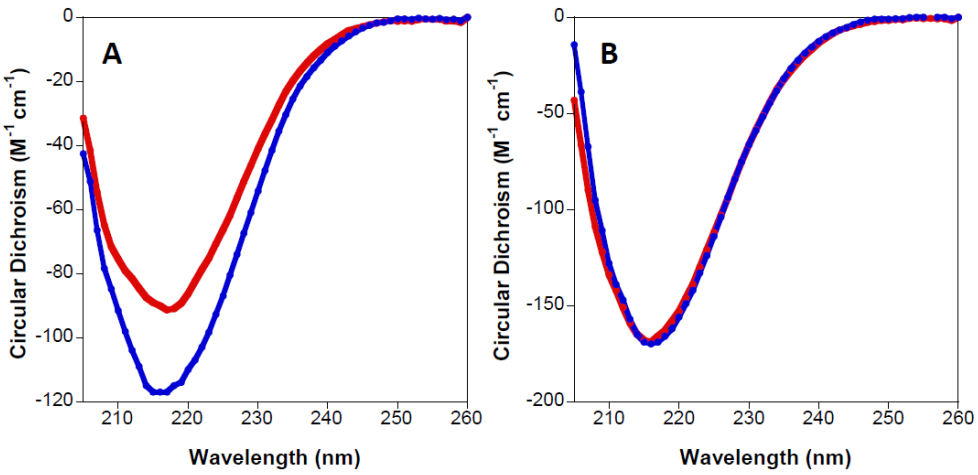

Figure 4.07 Circular Dichroism Spectra of Aβ Samples Incubated with Zn^{2+}.

A. $Aβ_{(1-40)}$ incubated with either no Zn^{2+} (red) or 0.05 mole equivalents of Zn^{2+} (blue). *B.* $Aβ_{(1-42)}$ incubated with either no Zn^{2+} (red) or 0.05 mole equivalents of Zn^{2+} (blue). CD readings were taken using a 0.1 cm path-length cuvette, and 20 μM Aβ samples were used, incubated with 5 mM HEPEs, at pH 7.4, under agitated conditions for over 200 hours.

4.3.4 Aβ Seeding with Zn^{2+}

It is notable that the influence of Zn^{2+} on Aβ formation does not occur in a stoichiometric manner; the data here have shown that even as little as 0.01 equivalents of Zn^{2+} substantially perturbs fibre formation. Thus, it is evident that a single Zn^{2+} ion can influence the assembly of many Aβ molecules, promoting and stabilising alternative assemblies rather than ThT binding amyloid fibres. This could occur through two potential mechanisms (Fig. 4.08): a seeding mechanism, in which Zn^{2+} binding causes an Aβ nucleus to adopt a conformation capable of recruiting monomeric Aβ to form the non-typical assemblies that have been observed here, or a dynamic exchange model, in which the rapid exchange of Zn^{2+} between Aβ molecules allows a greater number of Aβ molecules to be influenced by low levels of Zn^{2+} than one may otherwise expect.

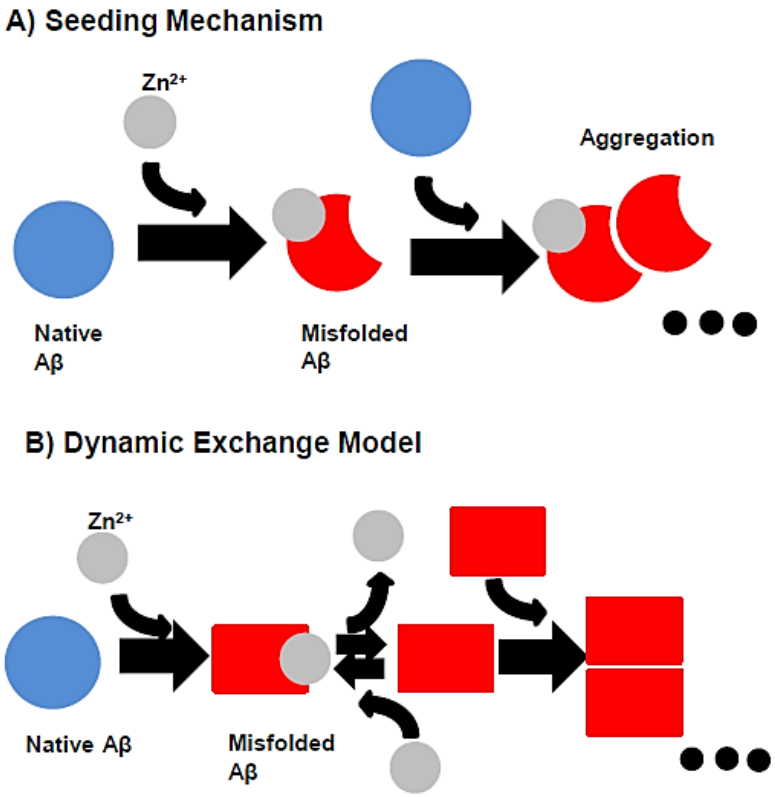

Figure 4.08 Mechanisms through which a Little Zn^{2+} May Affect Much Aβ.

Less than half a mole Zn^{2+} is required to abolish Aβ fibre growth in favour of alternative aggregative pathways. This may be because Zn^{2+} induces a conformational change in Aβ that nucleates non-fibrillar aggregation (*A*), or because Zn^{2+} is rapidly exchanged between Aβ peptides (*B*).

To investigate which mechanism is more likely, a seeding experiment (Fig. 4.09) analogous to the protein misfolding cyclic amplification experiments used for studying prion proteins (Barria et al, 2012) was carried out. In this experiment, monomeric Aβ was incubated with 0.4 mole equivalents of Zn^{2+} for a week, which was then used to seed a subsequent experiment, consisting of 10 % seed and 90 % monomeric Aβ, which in turn was incubated for a week and used to seed a further experiment.

This was repeated until there was only 0.0004 mole equivalents of Zn^{2+} present in the final experiment. It was found that ThT fluorescent signal generally increased between experiments, and by the final experiment the ThT fluorescence had approximately returned to that observed for monomeric Aβ incubated without Zn^{2+}. Supporting the ThT data, the TEM images demonstrate that Aβ aggregate species formed in later seeding experiments closely resembles the Aβ fibres produced in the absence of Zn^{2+}.

As the concentration of Zn^{2+} was reduced in sequential seeding experiments, Zn^{2+} induced aggregate species became less evident; this suggests that the dynamic exchange mechanism more accurately models how a small number of Zn^{2+} ions influence a large number of Aβ molecules. If a seeding mechanism was taking place, the Zn^{2+} induced aggregate species formed in the initial experiments would be able to promote formation of similar aggregates in sequential experiments, regardless of reductions in Zn^{2+} levels.

4.3.5 The Effect of Cu^{2+} and Zn^{2+} Mixtures on Aβ Misfolding

The presence of Cu^{2+} has also been shown to influence fibre formation (Bush, 2003; Chen et al, 2012; Chen et al, 2011; Faller et al, 2013; Matheou et al, 2015; Sarell et al, 2010; Viles, 2012). Additionally, both divalent metal ions are released at the synapse and are thought to chelate to Aβ via its histidine residues (Sarell et al, 2009). Consequently, it is striking that not only does Zn^{2+} influence Aβ fibre formation at much

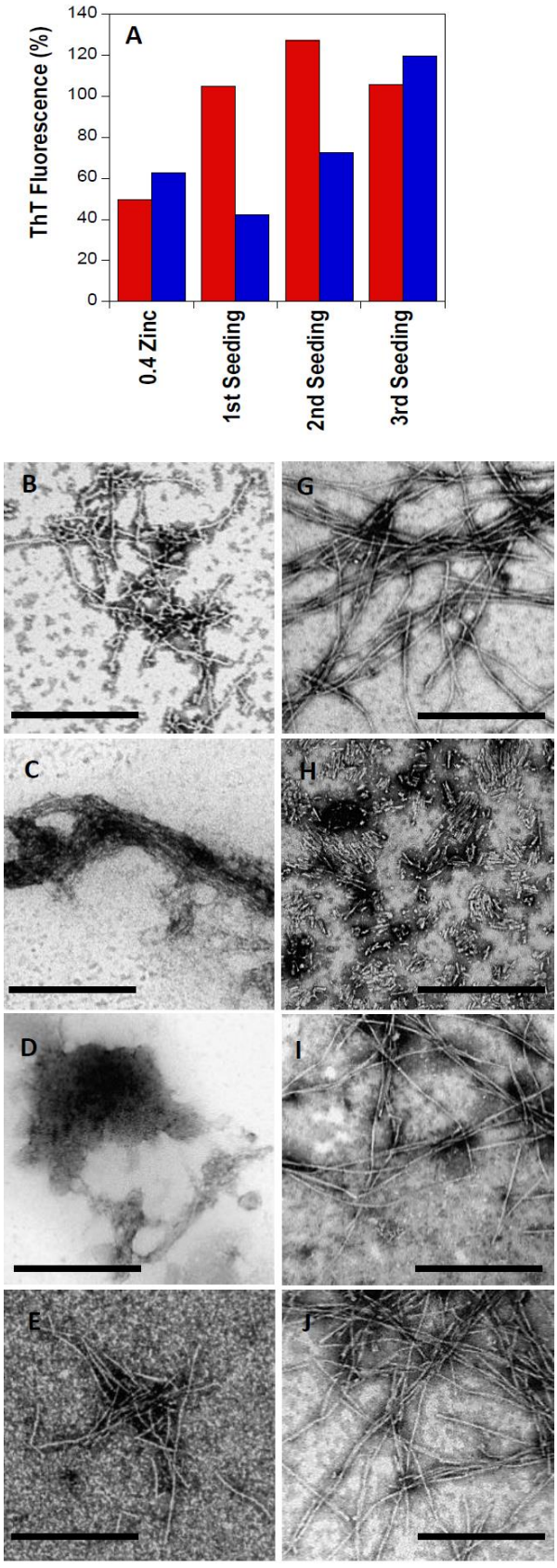

Figure 4.09 Aβ and Zn^{2+} Cross-Seeding Experiment.

A, Maximal ThT fluorescence of $Aβ_{(1-40)}$ (red) and $Aβ_{(1-42)}$ (blue) with 0.4 equivalents of Zn^{2+}, which after a week was used to seed monomeric Aβ (1st seeding), which in turn was also used to seed monomeric Aβ (2nd seeding), which again was used to seed monomeric Aβ (3rd seeding). Seeds were 10 % of final volume. Fluorescence is presented as a percentage of ThT fluorescence for mature $Aβ_{(1-40)}$ and $Aβ_{(1-42)}$ fibres grown in the absence of Zn^{2+}. Fibre growth was carried out at pH 7.4, with 10 μM Aβ, 30 mM HEPES, 10 mM NaCl and agitation, at 30 °C. *B – J.* Representative TEM images of mature $Aβ_{(1-42)}$ fibres (A), $Aβ_{(1-42)}$ grown with 0.4 equivalents of Zn^{2+} (B), 1st seeding for $Aβ_{(1-42)}$ (C), 2nd seeding for $Aβ_{(1-42)}$ (D), mature $Aβ_{(1-40)}$ fibres (G), $Aβ_{(1-40)}$ grown with 0.4 equivalents of Zn^{2+} (H), 1st seeding for $Aβ_{(1-40)}$ (I), 2nd seeding for $Aβ_{(1-40)}$ (J). Samples were stained with phosphotungstic acid. Scale bars are 500 nm. Zn^{2+} generated assemblies could not seed similar assemblies once Zn^{2+} was diluted.

lower equivalents than Cu^{2+}, but that it does so in a markedly different way. This is most evident for $A\beta_{(1-40)}$, for which substoichiometric Cu^{2+} accelerates fibre formation (Matheou et al, 2015; Sarell et al, 2010), while Zn^{2+} prevents fibre formation. To answer the question as to whether either of these metal ions could modulate or mask the other's effect, ThT fluorescence was used to follow $A\beta_{(1-40)}$ fibre growth in the presence of a variety of Cu^{2+}:Zn^{2+} mixtures. As is apparent in figure 4.10A, even when there was only a quarter as much Zn^{2+} as there was Cu^{2+}, the effect on fibre aggregation of Zn^{2+} predominated. In particular, ThT signal is reduced four-fold, and there is no acceleration in fibre growth. As the concentration of Zn^{2+} (100 – 300 μM) is generally thought to be higher than that of Cu^{2+} (15 – 250 μM) at the synapse (Hartter & Barnea, 1988; Kardos et al, 1989), the data suggests that *in vivo* the effect of Zn^{2+} may exert the greater influence on Aβ misfolding. This is supported by the TEM data, figure 4.10B; here the assembly outcome for mixtures of Zn^{2+} and Cu^{2+} (0.2 and 0.4 equivalents respectively) appears to be dominated by the presence of Zn^{2+}. $A\beta_{(1-40)}$ assembled into short fibril-like rods, that packed together in bundles, as is observed when $A\beta_{(1-40)}$ is incubated with Zn^{2+} in the absence of Cu^{2+}.

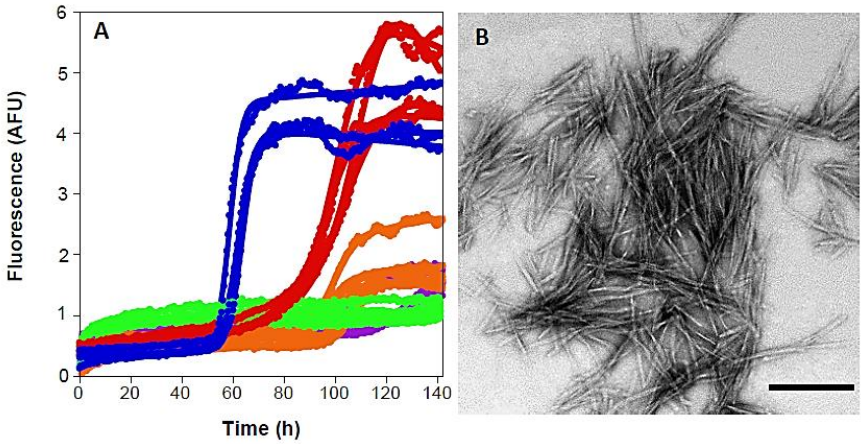

Figure 4.10 $A\beta_{(1-40)}$ Fibre Growth with Mixtures of Cu^{2+} and Zn^{2+}.

A. $A\beta_{(1-40)}$ fibre growth, monitored by Thioflavin T fluorescence, with no metal ions (red), 0.4 equivalents of Cu^{2+} (blue), 0.4 equivalents of both Cu^{2+} and Zn^{2+} (green), 0.4 equivalents of Cu^{2+} and 0.2 equivalents of Zn^{2+}(purple), and 0.4 equivalents of Cu^{2+} and 0.1 equivalents of Zn^{2+} (orange). Fibre growth was carried out at pH 7.4, with 10 μM $A\beta_{(1-40)}$, 30 mM HEPES, 10 mM NaCl and agitation, at 30 ^{o}C. (N = 3 – 6 Traces). *B.* Representative TEM image of $A\beta_{(1-40)}$ incubated with 0.4 mole equivalents of Cu^{2+} and 0.2 equivalents of Zn^{2+}. Samples were stained by phosphotungstic acid. Scale bar 200 nm. Assembly outcome is dominated by presence of Zn^{2+}.

DISCUSSION

4.4.1 Trace Zn^{2+} and Aβ Fibre Assembly

Here, it has been demonstrated that suprastoichiometric levels of Zn^{2+} completely abolish Aβ fibre growth, as has previously been reported (Garai et al, 2007; Ha et al, 2007; Raman et al, 2005; Sarell et al, 2010; Yoshiike et al, 2001), and induces $Aβ_{(1-40)}$ and $Aβ_{(1-42)}$ to form disordered tangled aggregates. As little as 0.01 mole equivalents of Zn^{2+} has also been shown to significantly influence the misfolding pathway of both $Aβ_{(1-40)}$ and $Aβ_{(1-42)}$. It is notable that the marked influence of such very low amounts of Zn^{2+} on Aβ assembly is even more remarkable when one considers the affinity of Zn^{2+} for Aβ. The effect is observable with 100 nM of Zn^{2+}, but Zn^{2+} affinity for Aβ is much weaker, ~ 10 μM, thus only a fraction of the 0.01 mole equivalents of Zn^{2+} will be bound to Aβ at any one time. It was surprising that a single Zn^{2+} ion can influence the aggregation of so many Aβ molecules, as each Zn^{2+} ion can only be bound to one or two Aβ molecules, at any one time. Ineed, Zn^{2+} cross-linking Aβ is insufficient to explain the very low substoichiometric amount of Zn^{2+} that effects fibre formation.

There are a number of potential mechanisms through which trace levels of Zn^{2+} could influence large numbers of Aβ molecules. For instance, the length of fibres may be restricted by Zn^{2+} bound Aβ peptide, capping the ends of fibres and limiting fibril length, or introducing sharp kinks into the fibre (Fig. 4.11). However, the stoichiometric ratio of Zn^{2+} to Aβ does not correlate clearly to fibre length. An alternative explanation could be the rapid exchange of Zn^{2+} between Aβ peptides. For fibrillogenesis, Aβ monomers need to adopt a specific conformation to bind to a growing fibre (Sgourakis et al, 2007; Srabasti Acharya, 2015; Yang & Teplow, 2008); however, Zn^{2+} may rapidly exchange between Aβ peptides, restricting the population of conformations typically available to them, and preventing the necessary conformation forming. These transient interactions with Zn^{2+} may also restrict fibril length or introduce kinks (Fig. 4.11).

A third possibility would be that Zn^{2+} binding promotes the formation of a unique seed, which may direct downstream Aβ aggregation through a template mechanism, though the seeding experiment showed this to be unlikely. Instead the data supports a dynamic exchange of Zn^{2+} between Aβ peptides as the most credible of these possibilities; this is consistent with ^{1}H NMR data that suggest a rapid exchange of Zn^{2+} between Aβ peptides (Danielsson et al, 2007 ; Syme & Viles, 2006). It is also notable that the data demonstrates that Zn^{2+} induced off-pathway assemblies do not readily form fibres, even once Zn^{2+} is removed. Interestingly, although assemblies generated with Zn^{2+}-$Aβ_{(1-40)}$ have a weak ThT fluorescence, studies using ss-NMR suggest the basic cross-β structure is maintained (Mithu et al, 2011), which is supported by the CD data presented here.

The data show that trace levels of Zn^{2+} influence $Aβ_{(1-40)}$ and $Aβ_{(1-42)}$ misfolding in distinct ways; with $Aβ_{(1-40)}$, Zn^{2+} induces formation of short rod-like structures that stack together in bundled structures, whereas with $Aβ_{(1-42)}$, Zn^{2+} typically promotes the formation of short crooked disordered fibrous assemblies that knit together. Solomonov *et al.* has shown that at 2 hours, Zn^{2+} promotes formation of disk shaped oligomers 10 nm in diameter (Solomonov et al, 2012); however, the structures presented here represent Zn^{2+}-Aβ at equilibrium. The dissimilarity in how substoichiometric levels of Zn^{2+} influence $Aβ_{(1-40)}$ and $Aβ_{(1-42)}$ isoforms may arise from differences in the fibril assembly pathways (Bitan et al, 2003; Chen & Glabe, 2006), as $Aβ_{(1-42)}$ fibre growth is believed to be nucleated by pentamer / hexamer oligomer units not formed in $Aβ_{(1-40)}$ fibrillogenesis (Bitan et al, 2003). Additionally, differences in the kinetics of aggregation for $Aβ_{(1-40)}$ and $Aβ_{(1-42)}$, may be a contributor, as $Aβ_{(1-42)}$ aggregates much more readily than $Aβ_{(1-40)}$ (Burdick et al, 1992).

The data presented here compliment a number of studies already in the literature. For instance, it has been well established, with ThT fluorescence, TEM, and atomic force

microscopy, that Zn^{2+} greatly perturbs amyloid fibril growth (Chen et al, 2012; Chen et al, 2011; Garai et al, 2007; Ha et al, 2007; Klug et al, 2003; Raman et al, 2005; Solomonov et al, 2012), and that metal ions, such as Zn^{2+} and Cu^{2+}, may influence $Aβ_{(1-40)}$ and $Aβ_{(1-42)}$ aggregation in markedly different ways (Chen et al, 2012; Chen et al, 2011; Sarell et al, 2010), as has been observed here. However, it has also been demonstrated here that levels of Zn^{2+} as low as 0.01 mole equivalents are sufficient to profoundly inhibit $Aβ_{(1-40)}$ and $Aβ_{(1-42)}$ fibre formation, and that this may occur through a rapid exchange of Zn^{2+} between Aβ molecules.

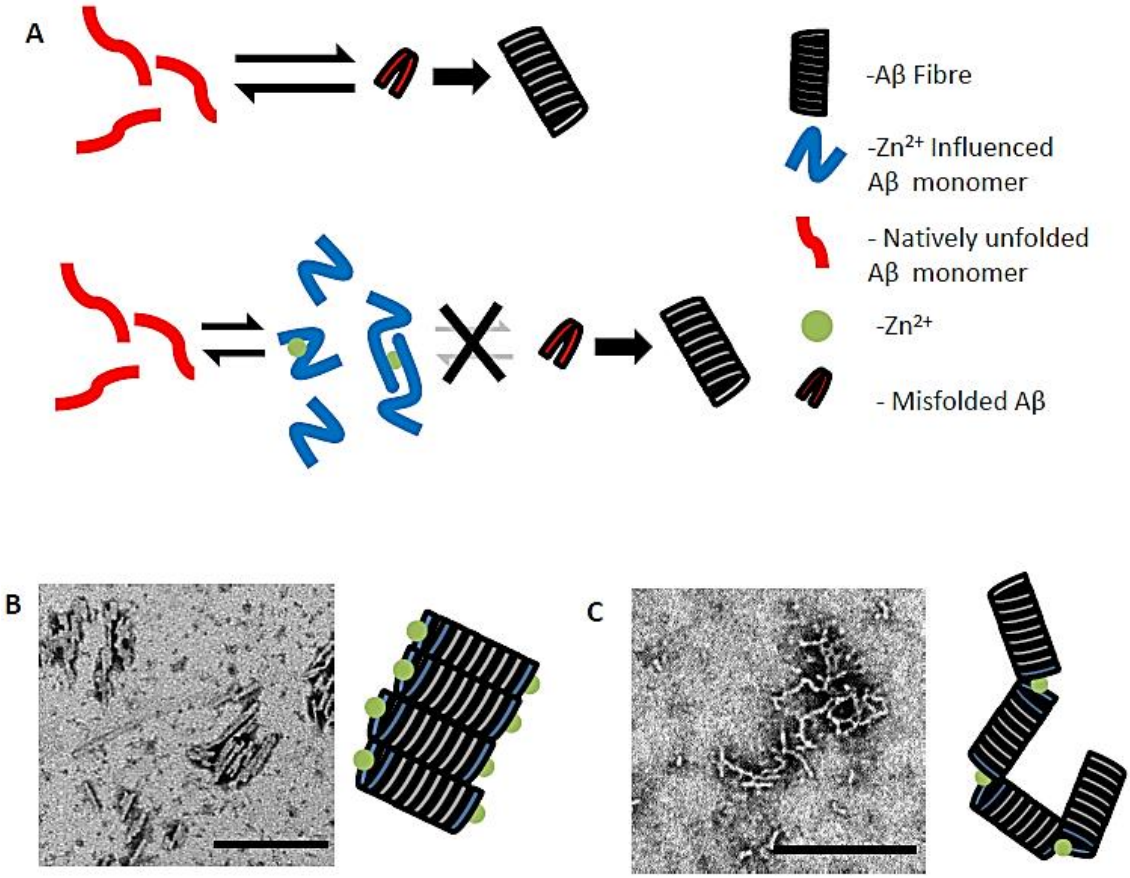

Figure 4.11 Schematics of Zn^{2+} Induced Aggregation.

A. Binding of Zn^{2+} to Aβ peptide in rapid exchange prevents a large number of Aβ molecules from forming fibres. A single Zn^{2+} ion may influence a great number of Aβ peptides through capping the ends of fibres, and inducing formation of bundles of short rods (*B*) or crooked assemblies (*C*). Scale bars, 200 nm.

Though this is supported by previous atomic-force microscopy data (Innocenti et al, 2010), it does not agree with a recent study on $A\beta_{(1-40)}$ using ThT binding, which found that though low levels of Zn^{2+} retarded fibre growth, 0.0125 – 0.125 mole equivalents of Zn^{2+} did not reduce the final amount of fibres formed (Abelein et al, 2015). This may be because the growth conditions used differed between experiments, as they used quiescent conditions, which generates fibres with differing biophysical properties to those grown under agitated conditions, as for our experiment (Paravastu et al, 2008; Petkova et al, 2005). The different observations may also arise from their use of phosphate buffer, as phosphate is known to co-precipitate with Zn^{2+} (Bachra & van Harskamp, 1970; Kejnovsky & Kypr, 1998), and may result in overestimation of the concentration of available Zn^{2+} ions in solution.

Several experiments were carried out to contextualise the results to an *in vivo* environment. *In vivo,* Zn^{2+} is released at the synapse with glutamate (Assaf & Chung, 1984; Howell et al, 1984; Nydegger et al, 2010; Qian & Noebels, 2006), so it was important to determine whether glutamate modulated the effect of Zn^{2+} upon Aβ. Glutamate did not prevent Zn^{2+}'s affect, indicating glutamate's affinity, K_{d1} = 600 μM at pH 7.4 (Dawson, 1986), for Zn^{2+} is not sufficient to prevent Zn^{2+} influencing Aβ assembly. Additionally, as levels of Zn^{2+} fluctuate in the brain with depolarisation (Kardos et al, 1989; Vogt et al, 2000), it was of interest to observe the effect of Zn^{2+} upon preformed mature fibrils and also the reversibility of Zn^{2+} induced aggregation. It was found that Zn^{2+} did not influence mature Aβ fibrils, nor did removal of Zn^{2+} enable aggregates formed with Zn^{2+} to revert and form fibres. This suggests the misfolding pathway of Zn^{2+} induced aggregate species is distinct from that of amyloid fibril growth; in contrast, protofibril assemblies of $A\beta_{(1-42)}$ generated by the presence of Cu^{2+} will rapidly seed fibre formation upon Cu^{2+} chelation (Matheou et al, 2015).

4.4.2 Contrasting and Dominating Influence of Zn^{2+} of Cu^{2+} in Fibre Assembly

Another divalent metal ion that is thought to be important in AD pathology is Cu^{2+} (Matheou et al, 2015; Sanokawa-Akakura et al, 2010; Sarell et al, 2010; Singh et al, 2013; Sparks & Schreurs, 2003; Viles, 2012). Interestingly, although the two divalent metal ions share a number of the same coordination ligands (Alies et al, 2013; Danielsson et al, 2007 ; Faller & Hureau, 2009; Minicozzi et al, 2008; Sarell et al, 2009; Silva & Saxena, 2013; Syme & Viles, 2006), there are marked differences in the influence of Zn^{2+} and Cu^{2+} on Aβ misfolding, as outlined in Table 4.1. In particular, substoichiometric Cu^{2+} much more markedly accentuates differences in $Aβ_{(1-40)}$ and $Aβ_{(1-42)}$ misfolding, as substoichiometric Cu^{2+} abolishes $Aβ_{(1-42)}$ fibre growth but accelerates $Aβ_{(1-40)}$ fibre growth (Matheou et al, 2015; Sarell et al, 2010), while substoichiometric Zn^{2+} prevents fibre growth for both alloforms. A further difference between Zn^{2+} and Cu^{2+} is the amount that is required to disrupt Aβ misfolding, with Zn^{2+} having a much greater influence at lower levels than Cu^{2+}. In particular, the influence of Cu^{2+} on Aβ assemblies is only apparent at stoichiometries of greater than 0.25 (Matheou et al, 2015; Sarell et al, 2010), 25 times greater than the 0.01 levels of Zn^{2+} required to disrupt fibre growth.

The differences in the effects of Cu^{2+} and Zn^{2+} may in part be due to differences in their on/off exchange rate with Aβ. Furthermore, unlike Cu^{2+}, Zn^{2+} is capable of forming flexible open coordination geometries with Aβ (Minicozzi et al, 2008), which enable Zn^{2+} to mediate Aβ cross-linking (Minicozzi et al, 2008; Sarell et al, 2010), while Cu^{2+} does not promote Aβ cross-linking at the concentrations used (Drew et al, 2009; Syme et al, 2004). Finally, it may also be that a single Zn^{2+} binding exerts longer-range intermolecular influence across an Aβ assembly than Cu^{2+} (or affects larger, specific, aggregates), enabling Zn^{2+} to affect Aβ aggregation at an exceptionally low substoichiometry, as it is the larger assembly that is essentially the Zn^{2+}'s binding partner. As the dose-dependent effect of Zn^{2+} upon Aβ aggregation would be

	Zn^{2+}		Cu^{2+}	
	Substochiometric	**Suprastochiometric**	**Substochiometric**	**Suprastochiometric**
$Aβ_{(1-40)}$	Stacks of short rod-like assemblies – Weak ThT signal	Networked tangled aggregates – Almost no ThT signal	Amyloid fibres – Strong ThT signal	Amorphous aggregates – No ThT signal
$Aβ_{(1-42)}$	Networked tangled aggregates – Weak ThT signal and off-pathway to fibre formation	Networked tangled aggregates – Almost no ThT signal	Oligomers and protofibrils – No ThT signal but on-pathway to fibre formation	Amorphous aggregates – No ThT signal

Table 4.01 Aβ Aggregate Species in the Presence of Metal Ions.

This table shows the predominant species of Aβ aggregate formed upon reaching equilibrium, after 200 hours, in the presence of Zn^{2+} and Cu^{2+}, at pH 7.4, with 10 μM Aβ, 30 Mm HEPES, 10 mM NaCl and agitation, at 30 ^{o}C.

proportional to the size of any such aggregate, future quantitative analysis of Aβ fibre kinetics at a range of Zn^{2+} concentrations could provide valuable insights into what sized Aβ assembly a single Zn^{2+} ion is able to influence.

As both Cu^{2+} and Zn^{2+} are elevated in AD, and both metal ions are released at the synapse, but differ in their relationship to Aβ, the present study sought to determine the net effect when $Aβ_{(1-40)}$ was incubated with mixtures of Zn^{2+} and Cu^{2+}. It was surprising that when both ions were present, Cu^{2+} had little influence upon $Aβ_{(1-40)}$ fibre growth. Although the affinity of Cu^{2+} for Aβ is much higher than Zn^{2+} (by more than 5 orders of magnitude), 50 pM and 10 μM respectively (Danielsson et al, 2007 ; Sarell et al, 2009), the rapid exchanging of Zn^{2+} between Aβ molecules may enable Zn^{2+} to influence a large number of Aβ peptide conformations, explaining Zn^{2+} induced aggregation dominating Aβ assembly outcomes in mixtures of substoichiometric Cu^{2+} and Zn^{2+}. Alternatively, differences in the size of the aggregates that Cu^{2+} and Zn^{2+} influence may facilitate Zn^{2+} determining assembly outcomes. Either way, these results highlight that Zn^{2+} may be important in AD pathology, not only through directly influencing Aβ misfolding, but through attenuating the effect of other factors, such as Cu^{2+}. For

instance, *in vivo*, Cu^{2+} levels may become elevated, but have no effect due to a dominant influence of Zn^{2+}, or alternatively, Cu^{2+} levels may remain stable, but changes in Zn^{2+} levels result in an associated change in the relationship between Cu^{2+} and Aβ. The fact that substoichiometric levels of Zn^{2+} influence Aβ misfolding differently to suprastoichiometric levels, and that Zn^{2+} may influence the effect of Cu^{2+}, provides an explanation as to why Zn^{2+} supplementation has been found to both attenuate and potentiate Alzheimer's like symptoms in animal studies (Adlard et al, 2008; Adlard et al, 2010; Corona et al, 2010; Linkous et al, 2009), as not only is Aβ misfolding extremely sensitive to Zn^{2+}, but also to the ratio of Aβ and Zn^{2+}, as well as its interplay with Cu^{2+}.

To conclude, since the first suggestion that Zn^{2+} can influence Aβ aggregation (Bush et al, 1994), both Zn^{2+} and Cu^{2+} homeostasis has been implicated in AD pathology, through a number of animal studies (Adlard et al, 2008; Adlard et al, 2010; Linkous et al, 2009; Sanokawa-Akakura et al, 2010; Singh et al, 2013; Sparks & Schreurs, 2003). Additionally, Zn^{2+} is prevalent at the glutamatergic neurons, that are in fact often described as zincergic neurons (Brown & Dyck, 2004; Takeda et al, 2013), and found to be greatly diminished in AD (Butterfield & Pocernich, 2003). This study highlights the many variables to be considered in delineating the role of Zn^{2+} and Cu^{2+} in AD pathology, as effect will be dependent on Aβ isoform, metal ion-Aβ stoichiometry, and relative metal ion concentrations. This complexity is underscored by finding that shifts of 0.01 equivalents of Zn^{2+} (100 nM) are sufficient to change the misfolding landscape of Aβ. However, a complex system also provides many routes for intervention, in this particular case, chelation/supplementation of Zn^{2+}/Cu^{2+} could provide such a route. A high-throughput screening in a yeast model of Aβ toxicity found that a Zn^{2+}/Cu^{2+} chelator, clioquinol, ameliorated Aβ toxicity (Matlack et al, 2014). Clioquinol has also been found to inhibit Aβ deposition and ameliorate symptoms, in a mouse model of AD (Cherny et al, 2001), further emphasising the potential importance of regulating metal homeostasis in Alzheimer's disease.

CHAPTER 5: The Effect of Cu^{2+} on $A\beta_{(1-40)}$ Fibre Stability

5.1 ABSTRACT

With substoichiometric Cu^{2+}, $A\beta_{(1-40)}$ forms fibres much more rapidly, and with an elevated pathogenicity. However, it is not clear how these fibres may differ in their physical properties, or how dependent their formation is on environment. As amyloid fibril stability has been linked to toxicity, $A\beta_{(1-40)}$ fibre stability was compared, with and without Cu^{2+}. In the presence of the denaturant guanidinium chloride, a protein denaturant, it was found that the fibres did not differ in their stability with Cu^{2+} present, but did appear to dissociate at surprisingly low concentrations of denaturant. In contrast, Aβ fibres were found to retain their ThT fluorescent structure at 90^{o}C, indicating that they have a high thermal stability. It was also found that Cu^{2+} increases rate of $A\beta_{(1-40)}$ fibre growth under both agitated and quiescent conditions, despite distinct $A\beta_{(1-40)}$ fibril morphologies forming in these two environments. These investigations suggest that increased rate of fibre formation is a general property of the Cu^{2+}-$A\beta_{(1-40)}$ interaction, independent of fibre morphology, and that Cu^{2+} does not confer an increase in $A\beta_{(1-40)}$ toxicity through a reduction in fibre stability.

5.2 INTRODUCTION

It is well established, at least for mammalian prion protein, that amyloid fibre stability is correlated with toxicity (Colby et al, 2009). This is illustrated by the high degree of covariance found between prion fibre stability and incubation time of prion disease pathology in mice; with the most stable fibres possessing the longest incubation time, it is suggested that a fibre's stability is inversely related to its toxicity (Colby et al, 2009). This is supported by work demonstrating that amyloid fibril fragmentation increases cytotoxicity (Xue et al, 2009; Xue et al, 2010). Thus, factors associated with AD pathology may impact disease aetiology through decreasing Aβ fibril stability, and leading to a concurrent increase in Aβ toxicity.

A particularly significant characteristic in AD is the alteration of metal ion concentration and homeostasis in the brain (Barnham & Bush, 2008), specifically Cu^{2+} ions. Chapter 3 demonstrated that Cu^{2+} accentuates differences in the aggregative properties of $A\beta_{(1-40)}$ and $A\beta_{(1-42)}$, accelerating $A\beta_{(1-40)}$ fibre growth, while stabilising $A\beta_{(1-42)}$ oligomers (Matheou et al, 2015). This was also found to increase the pathogenic potential of $A\beta_{(1-42)}$, presumably due to the greater toxicity of oligomers over fibres (Lambert et al, 1998; Lue et al, 1999). However, it has been previously reported that Cu^{2+} may also increase the cytotoxicity of $A\beta_{(1-40)}$ fibres (Sarell et al, 2010). Consequently, the hypothesis was advanced that Cu^{2+} may reduce $A\beta_{(1-40)}$ fibre stability, and in doing so, heighten fibril toxicity. To evaluate this hypothesis, fibril stability was investigated, with both chemical (Guanidinium Chloride (GdnCl)), and thermal denaturation, using ThT fluorescence and circular dichroism (CD) to measure fibre dissociation.

A caveat to generating amyloid fibres *in vitro* is that they may differ in morphology from amyloid fibres *in viv*o (Paravastu et al, 2008; Petkova et al, 2005). To establish that the increased rate of fibre growth with Cu^{2+} ions is not dependent on fibre morphology, the growth conditions of fibres were altered, growing them quiescently rather than in agitated conditions; this has been shown to switch fibril structure from a 2-fold to a 3-fold axial-symmetry (Petkova et al, 2005). The overall purpose of this study was to clarify how Cu^{2+} may influence $A\beta_{(1-40)}$ fibre properties, stability in particular, and how this may relate to AD progression *in vivo.*

5.3 RESULTS

5.3.1 Stability of Fibres in the Presence of Guanidinium Chloride

Prompted by the observation that, in the case of mammalian prions, fibril stability (ΔG of disassembly as measured by midpoint of unfolding in the presence of a chemical denaturant) is related to toxicity (Colby et al, 2009), this study sought to compare the

stability of fibres generated with Cu^{2+} and those generated without Cu^{2+}, to delineate whether a change in $A\beta_{(1-40)}$ fibre stability may be responsible for the potentiation of $A\beta_{(1-40)}$ fibre toxicity (Sarell et al, 2010). To obtain insight into the stability of fibres, they were exposed to a range of concentrations of GdnCl, a chemical denaturant, and followed fibre dissociation through measuring loss of ThT fluorescence, using a single-cell fluorescent spectrophotometer.

It was expected that the present would have a stability typical of globular proteins, or perhaps a higher stability. However, it was instead found that dissociation of fibres begins at ~ 0.03 M GdnCl, and ends by 1 M GdnCl with a midpoint of ~0.24 M GdnCl. This is illustrated in Figure 5.01, with ThT fluorescence signal for $A\beta_{(1-40)}$ fibres dropping from 900 AFU to 400 AFU with 1 M GdnCl.

Comparison of the normalised unfolding curves for $A\beta_{(1-40)}$ fibres generated with and without Cu^{2+} present appear essentially identical. This is emphasised by the similarity of the transition midpoints for the two fibres, 0.23 ± 0.009 M for fibres generated without Cu^{2+}, and 0.25 ± 0.014 M for fibres generated with Cu^{2+}. Curves were fitted as discussed in chapter 2 (Eq. 2.04).

A source of concern, was that despite no further dissociation occurring at > 1 M GdnCl, there was still a persistent fluorescent signal contributing ~30 – 50 % of the max fluorescence. It was determined that this could either be some erroneous artefact, perhaps from a scattering of the excitation beam, or, alternatively, be due to the presence of a durable sub-population of $A\beta_{(1-40)}$ fibres, capable of enduring an ever increasing concentration of GdnCl. The observation that $A\beta_{(1-40)}$ fibres should undergo a significant dissociation at a relatively low concentration of GdnCl was surprising, as amyloid fibrils are commonly found to be resistant to conditions that would denature most other proteins (Meersman & Dobson, 2006). A further source of concern was that GdnCl may interfere with ThT fluorescent signal. Consequently, verification of the

results with an alternative method for detecting the presence of β-sheet fibres was needed; for this, CD was used.

CD provides information on the secondary structure of a protein, and as β-sheet structures possess a negative peak at 217 nm, one is able to follow the dissociation of β-sheeted amyloid fibrils by measuring loss of signal at 217 nm. CD spectra were recorded in the presence and absence of 0.5 M GdnCl, because at this concentration of GdnCl, the fluorescence data (Fig 5.01b) would suggest, 80 % of amyloid fibres are dissociated if the persistent fluorescent signal is merely an artefact; however, if the continued fluorescent signal is instead due to a durable sub-population of fibres, one would expect only ~ 40 % loss of signal at 0.5 M GdnCl. As can be seen in figure 5.02, the addition of 0.5 M GdnCl caused a very marked 80 % drop in signal at 217 nm. This supports the fluorescent data, suggesting that relatively small amounts of GdnCl (1 M) will completely disassemble fibres.

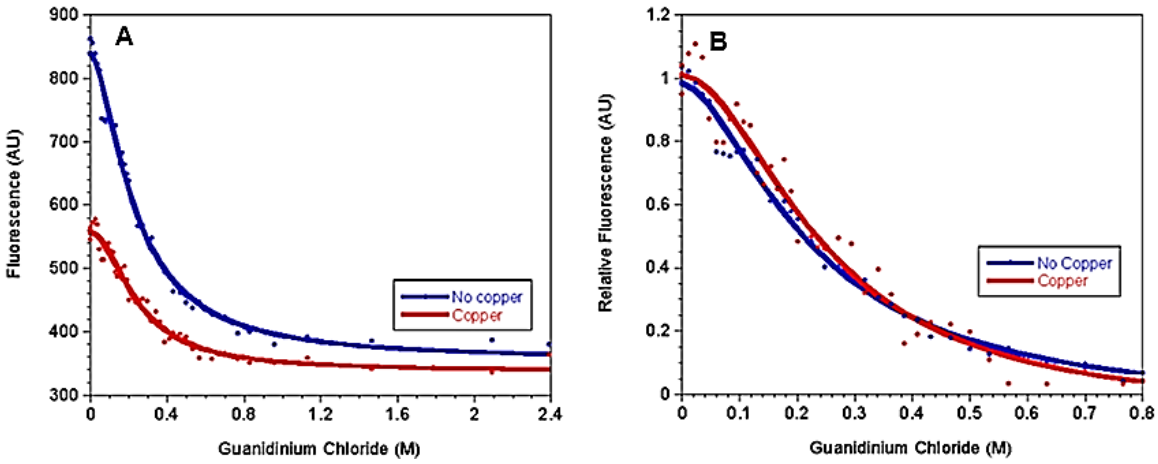

Figure 5.01 Stability of Aβ Fibres when Exposed to Guanidinium Chloride.

(A) Using a single-cell fluorescent spectrophotometer and measuring fluorescence at 489 nm, it was found that $A\beta_{(1\text{-}40)}$ fibres generated with 0.5 mol eq Cu^{2+} (*red trace*) and without Cu^{2+} (*blue trace*) begin to dissociate at ~0.03 M GdnCl. Additionally, loss of fluorescence plateaus at ~1.2 M GdnCl. (B) This figure shows the data normalised to both maximal and minimal ThT fluorescence. The transition midpoints for these curves are 0.23 M (with Cu^{2+}) and 0.25 M (without Cu^{2+}).

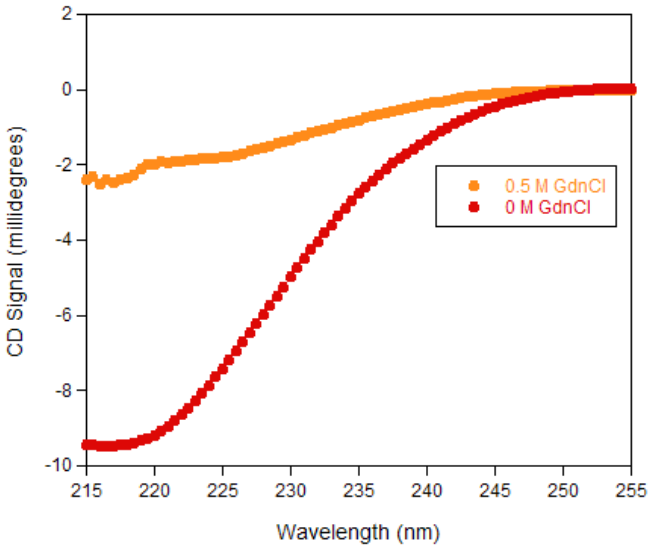

Figure 5.03 Verifying the Susceptibility of Aβ Fibres to Chemical Denaturation.

This figure shows the CD spectra (215 – 255 nm) of $A\beta_{(1-40)}$ fibres (grown with 60 µM amyloid-β, 30 mM HEPES, 5 mM NaCl, and 120 µM ThT) which had either been exposed to 0 M GdnCl, or 0.5 M GdnCl. CD readings were taken using a 0.1 cm path-length cuvette. A complete spectrum was obtained for fibres exposed to no GdnCl, showing a peak at 217 nm that corresponds to their β-sheet structure. For fibres exposed to 0.5 M GdnCl, GdnCl interfered with readings below ~220 nm; however, the data provides a reasonable estimate that the signal has dropped by ~ 80 %.

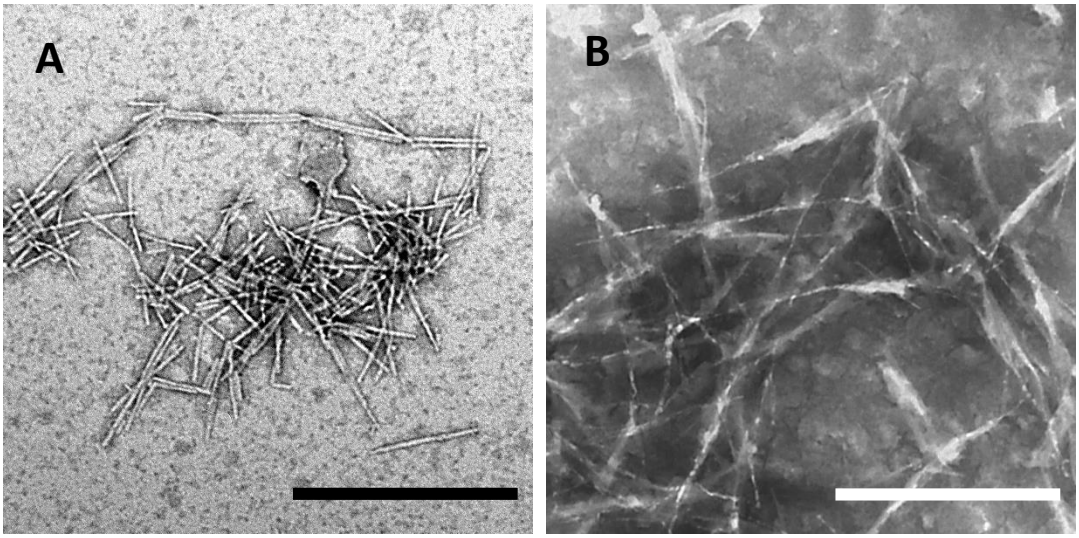

Figure 5.02 TEM images of Guanidinium Chloride Treated Aβ Fibres.

This figure shows representative TEM images of $A\beta_{(1-40)}$, in the absence of GdnCl (A), and in the presence of 0.5 M GdnCl (B). TEM images were stained with phosphopungstic acid. Scale bars are 500 nm.

The two CD samples were examined under TEM (Fig. 5.03), revealing the profound effect that 0.5 M GdnCl has upon $A\beta_{(1-40)}$ fibre integrity. It was found that in the presence of 0.5 M GdnCl, although a fibrous structure is maintained, the fibres lose their definition, no longer obviously being composed of distinct filaments with regular twists. Additionally, they appear much more diffuse, which is reflected by an increase in their width, expanding to be 20 – 50 nm wide, as opposed to 10 – 20 nm wide.

5.3.2 Thermal Stability of Amyloid-β Fibres

The investigations with GdnCl and $A\beta_{(1-40)}$ fibres prompted further probing of their stability. It was decided to assess how susceptible $A\beta_{(1-40)}$ fibres were to thermal denaturation, using ThT fluorescence. For this, a sample was placed in a water bath, and once it had incubated at the desired temperature for 5 minutes, was placed in a fluorescent spectrophotometer, cooled down to the initial temperature (10 ^{o}C), and a ThT fluorescence reading was taken. All fluorescent measurements were recorded at 10 ^{o}C, as fluorescence intensity may be temperature dependent. It was reasoned that thermal disassembly of fibres will happen rapidly (within 5 minutes), as the process of fibre disassembly is similar to the thermal unfolding of a globular protein, but that reassembly of Aβ into fibres would be slow, taking many hours in quiescent conditions. It was found that the fluorescent spectra of the sample was essentially unaltered with heating, as illustrated in Figure 5.04; additionally, the insert highlights that there was found to be no significant trend between fluctuations in fluorescence intensity and rising temperature. This suggests that Aβ fibres are stable at temperatures up to 90 ^{o}C.

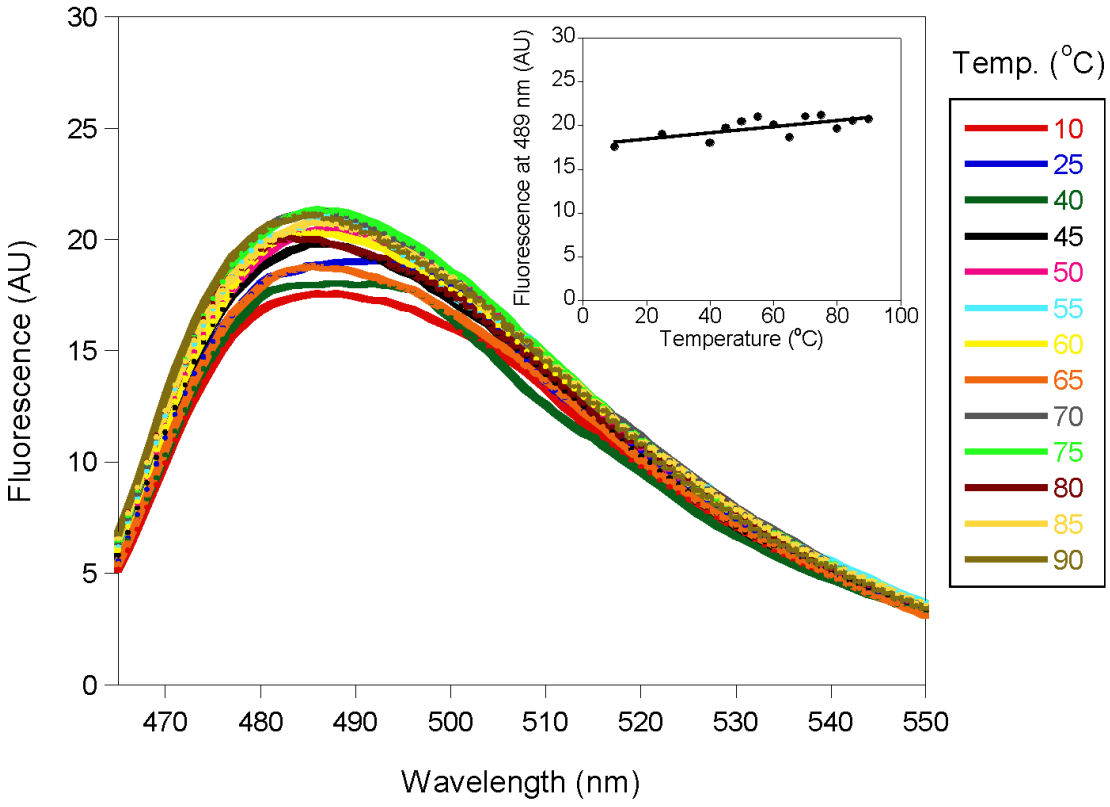

Figure 5.04 Aβ Fibres are Resistant to Thermal Denaturation

This figure shows fluorescent spectra for fibres (grown from 10 µM $A\beta_{(1\text{-}40)}$ with agitation) upon successive exposure to increasing temperatures. Samples were heated in a water bath to reach the desired temperature for 5 mins, and then cooled back down to 10 °C. The sample was then excited at 440 nm, and readings were taken from 420 nm to 600 nm in a fluorescent spectrophotometer. The *insert* summarises how the intensity of fluorescence at 489 nm changed with temperature.

5.3.3 Cu^{2+} Accelerates Fibre Growth under both Quiescent and Agitated Conditions

Fibres were grown using a 96-well plate assay, for which the binding of ThT to Aβ fibrils is used to monitor the kinetics of fibre formation. Fibres were initially generated using the same conditions as previously used (Sarell et al, 2010), with readings being taken every 30 min, and the plate undergoing 30 s of agitation prior to each fluorescence measurement. The concentration of $A\beta_{(1\text{-}40)}$ was 10 μM, with either no Cu^{2+} or half molar equivalence of Cu^{2+}. As shown in figures 5.05a and 5.05b, Cu^{2+} clearly influences fibre growth kinetics under these conditions, and a comparison of the median time needed to reach half-maximal ThT intensity (t_{50}) for fibres grown with Cu^{2+} (t_{50} = 73 hour median) and without Cu^{2+} (t_{50} = 126 hour median) supports the previous observation that Cu^{2+} approximately halves the t_{50} of Aβ fibre growth (Matheou et al, 2015; Sarell et al, 2010).

To assess whether the effect of Cu^{2+} on fibre growth kinetics was dependent upon fibre morphology, fibres were generated with no agitation; this changes fibre symmetry from 2-fold to 3-fold (Petkova et al, 2005). As growing fibres quiescently also greatly increases the time for fibres to form, the time between readings was changed to 2.8 hours. As illustrated in Figures 5.05C and 5.05D, Cu^{2+} still markedly influences fibre growth kinetics when fibres are grown quiescently, with the median t_{50} of fibre growth falling from 795 hours, for fibres grown without Cu^{2+}, to 565 hours, for fibres grown with Cu^{2+}. These results provide evidence to suggest that the manner in which Cu^{2+} alters the kinetics of Aβ fibre growth is not wholly dependent upon fibril structure.

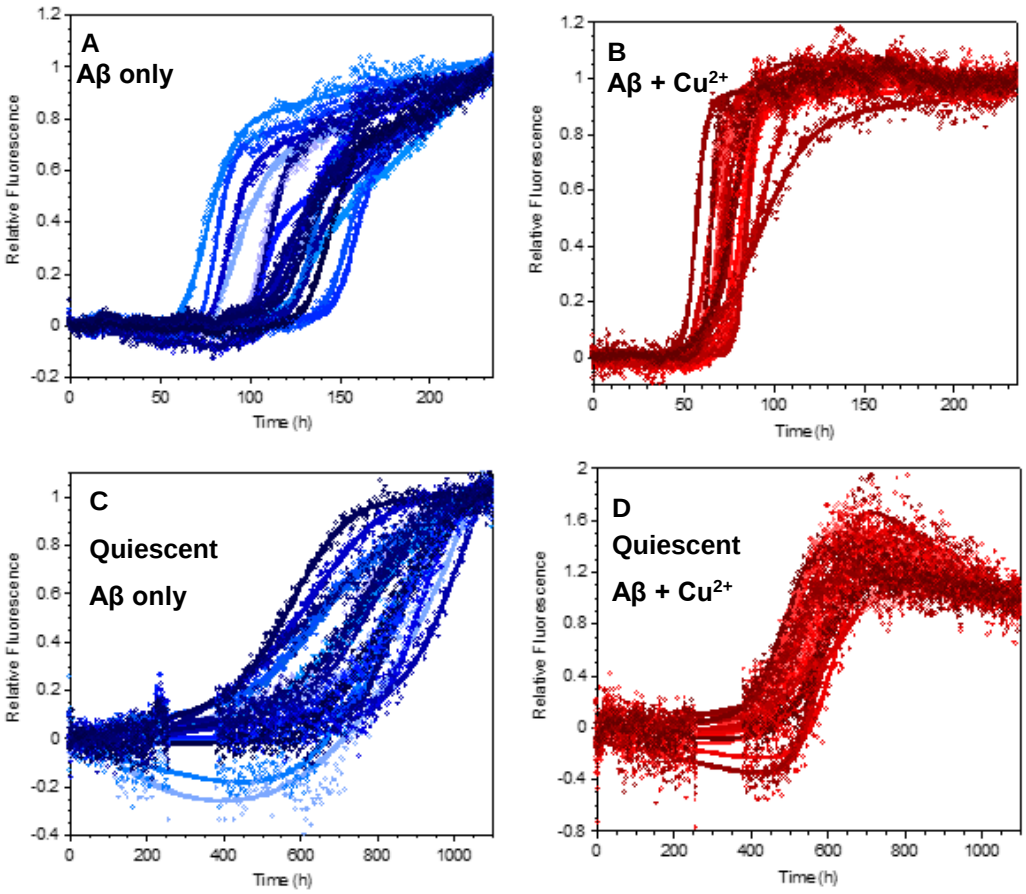

Figure 5.05 The Effect of Cu^{2+} on $Aβ_{(1-40)}$ Fibre Growth.

Fibre growth curves for 10 μM $Aβ_{(1-40)}$, with 0.5 mol eq Cu^{2+} (*red traces*) and without Cu^{2+} (*blue traces*) are shown. Fibres were grown with 20 μM ThT, 30 mM HEPES and 160 mM NaCl, at 30 ^{o}C and a pH of 7.4.ThT fluorescence is normalised to maximal fluorescence, and for each condition there are 20 representative traces from one 96-well plate. Figures *A* and *B* show samples that were agitated for 30 seconds every 30 mins; at these conditions, the median t_{50} for fibre growth was 73 hours with Cu^{2+} and 126 hours without Cu^{2+}. Figures *C* and *D* show samples that were grown without agitation; at these conditions, the median t_{50} for fibre growth was 565 hours with Cu^{2+} and 795 hours without Cu^{2+}.

5.4 Discussion

Here, the resistance of $A\beta_{(1-40)}$ fibres to both chemical and thermal denaturation has been investigated. Amyloid fibres are generally thought to be extremely resistant to thermal denaturing conditions, such as the amyloid fibres of insulin and Ure2p, both of which require over 100 ^{o}C for complete dissociation (Arora et al, 2004; Baxa et al, 2004). However, as discussed in a review on the pressure-temperature stability of amyloid fibres (Meersman & Dobson, 2006), amyloid fibres are thought to be relatively sensitive to chemical denaturation, in contrast to their high temperature resistance. Indeed, previous work with Aβ fibres has shown that < 1 M GdnCl causes substantial destabilisation of Aβ fibres (Chen et al, 2011; Lee et al, 2007). Although the data in this chapter is rather preliminary, the data suggests that Aβ may form fibres that are at once very resistant to thermal denaturation, while being highly sensitive to chemical denaturation. This supports the notion that though Aβ fibrils are thermodynamically stable, this stability is exceptionally dependent upon hydrophobic interactions (Meersman & Dobson, 2006), as evidenced by the $A\beta_{(1-40)}$ fibres readily dissociating in the presence of GdnCl, a chaotropic salt that increases the solubility of Aβ (Meersman & Dobson, 2006; Sawyer & Puckridge, 1973).

To determine whether generating $A\beta_{(1-40)}$ fibres in the presence of Cu^{2+} altered fibre stability, chemical denaturation was used, as Cu^{2+} has been found to dissociate $A\beta_{(1-42)}$ fibres (Matheou et al, 2015). Additionally, it has been found that amyloid fibre stability may influence fibre toxicity (Colby et al, 2009). It was found there was no significant difference in the sensitivity of the fibres to chemical denaturation, suggesting that the increase in toxicity conferred by Cu^{2+} ions is not associated with fibre stability. Thus, in this case, the heightened toxicity appears to come from elsewhere, potentially from Cu^{2+} redox activity, resulting in the generation of hydrogen peroxide and hydroxyl radicals, through Fenton/Haber-Weiss reactions (Huang et al, 1999; Liu et al, 2006; Opazo et al, 2002). This investigation, has also clarified the extent to which Cu^{2+}

accentuates differences in $A\beta_{(1-42)}$ and $A\beta_{(1-40)}$, as Cu^{2+} induces $A\beta_{(1-42)}$ fibres to rapidly dissociate into oligomers and protofibrils, as discussed in chapter 3, but has no apparent impact on $A\beta_{(1-40)}$ fibre stability.

In these investigations, it was also demonstrated that Cu^{2+} decreases the time taken for $A\beta_{(1-40)}$ to form fibres, for fibres generated both with and without agitation. This is significant, as fibres grown under these two conditions differ in their morphology (Petkova et al, 2005). Consequently, the results suggest that the means by which Cu^{2+} influences fibre growth kinetics is not dependent upon fibril structure, but instead arises from the interaction between Cu^{2+} and Aβ independently of final fibre structure, perhaps because binding of Cu^{2+} causes Aβ to approach its isoelectric point, and as a result become more prone to self-association (Sarell et al, 2010). Establishing that the accelerating effects of Cu^{2+} upon Aβ fibre formation is independent of fibre structure, strongly supports the notion that Cu^{2+} binding is capable of influencing Aβ fibril properties *in vivo*, regardless of differences in endogenous fibril morphology. Thus, delineating the mechanisms through which Cu^{2+} accentuates differences between $A\beta_{(1-40)}$ and $A\beta_{(1-42)}$ misfolding, as well as how it potentiates Aβ cytotoxicity, could help elucidate AD aetiology.

CHAPTER 6:

Conclusion

For a disease that is expected to afflict 1 in 85 people by 2050 (Prince et al, 2009), the underlying mechanisms of AD pathology are still fairly contentious; however, it is generally accepted that the misfolding and self-association of Aβ peptide in the brain is the primary event in disease onset. In particular, it is the assembly of Aβ into cross-β amyloid fibrils, and the formation of intermediate oligomeric species, that are thought to mediate disease pathology (Hardy & Higgins, 1992; Selkoe, 1991). Unfortunately, even with this knowledge we have still been unable to develop any effective treatments for this prevalent disease. Thus, it is now necessary to identify events that precede amyloid fibrillisation, as in doing so we would expand our window of diagnosis/intervention, while also increasing the number of drug targets to choose from.

One such event may be the dyshomeostasis of metal ions, as levels of Zn^{2+} and Cu^{2+} are found to be increased in the neuropil of AD patients, 2-fold and 4-fold respectively, and these metal ions are found directly bound to Aβ plaques (Dong et al, 2003; Lovell et al, 1998; Miller et al, 2006). Furthermore, a number of studies with mice and drosophila AD models have implicated Zn^{2+} and Cu^{2+} homeostasis as important determinants of disease phenotype (Adlard et al, 2008; Adlard et al, 2010; Corona et al, 2010; Hua et al, 2011; Linkous et al, 2009; Sparks & Schreurs, 2003). Unfortunately, the corresponding biophysical studies have often been conflicted (Faller et al, 2013; Viles, 2012). Early studies suggested that Zn^{2+} and Cu^{2+} induced the assembly of non-toxic amorphous aggregates (Raman et al, 2005; Yoshiike et al, 2001), and thus were not considered relevant to disease pathology. However, it has since been shown that when using substoichiometric levels of Cu^{2+} rather than the elevated levels previously used, $Aβ_{(1-40)}$ fibre formation is not only retained, but is accelerated, and with a potentiated cytotoxicity (Sarell et al, 2010), suggesting that the relationship between metal ions and Aβ self-assembly may be more complex than first thought. Furthermore, although previously it has been suggested that the affinities of Aβ for Zn^{2+} and Cu^{2+} are not sufficiently tight for their interaction to be significant *in vivo,* a combination of more

accurate affinity measurements, plus an appreciation for the high fluxes of Zn^{2+} and Cu^{2+} that occur at the synapse, has led to a general consensus that both Aβ-Zn^{2+} and Aβ-Cu^{2+} interactions likely occur at the synapse (Faller & Hureau, 2009; Frederickson, 1989; Hartter & Barnea, 1988; Kardos et al, 1989; Sarell et al, 2009; Viles, 2012; Vogt et al, 2000). The broad aim of this thesis was to further elucidate the potential role of metal ions in Aβ self-assembly and pathogenicity, looking at the metal ions Zn^{2+} and Cu^{2+}, and the Aβ alloforms $Aβ_{(1-40)}$ and $Aβ_{(1-42)}$.

There is special interest in $Aβ_{(1-42)}$, as it is the alloform most greatly implicated in AD, due to its elevation in early onset familial AD (Citron et al, 1997; Duff et al, 1996; Scheuner et al, 1996), as well as possessing a greater readiness to aggregate (particularly into soluble oligomers) and damage neurons (Burdick et al, 1992; Chen & Glabe, 2006; Lambert et al, 1998). During this thesis, it was found that the relationship between Cu^{2+} and $Aβ_{(1-40)}$ differs dramatically to that between Cu^{2+} and $Aβ_{(1-42),}$ as although suprastoichiometric levels of Cu^{2+} induces both $Aβ_{(1-42)}$ and $Aβ_{(1-40)}$ to form amorphous aggregates, substoichiometric levels of Cu^{2+} accelerate $Aβ_{(1-40)}$ fibre formation while causing $Aβ_{(1-42)}$ to form protofibrillar/oligomeric assemblies. Interestingly, chelation of Cu^{2+} enables $Aβ_{(1-42)}$ to resume fibril formation, and correspondingly, addition of Cu^{2+} to mature $Aβ_{(1-42)}$ fibres caused them disassemble into oligomers, suggesting these oligomeric species to be “on-pathway” to fibre formation. It was found that Cu^{2+} induced stabilisation of these intermediate oligomeric species enhanced the pathogenic potential of $Aβ_{(1-42)}$, as Cu^{2+}-$Aβ_{(1-42)}$ assemblies were seen to more greatly perturb the lipid membranes of artificial vesicles. These investigations suggest that Cu^{2+} may accentuate differences between $Aβ_{(1-40)}$ and $Aβ_{(1-42)}$ *in vivo*, a possibility that is reinforced by the observation that when $Aβ_{(1-40)}$ and $Aβ_{(1-42)}$ are mixed, as they would be *in vivo*, and incubated with Cu^{2+}, the aggregation of $Aβ_{(1-40)}$ and $Aβ_{(1-42)}$ remain distinct.

To substantiate the potential significance of Cu^{2+} to AD aetiology *in* vivo, these investigations sought to establish whether the effect of substoichiometric Cu^{2+} on $A\beta_{(1-40)}$ fibrillisation was dependent upon structure, as the structure of Aβ fibrils in AD patients is polymorphic (Lu et al, 2013; Watts et al, 2014). To obtain differing fibrillar structures fibres were grown in both agitated and quiescent conditions, which has been demonstrated to yield fibres that differ in their axial symmetry (Paravastu et al, 2008; Petkova et al, 2005). Additionally, as it was found Cu^{2+} destabilised $A\beta_{(1-42)}$ fibres, and that a reduction in fibril stability has been associated with an increase in disease pathology (Colby et al, 2009; Xue et al, 2009), an investigation was undertaken to determine whether Cu^{2+}reduced the stability of $A\beta_{(1-40)}$ fibres. It was found that substoichiometric Cu^{2+} accelerated formation of ThT binding fibres under both quiescent and agitated conditions, while not influencing fibril stability, suggesting that Cu^{2+} has a general effect on $A\beta_{(1-40)}$ fibre formation that is limited to fibril kinetics. This emphasises observation that Cu^{2+} influences the misfolding of $A\beta_{(1-42)}$ and $A\beta_{(1-40)}$ in considerably different ways, while also supporting the notion that Cu^{2+} may influence Aβ *in vivo.*

During this thesis, it has been found that trace levels of Zn^{2+} are able to have a profound effect on Aβ self-association through rapid exchanging between Aβ peptides, with as little as 0.01 mole equivalents dramatically influencing fibre growth. Additionally, the aggregate species that formed in the presence of substoichiometric levels of Zn^{2+} (stacks of rods for $A\beta_{(1-40)}$ and disordered tangles for $A\beta_{(1-42)}$) were different to those formed in the presence of Cu^{2+}. This suggested that the influence of Zn^{2+} upon Aβ aggregation is fundamentally different to that of Cu^{2+}. Indeed, it was determined Zn^{2+} induced aggregation to be irreversible, and mature Aβ fibres to be unperturbed by the addition of Zn^{2+}. This suggests that Zn^{2+} induced aggregates are thermodynamically isolated from Aβ fibres, representing an “off-pathway” aggregate formation. This differs to the inter-conversion seen when Cu^{2+} is added/stripped from Aβ aggregates. The difference between Cu^{2+} and Zn^{2+} may arise due to differences in coordination

geometry, affinity, ability to induce Aβ crosslinking, and/or the on/off rate of chelation (Faller et al, 2013; Viles, 2012). The difference between Cu^{2+} and Zn^{2+} may be significant *in vivo*, as it was demonstrated that Zn^{2+}'s effect on Aβ overpowers that of Cu^{2+}, at physiological levels of these ions. Thus, a shift in Zn^{2+} levels may cause a corresponding shift in Cu^{2+}'s capacity to induce oligomer formation.

This investigation into the relationship between metal ions and Aβ misfolding has demonstrated a number of distinct pathways that may be induced with Cu^{2+} and Zn^{2+}, pathways that are dependent upon Aβ alloform, which metal ion is used, and the metal ion to Aβ ratio. Indeed, the multitude of pathways may explain some previous disagreements in the literature (Faller et al, 2013; Viles, 2012). The results have also made it evident that Aβ aggregation is highly sensitive to small amounts of Cu^{2+} and Zn^{2+}, with substoichiometric levels able to completely abolish fibre growth, and Cu^{2+} able to disassemble fully formed $Aβ_{(1-42)}$ fibres. This is particularly significant, as it has been seen that soluble oligomers better correlate with disease progression than larger insoluble aggregates. Thus, Cu^{2+} dyshomeostasis may serve as a trigger for advancing AD, as a surge in Cu^{2+} may disassemble amyloid fibres into smaller oligomers (if Cu^{2+}/Zn^{2+} dyshomeostasis are not themselves a primary cause of Aβ aggregation). In the future, it would be useful to more thoroughly characterise Cu^{2+}/Zn^{2+} induced aggregate species, using atomic-force microscopy and X-ray diffraction. It would also be good to more accurately assess their pathogenic potential, using primary neuronal cultures to assess their effects on synaptic health.

A role for these metal ions in Aβ self-assembly opens up the potential of metal chelation therapies. However, it is significant that the chelators that have been investigated thus far chelate both Zn^{2+} and Cu^{2+} (Adlard et al, 2008; Faux et al, 2010; Grossi et al, 2009). As it has been found that these metal ions have contrasting effects, and that the effect of Zn^{2+} may overpower that of Cu^{2+}, it may be necessary to invest in the development of more specific chelators. Furthermore, as Cu^{2+} and Zn^{2+} may also

exacerbate AD pathology through alternative mechanisms, such as an increased release of Zn^{2+} and Cu^{2+} from the cell promoting Aβ cleavage from APP (Ayton et al, 2013; Bayer et al, 2003; Stelmashook et al, 2014), Cu^{2+} inducing Aβ redox activity (Huang et al, 1999; Liu et al, 2006; Nadal et al, 2008; Opazo et al, 2002), and disrupted Zn^{2+} signalling damaging memory function and leading to neuronal excitotoxicity (Koh & Choi, 1988; Marger et al, 2014; Vergnano et al, 2014), it is clear that Cu^{2+} and Zn^{2+} have both an important and complex role in AD pathology, that expands beyond Aβ misfolding. Future studies will have to consider the broad range of *in vivo* interactions that these metal ions participate in to accurately delineate how they may influence AD aetiology.

REFERENCES

Abelein A, Graslund A, Danielsson J (2015) Zinc as chaperone-mimicking agent for retardation of amyloid beta peptide fibril formation. *Proc Natl Acad Sci U S A*

Abramowitz M, Stegun, I. A. (1965) *Handbook of Mathematical Functions: with Formulas, Graphs, and Mathematical Tables* New York: Dover Publications.

Adamo AM, Oteiza PI (2010) Zinc deficiency and neurodevelopment: the case of neurons. *BioFactors* **36:** 117-124

Adlard PA, Cherny RA, Finkelstein DI, Gautier E, Robb E, Cortes M, Volitakis I, Liu X, Smith JP, Perez K, Laughton K, Li QX, Charman SA, Nicolazzo JA, Wilkins S, Deleva K, Lynch T, Kok G, Ritchie CW, Tanzi RE, Cappai R, Masters CL, Barnham KJ, Bush AI (2008) Rapid restoration of cognition in Alzheimer's transgenic mice with 8-hydroxy quinoline analogs is associated with decreased interstitial Abeta. *Neuron* **59:** 43-55

Adlard PA, Parncutt JM, Finkelstein DI, Bush AI (2010) Cognitive loss in zinc transporter-3 knock-out mice: a phenocopy for the synaptic and memory deficits of Alzheimer's disease? *J Neurosci* **30:** 1631-1636

Alies B, Sasaki I, Proux O, Sayen S, Guillon E, Faller P, Hureau C (2013) Zn impacts Cu coordination to amyloid-beta, the Alzheimer's peptide, but not the ROS production and the associated cell toxicity. *Chem Commun (Camb)* **49:** 1214-1216

Allen TM, Cleland LG (1980) Serum-induced leakage of liposome contents. *Biochim Biophys Acta* **597:** 418-426

Alzheimer A, Stelzmann RA, Schnitzlein HN, Murtagh FR (1995) An English translation of Alzheimer's 1907 paper, "Uber eine eigenartige Erkankung der Hirnrinde". *Clin Anat* **8:** 429-431

Andrick C, Broring K, Deuticke B, Haest CW (1991) Fast translocation of phosphatidylcholine to the outer membrane leaflet after its synthesis at the inner membrane surface in human erythrocytes. *Biochim Biophys Acta* **1064:** 235-241

Ariel Lipson, Stephen Lipson, Lipson H (2010) *Optical Physics*, 4th edn.: Cambridge University Press.

Arispe N, E. Rojas and H.B. Pollard (1993) Alzheimer disease amyloid b protein forms calcium channels in bilayer membranes: Blockade by tromethamine and aluminum. *Proc Natl Acad Sci* **90:** 567-571

Arispe N, Pollard HB, Rojas E (1996) Zn2+ interaction with Alzheimer amyloid beta protein calcium channels. *Proc Natl Acad Sci U S A* **93:** 1710-1715

Arora A, Ha C, Park CB (2004) Insulin amyloid fibrillation at above 100 degrees C: new insights into protein folding under extreme temperatures. *Protein Sci* **13:** 2429-2436

Ashley RH, Harroun TA, Hauss T, Breen KC, Bradshaw JP (2006) Autoinsertion of soluble oligomers of Alzheimer's Abeta(1-42) peptide into cholesterol-containing membranes is accompanied by relocation of the sterol towards the bilayer surface. *BMC Struct Biol* **6:** 21

Assaf SY, Chung SH (1984) Release of endogenous Zn2+ from brain tissue during activity. *Nature* **308:** 734-736

Atwood CS, Moir RD, Huang X, Scarpa RC, Bacarra NM, Romano DM, Hartshorn MA, Tanzi RE, Bush AI (1998) Dramatic aggregation of Alzheimer abeta by Cu(II) is induced by conditions representing physiological acidosis. *J Biol Chem* **273:** 12817-12826

Ayton S, Lei P, Bush AI (2013) Metallostasis in Alzheimer's disease. *Free Radic Biol Med* **62:** 76-89

Bachra BN, van Harskamp GA (1970) The effect of polyvalent metal ions on the stability of a buffer system for calcification in vitro. *Calcified tissue research* **4:** 359-365

Bailey JA, Maloney B, Ge YW, Lahiri DK (2011) Functional activity of the novel Alzheimer's amyloid beta-peptide interacting domain (AbetaID) in the APP and BACE1 promoter sequences and implications in activating apoptotic genes and in amyloidogenesis. *Gene* **488:** 13-22

Ballard C, Gauthier S, Corbett A, Brayne C, Aarsland D, Jones E (2011) Alzheimer’s disease. *Lancet* **377:** 1019-1031

Banci L, Bertini I, Cantini F, Ciofi-Baffoni S (2010) Cellular copper distribution: a mechanistic systems biology approach. *Cell Mol Life Sci* **67:** 2563-2589

Barnes N, Tsivkovskii R, Tsivkovskaia N, Lutsenko S (2005) The copper-transporting ATPases, menkes and wilson disease proteins, have distinct roles in adult and developing cerebellum. *J Biol Chem* **280:** 9640-9645

Barnham KJ, Bush AI (2008) Metals in Alzheimer's and Parkinson's diseases. *Curr Opin Chem Biol* **12:** 222-228

Barria MA, Gonzalez-Romero D, Soto C (2012) Cyclic amplification of prion protein misfolding. *Methods Mol Biol* **849:** 199-212

Barrier L, Ingrand S, Damjanac M, Rioux Bilan A, Hugon J, Page G (2007) Genotype-related changes of ganglioside composition in brain regions of transgenic mouse models of Alzheimer's disease. *Neurobiol Aging* **28:** 1863-1872

Barry AE, Klyubin I, Mc Donald JM, Mably AJ, Farrell MA, Scott M, Walsh DM, Rowan MJ (2011) Alzheimer's Disease Brain-Derived Amyloid-beta-Mediated Inhibition of LTP In Vivo Is Prevented by Immunotargeting Cellular Prion Protein. *J Neurosci* **31:** 7259-7263

Baruch-Suchodolsky R, Fischer B (2009) Abeta40, either soluble or aggregated, is a remarkably potent antioxidant in cell-free oxidative systems. *Biochemistry* **48:** 4354-4370

Baxa U, Ross PD, Wickner RB, Steven AC (2004) The N-terminal prion domain of Ure2p converts from an unfolded to a thermally resistant conformation upon filament formation. *J Mol Biol* **339:** 259-264

Bayer TA, Schafer S, Simons A, Kemmling A, Kamer T, Tepest R, Eckert A, Schussel K, Eikenberg O, Sturchler-Pierrat C, Abramowski D, Staufenbiel M, Multhaup G (2003) Dietary Cu stabilizes brain superoxide dismutase 1 activity and reduces amyloid Abeta production in APP23 transgenic mice. *Proc Natl Acad Sci U S A* **100:** 14187-14192

Bazinet RP, Laye S (2014) Polyunsaturated fatty acids and their metabolites in brain function and disease. *Nat Rev Neurosci* **15:** 771-785

Beatty WW, Salmon DP, Butters N, Heindel WC, Granholm EL (1988) Retrograde amnesia in patients with Alzheimer's disease or Huntington's disease. *Neurobiol Aging* **9:** 181-186

Becucci L, Vizza F, Duarte Y, Guidelli R (2014) The GM1 Ganglioside Forms GM1-Rich Gel Phase Microdomains within Lipid Rafts. *Coatings* **4:** 450

Ben-Ari Y, Khazipov R, Leinekugel X, Caillard O, Gaiarsa JL (1997) GABAA, NMDA and AMPA receptors: a developmentally regulated 'menage a trois'. *Trends Neurosci* **20:** 523-529

Benilova I, Karran E, De Strooper B (2012) The toxic Abeta oligomer and Alzheimer's disease: an emperor in need of clothes. *Nat Neurosci* **15:** 349-357

Biancalana M, Koide S (2010) Molecular mechanism of Thioflavin-T binding to amyloid fibrils. *Biochim Biophys Acta* **1804:** 1405-1412

Billingsley ML, Kincaid RL (1997) Regulated phosphorylation and dephosphorylation of tau protein: effects on microtubule interaction, intracellular trafficking and neurodegeneration. *Biochem J* **323 (Pt 3):** 577-591

Bitan G, Kirkitadze MD, Lomakin A, Vollers SS, Benedek GB, Teplow DB (2003) Amyloid beta - protein (Abeta) assembly: Abeta 40 and Abeta 42 oligomerize through distinct pathways. *Proc Natl Acad Sci U S A* **100:** 330-335

Breteler MM, Bots ML, Ott A, Hofman A (1998) Risk factors for vascular disease and dementia. *Haemostasis* **28:** 167-173

Brown CE, Dyck RH (2004) Distribution of zincergic neurons in the mouse forebrain. *J Comp Neurol* **479:** 156-167

Burdick D, Soreghan B, Kwon M, Kosmoski J, Knauer M, Henschen A, Yates J, Cotman C, Glabe C (1992) Assembly and aggregation properties of synthetic Alzheimer's A4/beta amyloid peptide analogs. *J Biol Chem* **267:** 546-554

Bush AI (2003) The metallobiology of Alzheimer's disease. *Trends Neurosci***:** 26:207-214

Bush AI, Pettingell WH, Multhaup G, d Paradis M, Vonsattel JP, Gusella JF, Beyreuther K, Masters CL, Tanzi RE (1994) Rapid induction of Alzheimer A beta amyloid formation by zinc. *Science* **265:** 1464-1467

Butterfield DA, Boyd-Kimball D (2005) The critical role of methionine 35 in Alzheimer's amyloid beta-peptide (1-42)-induced oxidative stress and neurotoxicity. *Biochim Biophys Acta* **1703:** 149-156

Butterfield DA, Castegna A, Lauderback CM, Drake J (2002) Evidence that amyloid beta-peptide-induced lipid peroxidation and its sequelae in Alzheimer's disease brain contribute to neuronal death. *Neurobiol Aging* **23:** 655-664

Butterfield DA, Pocernich CB (2003) The glutamatergic system and Alzheimer's disease: therapeutic implications. *CNS drugs* **17:** 641-652

Cai XD, Golde TE, Younkin SG (1993) Release of excess amyloid beta protein from a mutant amyloid beta protein precursor. *Science* **259:** 514-516

Ceccom J, Halley H, Daumas S, Lassalle JM (2014) A specific role for hippocampal mossy fiber's zinc in rapid storage of emotional memories. *Learning & memory* **21:** 287-297

Chang CC, Althaus JC, Carruthers CJ, Sutton MA, Steel DG, Gafni A (2013) Synergistic interactions between Alzheimer's Abeta40 and Abeta42 on the surface of primary neurons revealed by single molecule microscopy. *PLoS One* **8:** e82139

Chapman MR, Robinson LS, Pinkner JS, Roth R, Heuser J, Hammar M, Normark S, Hultgren SJ (2002) Role of Escherichia coli curli operons in directing amyloid fiber formation. *Science* **295:** 851-855

Chen WC, Hung CH (2001) Synthesis and characterization of iron N-confused porphyrins: Structural evidences of agostic interaction. *Inorganic Chemistry* **40:** 5070-+

Chen WT, Hong CJ, Lin YT, Chang WH, Huang HT, Liao JY, Chang YJ, Hsieh YF, Cheng CY, Liu HC, Chen YR, Cheng IH (2012) Amyloid-beta (Aβ) D7H mutation increases oligomeric Aβ42 and alters properties of Aβ-zinc/copper assemblies. *PLoS One* **7:** e35807

Chen WT, Liao YH, Yu HM, Cheng IH, Chen YR (2011) Distinct effects of Zn2+, Cu2+, Fe3+, and Al3+ on amyloid-beta stability, oligomerization, and aggregation: amyloid-beta destabilization promotes annular protofibril formation. *J Biol Chem* **286:** 9646-9656

Chen YR, Glabe CG (2006) Distinct early folding and aggregation properties of Alzheimer amyloid-beta peptides Abeta40 and Abeta42: stable trimer or tetramer formation by Abeta42. *J Biol Chem* **281:** 24414-24422

Chernoff YO (2004) Amyloidogenic domains, prions and structural inheritance: rudiments of early life or recent acquisition? *Curr Opin Chem Biol* **8:** 665-671

Cherny RA, Atwood CS, Xilinas ME, Gray DN, Jones WD, McLean CA, Barnham KJ, Volitakis I, Fraser FH, Kim Y, Huang X, Goldstein LE, Moir RD, Lim JT, Beyreuther K, Zheng H, Tanzi RE, Masters CL, Bush AI (2001) Treatment with a copper-zinc chelator markedly and rapidly inhibits beta-amyloid accumulation in Alzheimer's disease transgenic mice. *Neuron* **30:** 665-676

Choo-Smith LP, Garzon-Rodriguez W, Glabe CG, Surewicz WK (1997) Acceleration of amyloid fibril formation by specific binding of Abeta-(1-40) peptide to ganglioside-containing membrane vesicles. *J Biol Chem* **272:** 22987-22990

Christine CW, Choi DW (1990) Effect of zinc on NMDA receptor-mediated channel currents in cortical neurons. *J Neurosci* **10:** 108-116

Christopher Moyes PS (2008) *Principles of Animal Physiology*, 2nd edn.: Pearson College Div.

Cirrito JR, May PC, O'Dell MA, Taylor JW, Parsadanian M, Cramer JW, Audia JE, Nissen JS, Bales KR, Paul SM, DeMattos RB, Holtzman DM (2003) In vivo assessment of brain interstitial fluid with microdialysis reveals plaque-associated changes in amyloid-beta metabolism and half-life. *J Neurosci* **23:** 8844-8853

Citron M, Oltersdorf T, Haass C, McConlogue L, Hung AY, Seubert P, Vigo-Pelfrey C, Lieberburg I, Selkoe DJ (1992) Mutation of the beta-amyloid precursor protein in familial Alzheimer's disease increases beta-protein production. *Nature* **360:** 672-674

Citron M, Westaway D, Xia W, Carlson G, Diehl T, Levesque G, Johnson-Wood K, Lee M, Seubert P, Davis A, Kholodenko D, Motter R, Sherrington R, Perry B, Yao H, Strome R, Lieberburg I, Rommens J, Kim S, Schenk D, Fraser P, St George Hyslop P, Selkoe DJ (1997) Mutant presenilins of Alzheimer's disease increase production of 42-residue amyloid beta-protein in both transfected cells and transgenic mice. *Nat Med* **3:** 67-72

Clavaguera F, Bolmont T, Crowther RA, Abramowski D, Frank S, Probst A, Fraser G, Stalder AK, Beibel M, Staufenbiel M, Jucker M, Goedert M, Tolnay M (2009) Transmission and spreading of tauopathy in transgenic mouse brain. *Nat Cell Biol* **11:** 909-913

Cleary JP, Walsh DM, Hofmeister JJ, Shankar GM, Kuskowski MA, Selkoe DJ, Ashe KH (2005) Natural oligomers of the amyloid-beta protein specifically disrupt cognitive function. *Nat Neurosci* **8:** 79-84

Colby DW, Giles K, Legname G, Wille H, Baskakov IV, DeArmond SJ, Prusiner SB (2009) Design and construction of diverse mammalian prion strains. *Proc Natl Acad Sci U S A* **106:** 20417-20422

Colon W, Kelly JW (1992) Partial denaturation of transthyretin is sufficient for amyloid fibril formation in vitro. *Biochemistry* **31:** 8654-8660

Come JH, Fraser PE, Lansbury PT, Jr. (1993) A kinetic model for amyloid formation in the prion diseases: importance of seeding. *Proc Natl Acad Sci U S A* **90:** 5959-5963

Corder EH, Saunders AM, Strittmatter WJ, Schmechel DE, Gaskell PC, Small GW, Roses AD, Haines JL, Pericak-Vance MA (1993) Gene dose of apolipoprotein E type 4 allele and the risk of Alzheimer's disease in late onset families. *Science* **261:** 921-923

Corona C, Masciopinto F, Silvestri E, Viscovo AD, Lattanzio R, Sorda RL, Ciavardelli D, Goglia F, Piantelli M, Canzoniero LM, Sensi SL (2010) Dietary zinc supplementation of 3xTg-AD mice increases BDNF levels and prevents cognitive deficits as well as mitochondrial dysfunction. *Cell death & disease* **1:** e91

Crowhurst KA, Tollinger M, Forman-Kay JD (2002) Cooperative interactions and a non-native buried Trp in the unfolded state of an SH3 domain. *J Mol Biol* **322:** 163-178

Damante CA, Osz K, Nagy Z, Pappalardo G, Grasso G, Impellizzeri G, Rizzarelli E, Sovago I (2008) The Metal Loading Ability of beta-Amyloid N-Terminus: A Combined Potentiometric and Spectroscopic Study of Copper(II) Complexes with beta-Amyloid(1-16), Its Short or Mutated Peptide Fragments, and Its Polyethylene Glycol (PEG)-ylated Analogue. *Inorg Chem* **47**

Daniel L. Schacter DTG, Daniel M. Wegner (2011) Psychology. In *Pyschology*, p 80. New York: Worth Publishers

Danielsson J, Pierattelli R, Banci L, Gräslund A (2007) High-resolution NMR studies of the zinc-binding site of the Alzheimer's amyloid beta-peptide. *FEBS J***:** 274:246-259

Das SK, Ray K (2006) Wilson's disease: an update. *Nat Clin Pract Neurol* **2:** 482-493

Davies CA, Mann DM, Sumpter PQ, Yates PO (1987) A quantitative morphometric analysis of the neuronal and synaptic content of the frontal and temporal cortex in patients with Alzheimer's disease. *J Neurol Sci* **78:** 151-164

Dawson RMC, Elliot, D.C., Elliot, W.H., Jones, K.M (1986) *Data for Biochemical Research*, Oxford UK: Claredon Press.

de la Monte SM, Wands JR (2008) Alzheimer's disease is type 3 diabetes-evidence reviewed. *J Diabetes Sci Technol* **2:** 1101-1113

De Libero G, Mori L (2005) Recognition of lipid antigens by T cells. *Nat Rev Immunol* **5:** 485-496

De Strooper B, Annaert W (2000) Proteolytic processing and cell biological functions of the amyloid precursor protein. *J Cell Sci* **113 (Pt 11):** 1857-1870

Demuro A, Mina E, Kayed R, Milton SC, Parker I, Glabe CG (2005) Calcium dysregulation and membrane disruption as a ubiquitous neurotoxic mechanism of soluble amyloid oligomers. *J Biol Chem* **280:** 17294-17300

Der-Sarkissian A, Jao CC, Chen J, Langen R (2003) Structural organization of alpha-synuclein fibrils studied by site-directed spin labeling. *J Biol Chem* **278:** 37530-37535

Dong J, Atwood CS, Anderson VE, Siedlak SL, Smith MA, Perry G, Carey PR (2003) Metal binding and oxidation of amyloid-beta within isolated senile plaque cores: Raman microscopic evidence. *Biochemistry* **42:** 2768-2773

Donsante A, Tang J, Godwin SC, Holmes CS, Goldstein DS, Bassuk A, Kaler SG (2007) Differences in ATP7A gene expression underlie intrafamilial variability in Menkes disease/occipital horn syndrome. *J Med Genet* **44:** 492-497

Donsante A, Yi L, Zerfas PM, Brinster LR, Sullivan P, Goldstein DS, Prohaska J, Centeno JA, Rushing E, Kaler SG (2011) ATP7A gene addition to the choroid plexus results in long-term rescue of the lethal copper transport defect in a Menkes disease mouse model. *Mol Ther* **19:** 2114-2123

Dorlet P, Gambarelli S, Faller P, Hureau C (2009) Pulse EPR spectroscopy reveals the coordination sphere of copper(II) ions in the 1-16 amyloid-beta peptide: a key role of the first two N-terminus residues. *Angew Chem Int Ed Engl* **48:** 9273-9276

Drake A (1994a) Chapter 12: Optical Spectroscopy. In *Principles and Instrumentation. Microscopy, Optical Spectroscopy, and Macroscopic Techniques*, Christopher Jones BM, Adrian Thomas (ed), Vol. 22, pp 203-218. Methods in Molecular Biology

Drake A (1994b) Chapter 13: The Measurement of Electronic Absorption Spectra in The Ultraviolet and Visible. In *Principles and Instrumentation. Microscopy, Optical Spectroscopy, and Macroscopic Techniques*, Christopher Jones BM, Adrian Thomas (ed), Vol. 22, pp 173-182. Methods in Molecular Biology

Drake A (1994c) Chapter 16: Circular Dichroism. In *Principles and Instrumentation. Microscopy, Optical Spectroscopy, and Macroscopic Techniques*, Christopher Jones BM, Adrian Thomas (ed), Vol. 22, pp 151-172. Methods in Molecular Biology

Drew SC, Noble CJ, Masters CL, Hanson GR, Barnham KJ (2009) Pleomorphic copper coordination by Alzheimer's disease amyloid-beta peptide. *J Am Chem Soc* **131:** 1195-1207

Duff K, Eckman C, Zehr C, Yu X, Prada CM, Perez-tur J, Hutton M, Buee L, Harigaya Y, Yager D, Morgan D, Gordon MN, Holcomb L, Refolo L, Zenk B, Hardy J, Younkin S (1996) Increased amyloid-beta42(43) in brains of mice expressing mutant presenilin 1. *Nature* **383:** 710-713

Eanes ED, Glenner GG (1968) X-ray diffraction studies on amyloid filaments. *J Histochem Cytochem* **16:** 673-677

Egerton R (2005) *Physical Principles of Electron Microscopy*: Springer US.

Eichner T, Kalverda AP, Thompson GS, Homans SW, Radford SE (2011) Conformational conversion during amyloid formation at atomic resolution. *Mol Cell* **41:** 161-172

Eichner T, Radford SE (2011) A diversity of assembly mechanisms of a generic amyloid fold. *Mol Cell* **43:** 8-18

Englund EA, Gopi HN, Appella DH (2004) An efficient synthesis of a probe for protein function: 2,3-diaminopropionic acid with orthogonal protecting groups. *Org Lett* **6:** 213-215

Erni R, Rossell MD, Kisielowski C, Dahmen U (2009) Atomic-resolution imaging with a sub-50-pm electron probe. *Phys Rev Lett* **102:** 096101

Fabian-Fine R, Skehel P, Errington ML, Davies HA, Sher E, Stewart MG, Fine A (2001) Ultrastructural distribution of the alpha7 nicotinic acetylcholine receptor subunit in rat hippocampus. *J Neurosci* **21:** 7993-8003

Falkenberg B (2007) *Particle Metaphysics: A Critical Account of Subatomic Reality*, Berlin: Springer.

Faller P (2009) Copper and zinc binding to amyloid-beta: coordination, dynamics, aggregation, reactivity and metal-ion transfer. *Chembiochem* **10:** 2837-2845

Faller P, Hureau C (2009) Bioinorganic chemistry of copper and zinc ions coordinated to amyloid-beta peptide. *Dalton Trans***:** 1080-1094

Faller P, Hureau C, Berthoumieu O (2013) Role of metal ions in the self-assembly of the Alzheimer's amyloid-beta peptide. *Inorg Chem* **52:** 12193-12206

Faux NG, W. RC, Gunn A, Rembach A, Tsatsanis A, Bedo J, Harrison J, Lannfelt L, Blennow K, Zetterberg H, Ingelsson M, Masters CL, Tanzi RE, Cummings JL, Herd CM, Bush AI (2010) PBT2

rapidly improves cognition in Alzheimer's Disease: additional phase II analyses. *J Alzheimers Dis***:** 20:509-516

Ferri CP, Prince M, Brayne C, Brodaty H, Fratiglioni L, Ganguli M, Hall K, Hasegawa K, Hendrie H, Huang Y, Jorm A, Mathers C, Menezes PR, Rimmer E, Scazufca M, Alzheimer's Disease I (2005) Global prevalence of dementia: a Delphi consensus study. *Lancet* **366:** 2112-2117

Fezoui Y, Hartley DM, Harper JD, Khurana R, Walsh DM, Condron MM, Selkoe DJ, Lansbury PT, Jr., Fink AL, Teplow DB (2000) An improved method of preparing the amyloid beta-protein for fibrillogenesis and neurotoxicity experiments. *Amyloid* **7:** 166-178

Fisher RA (1921) On the "Probable Error" of a Coefficient of Correlation Deduced from a Small Sample. *Metron* **1:** 3-32

Fishman PH, Brady RO (1976) Biosynthesis and function of gangliosides. *Science* **194:** 906-915

Fisk L, Nalivaeva NN, Boyle JP, Peers CS, Turner AJ (2007) Effects of hypoxia and oxidative stress on expression of neprilysin in human neuroblastoma cells and rat cortical neurones and astrocytes. *Neurochem Res* **32:** 1741-1748

Forstl H, Kurz A (1999) Clinical features of Alzheimer's disease. *Eur Arch Psychiatry Clin Neurosci* **249:** 288-290

Fowler DM, Koulov AV, Alory-Jost C, Marks MS, Balch WE, Kelly JW (2006) Functional amyloid formation within mammalian tissue. *PLoS Biol* **4:** e6

Frears ER, Stephens DJ, Walters CE, Davies H, Austen BM (1999) The role of cholesterol in the biosynthesis of beta-amyloid. *Neuroreport* **10:** 1699-1705

Frederickson CJ (1989) Neurobiology of zinc and zinc-containing neurons. *Int Rev Neurobiol* **31:** 145-238

Fukada T, Yamasaki S, Nishida K, Murakami M, Hirano T (2011) Zinc homeostasis and signaling in health and diseases: Zinc signaling. *J Biol Inorg Chem* **16:** 1123-1134

Funato H, Yoshimura M, Kusui K, Tamaoka A, Ishikawa K, Ohkoshi N, Namekata K, Okeda R, Ihara Y (1998) Quantitation of amyloid beta-protein (A beta) in the cortex during aging and in Alzheimer's disease. *Am J Pathol* **152:** 1633-1640

Gabbita SP, Aksenov MY, Lovell MA, Markesbery WR (1999) Decrease in peptide methionine sulfoxide reductase in Alzheimer's disease brain. *J Neurochem* **73:** 1660-1666

Gabuzda D, Busciglio J, Chen LB, Matsudaira P, Yankner BA (1994) Inhibition of energy metabolism alters the processing of amyloid precursor protein and induces a potentially amyloidogenic derivative. *J Biol Chem* **269:** 13623-13628

Gaier ED, Eipper BA, Mains RE (2013) Copper signaling in the mammalian nervous system: synaptic effects. *J Neurosci Res* **91:** 2-19

Garai K, Sahoo B, Kaushalya SK, Desai R, Maiti S (2007) Zinc lowers amyloid-beta toxicity by selectively precipitating aggregation intermediates. *Biochemistry* **46:** 10655-10663

Geddes AJ, Parker KD, Atkins ED, Beighton E (1968) "Cross-beta" conformation in proteins. *J Mol Biol* **32:** 343-358

Glenner GG, Wong CW (1984) Alzheimer's disease and Down's syndrome: sharing of a unique cerebrovascular amyloid fibril protein. *Biochem Biophys Res Commun* **122:** 1131-1135

Goedert M, Spillantini MG, Jakes R, Rutherford D, Crowther RA (1989) Multiple isoforms of human microtubule-associated protein tau: sequences and localization in neurofibrillary tangles of Alzheimer's disease. *Neuron* **3:** 519-526

Goldsbury C, Kistler J, Aebi U, Arvinte T, Cooper GJ (1999) Watching amyloid fibrils grow by time-lapse atomic force microscopy. *J Mol Biol* **285:** 33-39

Goncalves SA, Matos JE, Outeiro TF (2010) Zooming into protein oligomerization in neurodegeneration using BiFC. *Trends Biochem Sci* **35:** 643-651

Greenfield N, Fasman GD (1969) Computed circular dichroism spectra for the evaluation of protein conformation. *Biochemistry* **8:** 4108-4116

Greenfield NJ (2006) Using circular dichroism spectra to estimate protein secondary structure. *Nature protocols* **1:** 2876-2890

Greenough MA, Volitakis I, Li QX, Laughton K, Evin G, Ho M, Dalziel AH, Camakaris J, Bush AI (2011) Presenilins promote the cellular uptake of copper and zinc and maintain copper chaperone of SOD1-dependent copper/zinc superoxide dismutase activity. *J Biol Chem* **286:** 9776-9786

Groenning M (2010) Binding mode of Thioflavin T and other molecular probes in the context of amyloid fibrils-current status. *Journal of chemical biology* **3:** 1-18

Grossi C, Francese S, Casini A, Rosi MC, Luccarini I, Fiorentini A, Gabbiani C, Messori L, Moneti G, Casamenti F (2009) Clioquinol decreases amyloid-beta burden and reduces working memory impairment in a transgenic mouse model of Alzheimer's disease. *J Alzheimers Dis* **17:** 423-440

Gunderson WA, Hernandez-Guzman J, Karr JW, Sun L, Szalai VA, Warncke K (2012) Local structure and global patterning of Cu2+ binding in fibrillar amyloid-beta [Abeta(1-40)] protein. *J Am Chem Soc* **134:** 18330-18337

Guo JP, Arai T, Miklossy J, McGeer PL (2006) Abeta and tau form soluble complexes that may promote self aggregation of both into the insoluble forms observed in Alzheimer's disease. *Proc Natl Acad Sci U S A* **103:** 1953-1958

Ha C, Ryu J, Park CB (2007) Metal ions differentially influence the aggregation and deposition of Alzheimer's beta-amyloid on a solid template. *Biochemistry* **46:** 6118-6125

Haass C, Koo EH, Mellon A, Hung AY, Selkoe DJ (1992) Targeting of cell-surface beta-amyloid precursor protein to lysosomes: alternative processing into amyloid-bearing fragments. *Nature* **357:** 500-503

Haass C, Lemere CA, Capell A, Citron M, Seubert P, Schenk D, Lannfelt L, Selkoe DJ (1995) The Swedish mutation causes early-onset Alzheimer's disease by beta-secretase cleavage within the secretory pathway. *Nat Med* **1:** 1291-1296

Haass C, Selkoe DJ (2007) Soluble protein oligomers in neurodegeneration: lessons from the Alzheimer's amyloid beta-peptide. *Nat Rev Mol Cell Biol***:** 8:101-112

Haines TH (2001) Do sterols reduce proton and sodium leaks through lipid bilayers? *Prog Lipid Res* **40:** 299-324

Hakomori S (2003) Structure, organization, and function of glycosphingolipids in membrane. *Curr Opin Hematol* **10:** 16-24

Hane F, Tran G, Attwood SJ, Leonenko Z (2013) Cu(2+) affects amyloid-beta (1-42) aggregation by increasing peptide-peptide binding forces. *PLoS One* **8:** e59005

Hansen KB, Ogden KK, Yuan H, Traynelis SF (2014) Distinct functional and pharmacological properties of Triheteromeric GluN1/GluN2A/GluN2B NMDA receptors. *Neuron* **81:** 1084-1096

Harada A, Oguchi K, Okabe S, Kuno J, Terada S, Ohshima T, Sato-Yoshitake R, Takei Y, Noda T, Hirokawa N (1994) Altered microtubule organization in small-calibre axons of mice lacking tau protein. *Nature* **369:** 488-491

Hardy J (1997) Amyloid, the presenilins and Alzheimer's disease. *Trends Neurosci* **20:** 154-159

Hardy J (2006) Has the amyloid cascade hypothesis for Alzheimer's disease been proved? *Curr Alzheimer Res***:** 3:71-73

Hardy J, Selkoe DJ (2002) The amyloid hypothesis of Alzheimer's disease: progress and problems on the road to therapeutics. *Science* **297:** 353-356

Hardy JA, Higgins GA (1992) Alzheimer's disease: the amyloid cascade hypothesis. *Science* **256:** 184-185

Hartley DM, Zhao C, Speier AC, Woodard GA, Li S, Li Z, Walz T (2008) Transglutaminase induces protofibril-like amyloid beta-protein assemblies that are protease-resistant and inhibit long-term potentiation. *J Biol Chem* **283:** 16790-16800

Hartter DE, Barnea A (1988) Evidence for release of copper in the brain: depolarization-induced release of newly taken-up 67copper. *Synapse* **2:** 412-415

Haupt C, Leppert J, Ronicke R, Meinhardt J, Yadav JK, Ramachandran R, Ohlenschlager O, Reymann KG, Gorlach M, Fandrich M (2012) Structural basis of beta-amyloid-dependent synaptic dysfunctions. *Angew Chem Int Ed Engl* **51:** 1576-1579

Hensley K, Carney JM, Mattson MP, Aksenova M, Harris M, Wu JF, Floyd RA, Butterfield DA (1994) A model for beta-amyloid aggregation and neurotoxicity based on free radical generation by the peptide: relevance to Alzheimer disease. *Proc Natl Acad Sci U S A* **91:** 3270-3274

Higaki J, Quon D, Zhong Z, Cordell B (1995) Inhibition of beta-amyloid formation identifies proteolytic precursors and subcellular site of catabolism. *Neuron* **14:** 651-659

Hiltunen M, van Groen T, Jolkkonen J (2009) Functional roles of amyloid-beta protein precursor and amyloid-beta peptides: evidence from experimental studies. *J Alzheimers Dis* **18:** 401-412

Holmes C, Boche D, Wilkinson D, Yadegarfar G, Hopkins V, Bayer A, Jones RW, Bullock R, Love S, Neal JW, Zotova E, Nicoll JA (2008) Long-term effects of Abeta42 immunisation in Alzheimer's disease: follow-up of a randomised, placebo-controlled phase I trial. *Lancet* **372:** 216-223

Horenstein J, Akabas MH (1998) Location of a high affinity Zn2+ binding site in the channel of alpha1beta1 gamma-aminobutyric acidA receptors. *Mol Pharmacol* **53:** 870-877

Hortschansky P, Christopeit T, Schroeckh V, Fandrich M (2005) Thermodynamic analysis of the aggregation propensity of oxidized Alzheimer's beta-amyloid variants. *Protein Sci* **14:** 2915-2918

House E, Collingwood J, Khan A, Korchazkina O, Berthon G, Exley C (2004) Aluminium, iron, zinc and copper influence the in vitro formation of amyloid fibrils of Abeta42 in a manner which may have consequences for metal chelation therapy in Alzheimer's disease. *J Alzheimers Dis* **6:** 291-301

House E, Mold M, Collingwood J, Baldwin A, Goodwin S, Exley C (2009) Copper abolishes the beta-sheet secondary structure of preformed amyloid fibrils of amyloid-beta(42). *J Alzheimers Dis* **18:** 811-817

Howell GA, Welch MG, Frederickson CJ (1984) Stimulation-induced uptake and release of zinc in hippocampal slices. *Nature* **308:** 736-738

Hsiao B, Dweck D, Luetje CW (2001) Subunit-dependent modulation of neuronal nicotinic receptors by zinc. *J Neurosci* **21:** 1848-1856

Hua H, Munter L, Harmeier A, Georgiev O, Multhaup G, Schaffner W (2011) Toxicity of Alzheimer's disease-associated Abeta peptide is ameliorated in a Drosophila model by tight control of zinc and copper availability. *Biological chemistry* **392:** 919-926

Huang X, Atwood CS, Hartshorn MA, Multhaup G, Goldstein LE, Scarpa RC, Cuajungco MP, Gray DN, Lim J, Moir RD, Tanzi RE, Bush AI (1999) The A beta peptide of Alzheimer's disease directly produces hydrogen peroxide through metal ion reduction. *Biochemistry* **38:** 7609-7616

Hung AY, Selkoe DJ (1994) Selective ectodomain phosphorylation and regulated cleavage of beta-amyloid precursor protein. *EMBO J* **13:** 534-542

Hutton M, Lendon CL, Rizzu P, Baker M, Froelich S, Houlden H, Pickering-Brown S, Chakraverty S, Isaacs A, Grover A, Hackett J, Adamson J, Lincoln S, Dickson D, Davies P, Petersen RC, Stevens M, de Graaff E, Wauters E, van Baren J, Hillebrand M, Joosse M, Kwon JM, Nowotny P, Che LK, Norton J, Morris JC, Reed LA, Trojanowski J, Basun H, Lannfelt L, Neystat M, Fahn S, Dark F, Tannenberg T, Dodd PR, Hayward N, Kwok JB, Schofield PR, Andreadis A, Snowden J, Craufurd D, Neary D, Owen F, Oostra BA, Hardy J, Goate A, van Swieten J, Mann D, Lynch T, Heutink P (1998) Association of missense and 5'-splice-site mutations in tau with the inherited dementia FTDP-17. *Nature* **393:** 702-705

Igbavboa U, Sun GY, Weisman GA, He Y, Wood WG (2009) Amyloid beta-protein stimulates trafficking of cholesterol and caveolin-1 from the plasma membrane to the Golgi complex in mouse primary astrocytes. *Neuroscience* **162:** 328-338

Innocenti M, Salvietti E, Guidotti M, Casini A, Bellandi S, Foresti ML, Gabbiani C, Pozzi A, Zatta P, Messori L (2010) Trace copper(II) or zinc(II) ions drastically modify the aggregation behavior of amyloid-beta1-42: an AFM study. *J Alzheimers Dis* **19:** 1323-1329

Iwata K, Fujiwara T, Matsuki Y, Akutsu H, Takahashi S, Naiki H, Goto Y (2006) 3D structure of amyloid protofilaments of beta2-microglobulin fragment probed by solid-state NMR. *Proc Natl Acad Sci U S A* **103:** 18119-18124

Jan A, Gokce O, Luthi-Carter R, Lashuel HA (2008) The ratio of monomeric to aggregated forms of Abeta40 and Abeta42 is an important determinant of amyloid-beta aggregation, fibrillogenesis, and toxicity. *J Biol Chem* **283:** 28176-28189

Jang H, Zheng J, Lal R, Nussinov R (2008) New structures help the modeling of toxic amyloidbeta ion channels. *Trends Biochem Sci* **33:** 91-100

Jarrett JT, Lansbury PT, Jr. (1993) Seeding "one-dimensional crystallization" of amyloid: a pathogenic mechanism in Alzheimer's disease and scrapie? *Cell* **73:** 1055-1058

Ji SR, Wu Y, Sui SF (2002) Cholesterol is an important factor affecting the membrane insertion of beta-amyloid peptide (A beta 1-40), which may potentially inhibit the fibril formation. *J Biol Chem* **277:** 6273-6279

Jiang D, Rauda I, Han S, Chen S, Zhou F (2012) Aggregation pathways of the amyloid β(1-42) peptide depend on its colloidal stability and ordered β-sheet stacking. *Langmuir* **28:** 12711-12721

Jimenez JL, Nettleton EJ, Bouchard M, Robinson CV, Dobson CM, Saibil HR (2002) The protofilament structure of insulin amyloid fibrils. *Proc Natl Acad Sci U S A* **99:** 9196-9201

Kaler SG (2011) ATP7A-related copper transport diseases-emerging concepts and future trends. *Nat Rev Neurol* **7:** 15-29

Kang J, Lemaire HG, Unterbeck A, Salbaum JM, Masters CL, Grzeschik KH, Multhaup G, Beyreuther K, Muller-Hill B (1987) The precursor of Alzheimer's disease amyloid A4 protein resembles a cell-surface receptor. *Nature* **325:** 733-736

Kang JE, Lim MM, Bateman RJ, Lee JJ, Smyth LP, Cirrito JR, Fujiki N, Nishino S, Holtzman DM (2009) Amyloid-beta dynamics are regulated by orexin and the sleep-wake cycle. *Science* **326:** 1005-1007

Kardos J, Kovacs I, Hajos F, Kalman M, Simonyi M (1989) Nerve endings from rat brain tissue release copper upon depolarization. A possible role in regulating neuronal excitability. *Neurosci Lett* **103:** 139-144

Karr JW, Szalai VA (2008) Cu(II) binding to monomeric, oligomeric, and fibrillar forms of the Alzheimer's disease amyloid-beta peptide. *Biochemistry* **47:** 5006-5016

Kayed R, Sokolov Y, Edmonds B, McIntire TM, Milton SC, Hall JE, Glabe CG (2004) Permeabilization of lipid bilayers is a common conformation-dependent activity of soluble amyloid oligomers in protein misfolding diseases. *J Biol Chem* **279:** 46363-46366

Kejnovsky E, Kypr J (1998) Millimolar concentrations of zinc and other metal cations cause sedimentation of DNA. *Nucleic Acids Res* **26:** 5295-5299

Kessels HW, Nabavi S, Malinow R (2013) Metabotropic NMDA receptor function is required for beta-amyloid-induced synaptic depression. *Proc Natl Acad Sci U S A* **110:** 4033-4038

Khachaturian ZS (1987) Hypothesis on the regulation of cytosol calcium concentration and the aging brain. *Neurobiol Aging* **8:** 345-346

Kheterpal I, Wetzel R, Cook KD (2003) Enhanced correction methods for hydrogen exchange-mass spectrometric studies of amyloid fibrils. *Protein Sci* **12:** 635-643

Kim BE, Turski ML, Nose Y, Casad M, Rockman HA, Thiele DJ (2010) Cardiac copper deficiency activates a systemic signaling mechanism that communicates with the copper acquisition and storage organs. *Cell Metab* **11:** 353-363

Kivipelto M, Solomon A (2006) Cholesterol as a risk factor for Alzheimer's disease - epidemiological evidence. *Acta Neurol Scand Suppl* **185:** 50-57

Klug GM, Losic D, Subasinghe SS, Aguilar MI, Martin LL, Small DH (2003) Beta-amyloid protein oligomers induced by metal ions and acid pH are distinct from those generated by slow spontaneous ageing at neutral pH. *Eur J Biochem* **270:** 4282-4293

Klyubin I, Betts V, Welzel AT, Blennow K, Zetterberg H, Wallin A, Lemere CA, Cullen WK, Peng Y, Wisniewski T, Selkoe DJ, Anwyl R, Walsh DM, Rowan MJ (2008) Amyloid beta protein dimer-containing human CSF disrupts synaptic plasticity: prevention by systemic passive immunization. *J Neurosci* **28:** 4231-4237

Klyubin I, Cullen WK, Hu NW, Rowan MJ (2012) Alzheimer's disease Abeta assemblies mediating rapid disruption of synaptic plasticity and memory. *Mol Brain* **5:** 25

Klyubin I, Walsh DM, Lemere CA, Cullen WK, Shankar GM, Betts V, Spooner ET, Jiang L, Anwyl R, Selkoe DJ, Rowan MJ (2005) Amyloid beta protein immunotherapy neutralizes Abeta oligomers that disrupt synaptic plasticity in vivo. *Nat Med* **11:** 556-561

Knops J, Suomensaari S, Lee M, McConlogue L, Seubert P, Sinha S (1995) Cell-type and amyloid precursor protein-type specific inhibition of A beta release by bafilomycin A1, a selective inhibitor of vacuolar ATPases. *J Biol Chem* **270:** 2419-2422

Knowles TP, Waudby CA, Devlin GL, Cohen SI, Aguzzi A, Vendruscolo M, Terentjev EM, Welland ME, Dobson CM (2009) An analytical solution to the kinetics of breakable filament assembly. *Science* **326:** 1533-1537

Kodama H, Fujisawa C, Bhadhprasit W (2011) Pathology, clinical features and treatments of congenital copper metabolic disorders--focus on neurologic aspects. *Brain Dev* **33:** 243-251

Kodama H, Murata Y, Kobayashi M (1999) Clinical manifestations and treatment of Menkes disease and its variants. *Pediatr Int* **41:** 423-429

Koh JY, Choi DW (1988) Zinc alters excitatory amino acid neurotoxicity on cortical neurons. *J Neurosci* **8:** 2164-2171

Koo EH, Squazzo SL, Selkoe DJ, Koo CH (1996) Trafficking of cell-surface amyloid beta-protein precursor. I. Secretion, endocytosis and recycling as detected by labeled monoclonal antibody. *J Cell Sci* **109 (Pt 5):** 991-998

Krebs MR, Bromley EH, Donald AM (2005) The binding of thioflavin-T to amyloid fibrils: localisation and implications. *J Struct Biol* **149:** 30-37

Kuperstein I, Broersen K, Benilova I, Rozenski J, Jonckheere W, Debulpaep M, Vandersteen A, Segers-Nolten I, Van Der Werf K, Subramaniam V, Braeken D, Callewaert G, Bartic C, D'Hooge R, Martins IC, Rousseau F, Schymkowitz J, De Strooper B (2010) Neurotoxicity of Alzheimer's disease Abeta peptides is induced by small changes in the Abeta42 to Abeta40 ratio. *EMBO J* **29:** 3408-3420

Lakowicz JR (2006) *Principles of Fluorescence Spectroscopy*, 3rd edn.: Springer US.

Lambert MP, Barlow AK, Chromy BA, Edwards C, Freed R, Liosatos M, Morgan TE, Rozovsky I, Trommer B, Viola KL, Wals P, Zhang C, Finch CE, Krafft GA, Klein WL (1998) Diffusible, nonfibrillar ligands derived from Abeta1-42 are potent central nervous system neurotoxins. *Proc Natl Acad Sci U S A* **95:** 6448-6453

Landes AM, Sperry SD, Strauss ME, Geldmacher DS (2001) Apathy in Alzheimer's disease. *J Am Geriatr Soc* **49:** 1700-1707

Lasagna-Reeves CA, Kayed R (2011) Astrocytes contain amyloid-beta annular protofibrils in Alzheimer's disease brains. *FEBS Lett* **585:** 3052-3057

Lashuel HA, Hartley DM, Petre BM, Wall JS, Simon MN, Walz T, Lansbury PT, Jr. (2003) Mixtures of wild-type and a pathogenic (E22G) form of Abeta40 in vitro accumulate protofibrils, including amyloid pores. *J Mol Biol* **332:** 795-808

Laurén J, Gimbel DA, Nygaard HB, Gilbert JW, Strittmatter SM (2009) Cellular prion protein mediates impairment of synaptic plasticity by amyloid-beta oligomers. *Nature* **457:** 1128-1132

Lazarov O, Lee M, Peterson DA, Sisodia SS (2002) Evidence that synaptically released beta-amyloid accumulates as extracellular deposits in the hippocampus of transgenic mice. *J Neurosci* **22:** 9785-9793

Lee JY, Cole TB, Palmiter RD, Koh JY (2000) Accumulation of zinc in degenerating hippocampal neurons of ZnT3-null mice after seizures: evidence against synaptic vesicle origin. *J Neurosci* **20:** RC79

Lee JY, Cole TB, Palmiter RD, Suh SW, Koh JY (2002) Contribution by synaptic zinc to the gender-disparate plaque formation in human Swedish mutant APP transgenic mice. *Proc Natl Acad Sci U S A* **99:** 7705-7710

Lee S, Fernandez EJ, Good TA (2007) Role of aggregation conditions in structure, stability, and toxicity of intermediates in the Abeta fibril formation pathway. *Protein Sci* **16:** 723-732

Lesne S, Koh MT, Kotilinek L, Kayed R, Glabe CG, Yang A, Gallagher M, Ashe KH (2006) A specific amyloid-beta protein assembly in the brain impairs memory. *Nature* **440:** 352-357

Lesné S, Koh MT, Kotilinek L, Kayed R, Glabe CG, Yang A, Gallagher M, Ashe KH (2006) A specific amyloid-beta protein assembly in the brain impairs memory. *Nature***:** 352-357

LeVine H, 3rd (1993) Thioflavine T interaction with synthetic Alzheimer's disease beta-amyloid peptides: detection of amyloid aggregation in solution. *Protein Sci* **2:** 404-410

Levy E, Carman MD, Fernandez-Madrid IJ, Power MD, Lieberburg I, van Duinen SG, Bots GT, Luyendijk W, Frangione B (1990) Mutation of the Alzheimer's disease amyloid gene in hereditary cerebral hemorrhage, Dutch type. *Science* **248:** 1124-1126

Li S, Hong S, Shepardson NE, Walsh DM, Shankar GM, Selkoe D (2009) Soluble oligomers of amyloid Beta protein facilitate hippocampal long-term depression by disrupting neuronal glutamate uptake. *Neuron* **62:** 788-801

Li S, Jin M, Koeglsperger T, Shepardson NE, Shankar GM, Selkoe DJ (2011) Soluble Abeta oligomers inhibit long-term potentiation through a mechanism involving excessive activation of extrasynaptic NR2B-containing NMDA receptors. *J Neurosci* **31:** 6627-6638

Lichtenthaler SF (2011) alpha-secretase in Alzheimer's disease: molecular identity, regulation and therapeutic potential. *J Neurochem* **116:** 10-21

Lin DD, Cohen AS, Coulter DA (2001) Zinc-induced augmentation of excitatory synaptic currents and glutamate receptor responses in hippocampal CA3 neurons. *Journal of neurophysiology* **85:** 1185-1196

Linkous DH, Adlard PA, Wanschura PB, Conko KM, Flinn JM (2009) The effects of enhanced zinc on spatial memory and plaque formation in transgenic mice. *J Alzheimers Dis* **18:** 565-579

Liu G, Huang W, Moir RD, Vanderburg CR, Lai B, Peng Z, Tanzi RE, Rogers JT, Huang X (2006) Metal exposure and Alzheimer's pathogenesis. *J Struct Biol* **155:** 45-51

Lo JC, Loh KK, Zheng H, Sim SK, Chee MW (2014) Sleep duration and age-related changes in brain structure and cognitive performance. *Sleep* **37:** 1171-1178

Lomakin A, Chung DS, Benedek GB, Kirschner DA, Teplow DB (1996) On the nucleation and growth of amyloid beta-protein fibrils: detection of nuclei and quantitation of rate constants. *Proc Natl Acad Sci U S A* **93:** 1125-1129

Lopez-Toledano MA, Shelanski ML (2004) Neurogenic effect of beta-amyloid peptide in the development of neural stem cells. *J Neurosci* **24:** 5439-5444

Lovell MA, Robertson JD, Teesdale WJ, Campbell JL, Markesbery WR (1998) Copper, iron and zinc in Alzheimer's disease senile plaques. *J Neurol Sci* **18:** 47-52

Lovell MA, Xie C, Gabbita SP, Markesbery WR (2000) Decreased thioredoxin and increased thioredoxin reductase levels in Alzheimer's disease brain. *Free Radic Biol Med* **28:** 418-427

Lu JX, Qiang W, Yau WM, Schwieters CD, Meredith SC, Tycko R (2013) Molecular structure of beta-amyloid fibrils in Alzheimer's disease brain tissue. *Cell* **154:** 1257-1268

Lue LF, Kuo YM, Roher AE, Brachova L, Shen Y, Sue L, Beach T, Kurth JH, Rydel RE, Rogers J (1999) Soluble amyloid beta peptide concentration as a predictor of synaptic change in Alzheimer's disease. *Am J Pathol* **155:** 853-862

Luo L, Tully T, White K (1992) Human amyloid precursor protein ameliorates behavioral deficit of flies deleted for Appl gene. *Neuron* **9:** 595-605

Luo Y, Bolon B, Damore MA, Fitzpatrick D, Liu H, Zhang J, Yan Q, Vassar R, Citron M (2003) BACE1 (beta-secretase) knockout mice do not acquire compensatory gene expression changes or develop neural lesions over time. *Neurobiol Dis* **14:** 81-88

Lynch MA (2004) Long-term potentiation and memory. *Physiol Rev* **84:** 87-136

Manczak M, Reddy PH (2013) Abnormal interaction of oligomeric amyloid-beta with phosphorylated tau: implications to synaptic dysfunction and neuronal damage. *J Alzheimers Dis* **36:** 285-295

Marger L, Schubert CR, Bertrand D (2014) Zinc: an underappreciated modulatory factor of brain function. *Biochem Pharmacol* **91:** 426-435

Marks N, Berg MJ, Saito M, Saito M (2008) Glucosylceramide synthase decrease in frontal cortex of Alzheimer brain correlates with abnormal increase in endogenous ceramides: consequences to morphology and viability on enzyme suppression in cultured primary neurons. *Brain Res* **1191:** 136-147

Masamoto K, Tanishita K (2009) Oxygen transport in brain tissue. *J Biomech Eng* **131:** 074002

Mason RP, Shoemaker WJ, Shajenko L, Chambers TE, Herbette LG (1992) Evidence for changes in the Alzheimer's disease brain cortical membrane structure mediated by cholesterol. *Neurobiol Aging* **13:** 413-419

Masters CL, Simms G, Weinman NA, Multhaup G, McDonald BL, Beyreuther K (1985) Amyloid plaque core protein in Alzheimer disease and Down syndrome. *Proc Natl Acad Sci U S A* **82:** 4245-4249

Matheou CJ, Younan ND, Viles JH (2015) Cu2+ accentuates distinct misfolding of Abeta(1-40) and Abeta(1-42) peptides, and potentiates membrane disruption. *Biochem J* **466:** 233-242

Matlack KE, Tardiff DF, Narayan P, Hamamichi S, Caldwell KA, Caldwell GA, Lindquist S (2014) Clioquinol promotes the degradation of metal-dependent amyloid-beta (Abeta) oligomers to restore endocytosis and ameliorate Abeta toxicity. *Proc Natl Acad Sci U S A* **111:** 4013-4018

Matsumura S, Shinoda K, Yamada M, Yokojima S, Inoue M, Ohnishi T, Shimada T, Kikuchi K, Masui D, Hashimoto S, Sato M, Ito A, Akioka M, Takagi S, Nakamura Y, Nemoto K, Hasegawa Y, Takamoto H, Inoue H, Nakamura S, Nabeshima Y, Teplow DB, Kinjo M, Hoshi M (2011) Two distinct amyloid beta-protein (Abeta) assembly pathways leading to oligomers and fibrils identified by combined fluorescence correlation spectroscopy, morphology, and toxicity analyses. *J Biol Chem* **286:** 11555-11562

Mattson MP (1994) Secreted forms of beta-amyloid precursor protein modulate dendrite outgrowth and calcium responses to glutamate in cultured embryonic hippocampal neurons. *J Neurobiol* **25:** 439-450

Mattson MP (1997) Cellular actions of beta-amyloid precursor protein and its soluble and fibrillogenic derivatives. *Physiol Rev* **77:** 1081-1132

Mattson MP (2004) Pathways towards and away from Alzheimer's disease. *Nature* **430:** 631-639

Mattson MP, Cheng B, Davis D, Bryant K, Lieberburg I, Rydel RE (1992) beta-Amyloid peptides destabilize calcium homeostasis and render human cortical neurons vulnerable to excitotoxicity. *J Neurosci* **12:** 376-389

Mattsson N, Blennow K, Zetterberg H (2009) CSF biomarkers: pinpointing Alzheimer pathogenesis. *Ann N Y Acad Sci* **1180:** 28-35

McLaurin J, Chakrabartty A (1996) Membrane disruption by Alzheimer beta-amyloid peptides mediated through specific binding to either phospholipids or gangliosides. Implications for neurotoxicity. *J Biol Chem* **271:** 26482-26489

McLaurin J, Chakrabartty A (1997) Characterization of the interactions of Alzheimer beta-amyloid peptides with phospholipid membranes. *Eur J Biochem* **245:** 355-363

Mecocci P, MacGarvey U, Beal MF (1994) Oxidative damage to mitochondrial DNA is increased in Alzheimer's disease. *Ann Neurol* **36:** 747-751

Meersman F, Dobson CM (2006) Probing the pressure-temperature stability of amyloid fibrils provides new insights into their molecular properties. *Biochim Biophys Acta* **1764:** 452-460

Mega MS, Cummings JL, Fiorello T, Gornbein J (1996) The spectrum of behavioral changes in Alzheimer's disease. *Neurology* **46:** 130-135

Meinhardt J, Sachse C, Hortschansky P, Grigorieff N, Fandrich M (2009) Abeta(1-40) fibril polymorphism implies diverse interaction patterns in amyloid fibrils. *J Mol Biol* **386:** 869-877

Meraz-Rios MA, Lira-De Leon KI, Campos-Pena V, De Anda-Hernandez MA, Mena-Lopez R (2010) Tau oligomers and aggregation in Alzheimer's disease. *J Neurochem* **112:** 1353-1367

Milanesi L, Sheynis T, Xue WF, Orlova EV, Hellewell AL, Jelinek R, Hewitt EW, Radford SE, Saibil HR (2012) Direct three-dimensional visualization of membrane disruption by amyloid fibrils. *Proc Natl Acad Sci U S A* **109:** 20455-20460

Miller LM, Wang Q, Telivala TP, Smith RJ, Lanzirotti A, Miklossy J (2006) Synchrotron-based infrared and X-ray imaging shows focalized accumulation of Cu and Zn co-localized with beta-amyloid deposits in Alzheimer's disease. *J Struct Biol* **155:** 30-37

Minicozzi V, Stellato F, Comai M, Dalla Serra M, Potrich C, Meyer-Klaucke W, Morante S (2008) Identifying the minimal copper- and zinc-binding site sequence in amyloid-beta peptides. *J Biol Chem***:** 283:10784-10792

Miravalle L, Tokuda T, Chiarle R, Giaccone G, Bugiani O, Tagliavini F, Frangione B, Ghiso J (2000) Substitutions at codon 22 of Alzheimer's abeta peptide induce diverse conformational changes and apoptotic effects in human cerebral endothelial cells. *J Biol Chem* **275:** 27110-27116

Mithu VS, Sarkar B, Bhowmik D, Chandrakesan M, Maiti S, Madhu PK (2011) Zn(++) binding disrupts the Asp(23)-Lys(28) salt bridge without altering the hairpin-shaped cross-beta Structure of Abeta(42) amyloid aggregates. *Biophys J* **101:** 2825-2832

Mocchetti I (2005) Exogenous gangliosides, neuronal plasticity and repair, and the neurotrophins. *Cell Mol Life Sci* **62:** 2283-2294

Mold M, Ouro-Gnao L, Wieckowski BM, Exley C (2013) Copper prevents amyloid-beta(1-42) from forming amyloid fibrils under near-physiological conditions in vitro. *Sci Rep* **3:** 1256

Nadal RC, Rigby SE, Viles JH (2008) Amyloid beta-Cu2+ complexes in both monomeric and fibrillar forms do not generate H2O2 catalytically but quench hydroxyl radicals. *Biochemistry* **47:** 11653-11664

Nakanishi K, Berova N, Woody R (1994) *Circular Dichroism: Principles and Applications*: VCH.

Nalivaeva NN, Belyaev ND, Zhuravin IA, Turner AJ (2012) The Alzheimer's amyloid-degrading peptidase, neprilysin: can we control it? *International journal of Alzheimer's disease* **2012:** 383796

Nalivaevaa NN, Fisk L, Kochkina EG, Plesneva SA, Zhuravin IA, Babusikova E, Dobrota D, Turner AJ (2004) Effect of hypoxia/ischemia and hypoxic preconditioning/reperfusion on expression of some amyloid-degrading enzymes. *Ann N Y Acad Sci* **1035:** 21-33

Naslund J, Schierhorn A, Hellman U, Lannfelt L, Roses AD, Tjernberg LO, Silberring J, Gandy SE, Winblad B, Greengard P, et al. (1994) Relative abundance of Alzheimer A beta amyloid peptide variants in Alzheimer disease and normal aging. *Proc Natl Acad Sci U S A* **91:** 8378-8382

Nelson R, Eisenberg D (2006) Recent atomic models of amyloid fibril structure. *Curr Opin Struct Biol* **16:** 260-265

Nielsen JT, Bjerring M, Jeppesen MD, Pedersen RO, Pedersen JM, Hein KL, Vosegaard T, Skrydstrup T, Otzen DE, Nielsen NC (2009) Unique identification of supramolecular structures in amyloid fibrils by solid-state NMR spectroscopy. *Angew Chem Int Ed Engl* **48:** 2118-2121

Nilsberth C, Westlind-Danielsson A, Eckman CB, Condron MM, Axelman K, Forsell C, Stenh C, Luthman J, Teplow DB, Younkin SG, Naslund J, Lannfelt L (2001) The 'Arctic' APP mutation (E693G) causes Alzheimer's disease by enhanced Abeta protofibril formation. *Nat Neurosci* **4:** 887-893

Noy D, Solomonov I, Sinkevich O, Arad T, Kjaer K, Sagi I (2008) Zinc-amyloid beta interactions on a millisecond time-scale stabilize non-fibrillar Alzheimer-related species. *J Am Chem Soc* **130:** 1376-1383

Nydegger I, Rumschik SM, Kay AR (2010) Zinc is externalized rather than released during synaptic transmission. *ACS chemical neuroscience* **1:** 728-736

O'Nuallain B, Freir DB, Nicoll AJ, Risse E, Ferguson N, Herron CE, Collinge J, Walsh DM (2010) Amyloid beta-protein dimers rapidly form stable synaptotoxic protofibrils. *J Neurosci* **30:** 14411-14419

Ohvo-Rekila H, Ramstedt B, Leppimaki P, Slotte JP (2002) Cholesterol interactions with phospholipids in membranes. *Prog Lipid Res* **41:** 66-97

Olson MI, Shaw CM (1969) Presenile dementia and Alzheimer's disease in mongolism. *Brain* **92:** 147-156

Opazo C, Huang X, Cherny RA, Moir RD, Roher AE, White AR, Cappai R, Masters CL, Tanzi RE, Inestrosa NC, Bush AI (2002) Metalloenzyme-like activity of Alzheimer's disease beta-amyloid. Cu-dependent catalytic conversion of dopamine, cholesterol, and biological reducing agents to neurotoxic H(2)O(2). *J Biol Chem* **277:** 40302-40308

Pamplona R, Dalfo E, Ayala V, Bellmunt MJ, Prat J, Ferrer I, Portero-Otin M (2005) Proteins in human brain cortex are modified by oxidation, glycoxidation, and lipoxidation. Effects of Alzheimer disease and identification of lipoxidation targets. *J Biol Chem* **280:** 21522-21530

Paoletti P, Vergnano AM, Barbour B, Casado M (2009) Zinc at glutamatergic synapses. *Neuroscience* **158:** 126-136

Paravastu AK, Leapman RD, Yau WM, Tycko R (2008) Molecular structural basis for polymorphism in Alzheimer's beta-amyloid fibrils. *Proc Natl Acad Sci U S A* **105:** 18349-18354

Parthasarathy S, Long F, Miller Y, Xiao Y, McElheny D, Thurber K, Ma B, Nussinov R, Ishii Y (2011) Molecular-level examination of Cu2+ binding structure for amyloid fibrils of 40-residue Alzheimer's beta by solid-state NMR spectroscopy. *J Am Chem Soc* **133:** 3390-3400

Parvathy S, Hussain I, Karran EH, Turner AJ, Hooper NM (1999) Cleavage of Alzheimer's amyloid precursor protein by alpha-secretase occurs at the surface of neuronal cells. *Biochemistry* **38:** 9728-9734

Patel AR, Kanazawa KK, Frank CW (2009) Antibody binding to a tethered vesicle assembly using QCM-D. *Anal Chem* **81:** 6021-6029

Pauwels K, Williams TL, Morris KL, Jonckheere W, Vandersteen A, Kelly G, Schymkowitz J, Rousseau F, Pastore A, Serpell LC, Broersen K (2012) Structural basis for increased toxicity of pathological abeta42:abeta40 ratios in Alzheimer disease. *J Biol Chem* **287:** 5650-5660

Pedersen JT, Østergaard J, Rozlosnik N, Gammelgaard B, Heegaard NH (2011) Cu(II) mediates kinetically distinct, non-amyloidogenic aggregation of amyloid-beta peptides. *J Biol Chem* **286:** 26952-26963

Petkova AT, Leapman RD, Guo Z, Yau WM, Mattson MP, Tycko R (2005) Self-propagating, molecular-level polymorphism in Alzheimer's beta-amyloid fibrils. *Science* **307:** 262-265

Pillot T, Goethals M, Vanloo B, Talussot C, Brasseur R, Vandekerckhove J, Rosseneu M, Lins L (1996) Fusogenic properties of the C-terminal domain of the Alzheimer beta-amyloid peptide. *J Biol Chem* **271:** 28757-28765

Poorkaj P, Bird TD, Wijsman E, Nemens E, Garruto RM, Anderson L, Andreadis A, Wiederholt WC, Raskind M, Schellenberg GD (1998) Tau is a candidate gene for chromosome 17 frontotemporal dementia. *Ann Neurol* **43:** 815-825

Prana (2014) Prana Biotechnology announces top line results of Phase 2 IMAGINE trial of PBT2 in Alzheimer's disease. *Alzheimer's disease, Investor Announcement*

Prince M, Jackson J, Ferri CP, Sousa R, Albanese E, Ribeiro WS, Honyashiki M (2009) Alzheimer's disease international world alzheimer report. *In International AsD (ed)***:** pp. 1-96

Prusiner SB (1998) Prions. *Proc Natl Acad Sci U S A* **95:** 13363-13383

Puzzo D, Privitera L, Fa M, Staniszewski A, Hashimoto G, Aziz F, Sakurai M, Ribe EM, Troy CM, Mercken M, Jung SS, Palmeri A, Arancio O (2011) Endogenous amyloid-beta is necessary for hippocampal synaptic plasticity and memory. *Ann Neurol* **69:** 819-830

Puzzo D, Privitera L, Leznik E, Fa M, Staniszewski A, Palmeri A, Arancio O (2008) Picomolar amyloid-beta positively modulates synaptic plasticity and memory in hippocampus. *J Neurosci* **28:** 14537-14545

Qian J, Noebels JL (2006) Exocytosis of vesicular zinc reveals persistent depression of neurotransmitter release during metabotropic glutamate receptor long-term depression at the hippocampal CA3-CA1 synapse. *J Neurosci* **26:** 6089-6095

Que EL, Domaille DW, Chang CJ (2008) Metals in neurobiology: probing their chemistry and biology with molecular imaging. *Chem Rev* **108:** 1517-1549

Querfurth HW, LaFerla FM (2010) Alzheimer's disease. *N Engl J Med* **362:** 329-344

Quintarelli G, Zito R, Cifonelli JA (1971) On phosphotungstic acid staining. I. *J Histochem Cytochem* **19:** 641-647

Quist A, Doudevski I, Lin H, Azimova R, Ng D, Frangione B, Kagan B, Ghiso J, Lal R (2005) Amyloid ion channels: a common structural link for protein-misfolding disease. *Proc Natl Acad Sci U S A* **102:** 10427-10432

Raman B, Ban T, Yamaguchi K, Sakai M, Kawai T, Naiki H, Goto Y (2005) Metal ion-dependent effects of clioquinol on the fibril growth of an amyloid {beta} peptide. *J Biol Chem* **280:** 16157-16162

Ravona-Springer R, Davidson M, Noy S (2003) Is the distinction between Alzheimer's disease and vascular dementia possible and relevant? *Dialogues Clin Neurosci* **5:** 7-15

Riccio A, Ahn S, Davenport CM, Blendy JA, Ginty DD (1999) Mediation by a CREB family transcription factor of NGF-dependent survival of sympathetic neurons. *Science* **286:** 2358-2361

Roberts GW (1988) Immunocytochemistry of neurofibrillary tangles in dementia pugilistica and Alzheimer's disease: evidence for common genesis. *Lancet* **2:** 1456-1458

Roses AD (1997) Alzheimer's disease: the genetics of risk. *Hosp Pract (1995)* **32:** 51-55, 58-63, 67-59

Roth GS, Joseph JA, Mason RP (1995) Membrane alterations as causes of impaired signal transduction in Alzheimer's disease and aging. *Trends Neurosci* **18:** 203-206

Roychaudhuri R, Yang M, Hoshi MM, Teplow DB (2009) Amyloid beta-protein assembly and Alzheimer disease. *J Biol Chem* **284:** 4749-4753

Sabate R, Gallardo M, Estelrich J (2005) Temperature dependence of the nucleation constant rate in beta amyloid fibrillogenesis. *Int J Biol Macromol* **35:** 9-13

Salbaum JM, Ruddle FH (1994) Embryonic expression pattern of amyloid protein precursor suggests a role in differentiation of specific subsets of neurons. *J Exp Zool* **269:** 116-127

Sanokawa-Akakura R, Cao W, Allan K, Patel K, Ganesh A, Heiman G, Burke R, Kemp FW, Bogden JD, Camakaris J, Birge RB, Konsolaki M (2010) Control of Alzheimer's amyloid beta toxicity by the high molecular weight immunophilin FKBP52 and copper homeostasis in Drosophila. *PLoS One* **5:** e8626

Sarell CJ, Syme CD, Rigby SE, Viles JH (2009) Copper(II) binding to amyloid-beta fibrils of Alzheimer's disease reveals a picomolar affinity: stoichiometry and coordination geometry are independent of Abeta oligomeric form. *Biochemistry* **48:** 4388-4402

Sarell CJ, Wilkinson SR, Viles JH (2010) Substoichiometric levels of Cu2+ ions accelerate the kinetics of fiber formation and promote cell toxicity of amyloid-{beta} from Alzheimer disease. *J Biol Chem* **285:** 41533-41540

Sawaya MR, Sambashivan S, Nelson R, Ivanova MI, Sievers SA, Apostol MI, Thompson MJ, Balbirnie M, Wiltzius JJ, McFarlane HT, Madsen AO, Riekel C, Eisenberg D (2007) Atomic structures of amyloid cross-beta spines reveal varied steric zippers. *Nature* **447:** 453-457

Sawyer WH, Puckridge J (1973) The dissociation of proteins by chaotropic salts. *J Biol Chem* **248:** 8429-8433

Scherzinger E, Sittler A, Schweiger K, Heiser V, Lurz R, Hasenbank R, Bates GP, Lehrach H, Wanker EE (1999) Self-assembly of polyglutamine-containing huntingtin fragments into amyloid-like fibrils: implications for Huntington's disease pathology. *Proc Natl Acad Sci U S A* **96:** 4604-4609

Scheuner D, Eckman C, Jensen M, Song X, Citron M, Suzuki N, Bird TD, Hardy J, Hutton M, Kukull, W., Larson E, Levy-Lahad E, Viitanen M, Peskind E, Poorkaj P, Schellenberg G (1996)

Secreted amyloid beta-protein similar to that in the senile plaques of Alzheimer's disease is increased in vivo by the presenilin 1 and 2 and APP mutations linked to familial Alzheimer's disease. *Nat Med* **2:** 864-870

Schlief ML, West T, Craig AM, Holtzman DM, Gitlin JD (2006) Role of the Menkes copper-transporting ATPase in NMDA receptor-mediated neuronal toxicity. *Proc Natl Acad Sci U S A* **103:** 14919-14924

Schmidt M, Rohou A, Lasker K, Yadav JK, Schiene-Fischer C, Fandrich M, Grigorieff N (2015) Peptide dimer structure in an Abeta(1-42) fibril visualized with cryo-EM. *Proc Natl Acad Sci U S A* **112:** 11858-11863

Schnabel J (2011) Amyloid: little proteins, big clues. *Nature* **475:** S12-14

Selkoe DJ (1991) The molecular pathology of Alzheimer's disease. *Neuron* **6:** 487-498

Selkoe DJ (2002) Alzheimer's disease is a synaptic failure. *Science* **298:** 789-791

Selkoe DJ (2008) Soluble oligomers of the amyloid beta-protein impair synaptic plasticity and behavior. *Behav Brain Res* **192:** 106-113

Sen P, Fatima S, Ahmad B, Khan RH (2009) Interactions of thioflavin T with serum albumins: spectroscopic analyses. *Spectrochimica acta Part A, Molecular and biomolecular spectroscopy* **74:** 94-99

Sensi SL, Paoletti P, Koh JY, Aizenman E, Bush AI, Hershfinkel M (2011) The neurophysiology and pathology of brain zinc. *J Neurosci* **31:** 16076-16085

Serpell LC, Sunde M, Benson MD, Tennent GA, Pepys MB, Fraser PE (2000) The protofilament substructure of amyloid fibrils. *J Mol Biol* **300:** 1033-1039

Seubert P, Vigo-Pelfrey C, Esch F, Lee M, Dovey H, Davis D, Sinha S, Schlossmacher M, Whaley J, Swindlehurst C, et al. (1992) Isolation and quantification of soluble Alzheimer's beta-peptide from biological fluids. *Nature* **359:** 325-327

Sgourakis NG, Merced-Serrano M, Boutsidis C, Drineas P, Du Z, Wang C, Garcia AE (2011) Atomic-level characterization of the ensemble of the Abeta(1-42) monomer in water using unbiased molecular dynamics simulations and spectral algorithms. *J Mol Biol* **405:** 570-583

Sgourakis NG, Yan Y, McCallum SA, Wang C, Garcia AE (2007) The Alzheimer's peptides Abeta40 and 42 adopt distinct conformations in water: a combined MD / NMR study. *J Mol Biol* **368:** 1448-1457

Shankar GM, Li S, Mehta TH, Garcia-Munoz A, Shepardson NE, Smith I, Brett FM, Farrell MA, Rowan MJ, Lemere CA, Regan CM, Walsh DM, Sabatini BL, Selkoe DJ (2008) Amyloid-beta protein dimers isolated directly from Alzheimer's brains impair synaptic plasticity and memory. *Nat Med* **14:** 837-842

Sharma AK, Pavlova ST, Kim J, Kim J, Mirica LM (2013) The effect of Cu(2+) and Zn(2+) on the Abeta42 peptide aggregation and cellular toxicity. *Metallomics* **5:** 1529-1536

Sharonova IN, Vorobjev VS, Haas HL (1998) High-affinity copper block of GABA(A) receptor-mediated currents in acutely isolated cerebellar Purkinje cells of the rat. *Eur J Neurosci* **10:** 522-528

Shen CL, Murphy RM (1995) Solvent effects on self-assembly of beta-amyloid peptide. *Biophys J* **69:** 640-651

Sheng JG, Price DL, Koliatsos VE (2002) Disruption of corticocortical connections ameliorates amyloid burden in terminal fields in a transgenic model of Abeta amyloidosis. *J Neurosci* **22:** 9794-9799

Shin BK, Saxena S (2011) Substantial Contribution of the Two Imidazole Rings of the His13-His14 Dyad to Cu(II) Binding in Amyloid-beta(1-16) at Physiological pH and Its Significance. *J Phys Chem A* **115:** 9590-9602

Shirotani K, Tsubuki S, Iwata N, Takaki Y, Harigaya W, Maruyama K, Kiryu-Seo S, Kiyama H, Iwata H, Tomita T, Iwatsubo T, Saido TC (2001) Neprilysin degrades both amyloid beta peptides 1-40 and 1-42 most rapidly and efficiently among thiorphan- and phosphoramidon-sensitive endopeptidases. *J Biol Chem* **276:** 21895-21901

Sigel H, Sigel A, Sigel R (2009) *Metal Ions in Life Sciences*, Vol. 5, Cambridge: Royal Society of Chemistry.

Sikorski P, Atkins ED, Serpell LC (2003) Structure and texture of fibrous crystals formed by Alzheimer's abeta(11-25) peptide fragment. *Structure* **11:** 915-926

Silva KI, Saxena S (2013) Zn(II) ions substantially perturb Cu(II) ion coordination in amyloid-beta at physiological pH. *J Phys Chem B* **117:** 9386-9394

Simons M, Keller P, De Strooper B, Beyreuther K, Dotti CG, Simons K (1998) Cholesterol depletion inhibits the generation of beta-amyloid in hippocampal neurons. *Proc Natl Acad Sci U S A* **95:** 6460-6464

Singh SK, Sinha P, Mishra L, Srikrishna S (2013) Neuroprotective Role of a Novel Copper Chelator against Abeta 42 Induced Neurotoxicity. *Int J Alzheimers Dis* **2013:** 567128

Sinha S, Anderson JP, Barbour R, Basi GS, Caccavello R, Davis D, Doan M, Dovey HF, Frigon N, Hong J, Jacobson-Croak K, Jewett N, Keim P, Knops J, Lieberburg I, Power M, Tan H, Tatsuno G, Tung J, Schenk D, Seubert P, Suomensaari SM, Wang S, Walker D, Zhao J, McConlogue L, John V (1999) Purification and cloning of amyloid precursor protein beta-secretase from human brain. *Nature* **402:** 537-540

Smith DP, Ciccotosto GD, Tew DJ, Fodero-Tavoletti MT, Johanssen T, Masters CL, Barnham KJ, Cappai R (2007) Concentration dependent Cu2+ induced aggregation and dityrosine formation of the Alzheimer's disease amyloid-beta peptide. *Biochemistry* **46:** 2881-2891

Snyder EM, Nong Y, Almeida CG, Paul S, Moran T, Choi EY, Nairn AC, Salter MW, Lombroso PJ, Gouras GK, Greengard P (2005) Regulation of NMDA receptor trafficking by amyloid-beta. *Nat Neurosci* **8:** 1051-1058

Sokolov Y, Kozak JA, Kayed R, Chanturiya A, Glabe C, Hall JE (2006) Soluble amyloid oligomers increase bilayer conductance by altering dielectric structure. *J Gen Physiol* **128:** 637-647

Solomonov I, Korkotian E, Born B, Feldman Y, Bitler A, Rahimi F, Li H, Bitan G, Sagi I (2012) Zn2+-Abeta40 complexes form metastable quasi-spherical oligomers that are cytotoxic to cultured hippocampal neurons. *J Biol Chem* **287:** 20555-20564

Sparks DL, Schreurs BG (2003) Trace amounts of copper in water induce beta-amyloid plaques and learning deficits in a rabbit model of Alzheimer's disease. *Proc Natl Acad Sci U S A* **100:** 11065-11069

Spillantini MG, Bird TD, Ghetti B (1998) Frontotemporal dementia and Parkinsonism linked to chromosome 17: a new group of tauopathies. *Brain Pathol* **8:** 387-402

Srabasti Acharya LJL (2015) Reconfiguration of the Alzheimer's Peptide Kinetically Controls Aggregation in Alzheimer's Disease. *Biophys J* **108:** 65a-66a

Stelmashook EV, Isaev NK, Genrikhs EE, Amelkina GA, Khaspekov LG, Skrebitsky VG, Illarioshkin SN (2014) Role of zinc and copper ions in the pathogenetic mechanisms of Alzheimer's and Parkinson's diseases. *Biochemistry (Mosc)* **79:** 391-396

Stickgold R, Walker MP (2005) Sleep and memory: the ongoing debate. *Sleep* **28:** 1225-1227

Stine WB, Jr., Dahlgren KN, Krafft GA, LaDu MJ (2003) In vitro characterization of conditions for amyloid-beta peptide oligomerization and fibrillogenesis. *J Biol Chem* **278:** 11612-11622

Stsiapura VI, Maskevich AA, Kuzmitsky VA, Turoverov KK, Kuznetsova IM (2007) Computational study of thioflavin T torsional relaxation in the excited state. *J Phys Chem A* **111:** 4829-4835

Student (1908) The probable error of mean. *Biometrika* **6:** 1-25

Subasinghe S, Unabia S, Barrow CJ, Mok SS, Aguilar MI, Small DH (2003) Cholesterol is necessary both for the toxic effect of Abeta peptides on vascular smooth muscle cells and for Abeta binding to vascular smooth muscle cell membranes. *J Neurochem* **84:** 471-479

Sunde M, Serpell LC, Bartlam M, Fraser PE, Pepys MB, Blake CC (1997) Common core structure of amyloid fibrils by synchrotron X-ray diffraction. *J Mol Biol* **273:** 729-739

Suzuki T, Oishi M, Marshak DR, Czernik AJ, Nairn AC, Greengard P (1994) Cell cycle-dependent regulation of the phosphorylation and metabolism of the Alzheimer amyloid precursor protein. *EMBO J* **13:** 1114-1122

Syme CD, Nadalm RC, Rigby SE, Viles JH (2004) Copper binding to the amyloid-beta (Abeta) peptide associated with Alzheimer's disease: folding, coordination geometry, pH dependence, stoichiometry, and affinity of Abeta-(1-28): insights from a range of complementary spectroscopic techniques. *J Biol Chem***:** 279:18169-18177

Syme CD, Viles JH (2006) Solution 1H NMR investigation of Zn2+ and Cd2+ binding to amyloid-beta peptide (Abeta) of Alzheimer's disease. *Biochim Biophys Acta* **1764:** 246-256

Szewczyk B (2013) Zinc homeostasis and neurodegenerative disorders. *Front Aging Neurosci* **5:** 33

Tabaton M, Zhu X, Perry G, Smith MA, Giliberto L (2010) Signaling effect of amyloid-beta(42) on the processing of AbetaPP. *Exp Neurol* **221:** 18-25

Tackenberg C, Grinschgl S, Trutzel A, Santuccione AC, Frey MC, Konietzko U, Grimm J, Brandt R, Nitsch RM (2013) NMDA receptor subunit composition determines beta-amyloid-induced neurodegeneration and synaptic loss. *Cell death & disease* **4:** e608

Takeda A (2011) Zinc signaling in the hippocampus and its relation to pathogenesis of depression. *Mol Neurobiol* **44:** 166-174

Takeda A, Nakamura M, Fujii H, Tamano H (2013) Synaptic Zn(2+) homeostasis and its significance. *Metallomics* **5:** 417-423

Taketo M, Yoshioka T (2000) Developmental change of GABA(A) receptor-mediated current in rat hippocampus. *Neuroscience* **96:** 507-514

Taniguchi T, Kawamata T, Mukai H, Hasegawa H, Isagawa T, Yasuda M, Hashimoto T, Terashima A, Nakai M, Mori H, Ono Y, Tanaka C (2001) Phosphorylation of tau is regulated by PKN. *J Biol Chem* **276:** 10025-10031

Taubenfeld SM, Milekic MH, Monti B, Alberini CM (2001) The consolidation of new but not reactivated memory requires hippocampal C/EBPbeta. *Nat Neurosci* **4:** 813-818

Teplow DB, Lazo ND, Bitan G, Bernstein S, Wyttenbach T, Bowers MT, Baumketner A, Shea JE, Urbanc B, Cruz L, Borreguero J, Stanley HE (2006) Elucidating amyloid beta-protein folding and assembly: A multidisciplinary approach. *Acc Chem Res* **39:** 635-645

Terry RD, Masliah E, Salmon DP, Butters N, DeTeresa R, Hill R, Hansen LA, Katzman R (1991) Physical basis of cognitive alterations in Alzheimer's disease: synapse loss is the major correlate of cognitive impairment. *Ann Neurol* **30:** 572-580

Torok M, Milton S, Kayed R, Wu P, McIntire T, Glabe CG, Langen R (2002) Structural and dynamic features of Alzheimer's Abeta peptide in amyloid fibrils studied by site-directed spin labeling. *J Biol Chem* **277:** 40810-40815

Tougu V, Karafin A, Zovo K, Chung RS, Howells C, West AK, Palumaa P (2009) Zn(II)- and Cu(II)-induced non-fibrillar aggregates of amyloid-beta (1-42) peptide are transformed to amyloid fibrils, both spontaneously and under the influence of metal chelators. *J Neurochem* **110:** 1784-1795

Trombley PQ, Shepherd GM (1996) Differential modulation by zinc and copper of amino acid receptors from rat olfactory bulb neurons. *Journal of neurophysiology* **76:** 2536-2546

Tycko R, Sciarretta KL, Orgel JP, Meredith SC (2009) Evidence for novel beta-sheet structures in Iowa mutant beta-amyloid fibrils. *Biochemistry* **48:** 6072-6084

Uriu-Adams JY, Keen CL (2005) Copper, oxidative stress, and human health. *Mol Aspects Med* **26:** 268-298

Uversky VN, Li J, Fink AL (2001) Metal-triggered structural transformations, aggregation, and fibrillation of human alpha-synuclein. A possible molecular NK between Parkinson's disease and heavy metal exposure. *J Biol Chem* **276:** 44284-44296

Uversky VN, Oldfield CJ, Dunker AK (2008) Intrinsically disordered proteins in human diseases: introducing the D2 concept. *Annu Rev Biophys* **37:** 215-246

Valdes-Gonzalez T, Inagawa J, Ido T (2001) Neuropeptides interact with glycolipid receptors: a surface plasmon resonance study. *Peptides* **22:** 1099-1106

Van Broeckhoven C, Haan J, Bakker E, Hardy JA, Van Hul W, Wehnert A, Vegter-Van der Vlis M, Roos RA (1990) Amyloid beta protein precursor gene and hereditary cerebral hemorrhage with amyloidosis (Dutch). *Science* **248:** 1120-1122

Vassar R, Bennett BD, Babu-Khan S, Kahn S, Mendiaz EA, Denis P, Teplow DB, Ross S, Amarante P, Loeloff R, Luo Y, Fisher S, Fuller J, Edenson S, Lile J, Jarosinski MA, Biere AL, Curran E, Burgess T, Louis JC, Collins F, Treanor J, Rogers G, Citron M (1999) Beta-secretase cleavage of Alzheimer's amyloid precursor protein by the transmembrane aspartic protease BACE. *Science* **286:** 735-741

Vergnano AM, Rebola N, Savtchenko LP, Pinheiro PS, Casado M, Kieffer BL, Rusakov DA, Mulle C, Paoletti P (2014) Zinc dynamics and action at excitatory synapses. *Neuron* **82:** 1101-1114

Viles JH (2012) Metal ions and amyloid fiber formation in neurodegenerative diseases. Copper, zinc and iron in Alzheimer's, Parkinson's and prion diseases. *Coord Chem Rev* **256:** 2271-2284

Viles JH, Cohen FE, Prusiner SB, Goodin DB, Wright PE, Dyson HJ (1999) Copper binding to the prion protein: structural implications of four identical cooperative binding sites. *Proc Natl Acad Sci U S A* **96:** 2042-2047

Vivekanandan S, Brender JR, Lee SY, Ramamoorthy A (2011) A partially folded structure of amyloid-beta(1-40) in an aqueous environment. *Biochem Biophys Res Commun* **411:** 312-316

Vlachova V, Zemkova H, Vyklicky L, Jr. (1996) Copper modulation of NMDA responses in mouse and rat cultured hippocampal neurons. *Eur J Neurosci* **8:** 2257-2264

Vogt K, Mellor J, Tong G, Nicoll R (2000) The actions of synaptically released zinc at hippocampal mossy fiber synapses. *Neuron* **26:** 187-196

Waldemar G, Dubois B, Emre M, Georges J, McKeith IG, Rossor M, Scheltens P, Tariska P, Winblad B, Efns (2007) Recommendations for the diagnosis and management of Alzheimer's disease and other disorders associated with dementia: EFNS guideline. *Eur J Neurol* **14:** e1-26

Walsh DM, Hartley DM, Kusumoto Y, Fezoui Y, Condron MM, Lomakin A, Benedek GB, Selkoe DJ, Teplow DB (1999) Amyloid beta-protein fibrillogenesis. Structure and biological activity of protofibrillar intermediates. *J Biol Chem* **274:** 25945-25952

Walsh DM, Klyubin I, Fadeeva JV, Cullen WK, Anwyl R, Wolfe MS, Rowan MJ, Selkoe DJ (2002) Naturally secreted oligomers of amyloid beta protein potently inhibit hippocampal long-term potentiation in vivo. *Nature* **416:** 535-539

Wang DS, Lipton RB, Katz MJ, Davies P, Buschke H, Kuslansky G, Verghese J, Younkin SG, Eckman C, Dickson DW (2005) Decreased neprilysin immunoreactivity in Alzheimer disease, but not in pathological aging. *J Neuropathol Exp Neurol* **64:** 378-385

Wang J, Dickson DW, Trojanowski JQ, Lee VM (1999) The levels of soluble versus insoluble brain Abeta distinguish Alzheimer's disease from normal and pathologic aging. *Exp Neurol* **158:** 328-337

Wang L, Lashuel HA, Walz T, Colon W (2002) Murine apolipoprotein serum amyloid A in solution forms a hexamer containing a central channel. *Proc Natl Acad Sci U S A* **99:** 15947-15952

Wasco W, Bupp K, Magendantz M, Gusella JF, Tanzi RE, Solomon F (1992) Identification of a mouse brain cDNA that encodes a protein related to the Alzheimer disease-associated amyloid beta protein precursor. *Proc Natl Acad Sci U S A* **89:** 10758-10762

Wasco W, Gurubhagavatula S, Paradis MD, Romano DM, Sisodia SS, Hyman BT, Neve RL, Tanzi RE (1993) Isolation and characterization of APLP2 encoding a homologue of the Alzheimer's associated amyloid beta protein precursor. *Nat Genet* **5:** 95-100

Watts JC, Condello C, Stohr J, Oehler A, Lee J, DeArmond SJ, Lannfelt L, Ingelsson M, Giles K, Prusiner SB (2014) Serial propagation of distinct strains of Abeta prions from Alzheimer's disease patients. *Proc Natl Acad Sci U S A* **111:** 10323-10328

Weidemann A, Konig G, Bunke D, Fischer P, Salbaum JM, Masters CL, Beyreuther K (1989) Identification, biogenesis, and localization of precursors of Alzheimer's disease A4 amyloid protein. *Cell* **57:** 115-126

Weiser T, Wienrich M (1996) The effects of copper ions on glutamate receptors in cultured rat cortical neurons. *Brain Res* **742:** 211-218

Welge V, Fiege O, Lewczuk P, Mollenhauer B, Esselmann H, Klafki HW, Wolf S, Trenkwalder C, Otto M, Kornhuber J, Wiltfang J, Bibl M (2009) Combined CSF tau, p-tau181 and amyloid-beta 38/40/42 for diagnosing Alzheimer's disease. *J Neural Transm* **116:** 203-212

Wetzel R (2006) Amyloid fibrils--common threads in the natural history of proteins. *Acc Chem Res* **39:** 567

White AR, Reyes R, Mercer JF, Camakaris J, Zheng H, Bush AI, Multhaup G, Beyreuther K, Masters CL, Cappai R (1999) Copper levels are increased in the cerebral cortex and liver of APP and APLP2 knockout mice. *Brain Res* **842:** 439-444

Whitmore L, Wallace BA (2008) Protein secondary structure analyses from circular dichroism spectroscopy: methods and reference databases. *Biopolymers* **89:** 392-400

Wickner RB (1994) [URE3] as an altered URE2 protein: evidence for a prion analog in Saccharomyces cerevisiae. *Science* **264:** 566-569

Williams DR, Lees AJ (2009) Progressive supranuclear palsy: clinicopathological concepts and diagnostic challenges. *Lancet Neurol* **8:** 270-279

Williams TL, Day IJ, Serpell LC (2010) The effect of Alzheimer's Abeta aggregation state on the permeation of biomimetic lipid vesicles. *Langmuir* **26:** 17260-17268

Williams TL, Serpell LC (2011) Membrane and surface interactions of Alzheimer's Abeta peptide--insights into the mechanism of cytotoxicity. *The FEBS journal* **278:** 3905-3917

Wirtz KW (1991) Phospholipid transfer proteins. *Annu Rev Biochem* **60:** 73-99

Wood SJ, Maleeff B, Hart T, Wetzel R (1996) Physical, morphological and functional differences between ph 5.8 and 7.4 aggregates of the Alzheimer's amyloid peptide Abeta. *J Mol Biol* **256:** 870-877

Wu J, Anwyl R, Rowan MJ (1995) beta-Amyloid selectively augments NMDA receptor-mediated synaptic transmission in rat hippocampus. *Neuroreport* **6:** 2409-2413

Xiao Y, Ma B, McElheny D, Parthasarathy S, Long F, Hoshi M, Nussinov R, Ishii Y (2015) Abeta(1-42) fibril structure illuminates self-recognition and replication of amyloid in Alzheimer's disease. *Nat Struct Mol Biol* **22:** 499-505

Xue WF, Hellewell AL, Gosal WS, Homans SW, Hewitt EW, Radford SE (2009) Fibril fragmentation enhances amyloid cytotoxicity. *J Biol Chem* **284:** 34272-34282

Xue WF, Hellewell AL, Hewitt EW, Radford SE (2010) Fibril fragmentation in amyloid assembly and cytotoxicity: when size matters. *Prion* **4:** 20-25

Xue WF, Homans SW, Radford SE (2008) Systematic analysis of nucleation-dependent polymerization reveals new insights into the mechanism of amyloid self-assembly. *Proc Natl Acad Sci U S A* **105:** 8926-8931

Yan R, Bienkowski MJ, Shuck ME, Miao H, Tory MC, Pauley AM, Brashier JR, Stratman NC, Mathews WR, Buhl AE, Carter DB, Tomasselli AG, Parodi LA, Heinrikson RL, Gurney ME (1999) Membrane-anchored aspartyl protease with Alzheimer's disease beta-secretase activity. *Nature* **402:** 533-537

Yang M, Teplow DB (2008) Amyloid beta-protein monomer folding: free-energy surfaces reveal alloform-specific differences. *J Mol Biol* **384:** 450-464

Yankner BA, Lu T (2009) Amyloid beta-protein toxicity and the pathogenesis of Alzheimer disease. *J Biol Chem* **284:** 4755-4759

Yeagle PL (1991) Modulation of membrane function by cholesterol. *Biochimie* **73:** 1303-1310

Yip CM, Elton EA, Darabie AA, Morrison MR, McLaurin J (2001) Cholesterol, a modulator of membrane-associated Abeta-fibrillogenesis and neurotoxicity. *J Mol Biol* **311:** 723-734

Yoshiike Y, Tanemura K, Murayama O, Akagi T, Murayama M, Sato S, Sun X, Tanaka N, Takashima A (2001) New insights on how metals disrupt amyloid beta-aggregation and their effects on amyloid-beta cytotoxicity. *J Biol Chem* **276:** 32293-32299

You H, Tsutsui S, Hameed S, Kannanayakal TJ, Chen L, Xia P, Engbers JD, Lipton SA, Stys PK, Zamponi GW (2012) Abeta neurotoxicity depends on interactions between copper ions, prion protein, and N-methyl-D-aspartate receptors. *Proc Natl Acad Sci U S A* **109:** 1737-1742

Younan ND, Sarell CJ, Davies P, Brown DR, Viles JH (2013) The cellular prion protein traps Alzheimer's Abeta in an oligomeric form and disassembles amyloid fibers. *FASEB J* **27:** 1847-1858

Yu WH, Lukiw WJ, Bergeron C, Niznik HB, Fraser PE (2001) Metallothionein III is reduced in Alzheimer's disease. *Brain Res* **894:** 37-45

Yuan H, Hansen KB, Zhang J, Pierson TM, Markello TC, Fajardo KV, Holloman CM, Golas G, Adams DR, Boerkoel CF, Gahl WA, Traynelis SF (2014) Functional analysis of a de novo GRIN2A missense mutation associated with early-onset epileptic encephalopathy. *Nat Commun* **5:** 3251

Zagorski MG, Barrow CJ (1992) NMR studies of amyloid beta-peptides: proton assignments, secondary structure, and mechanism of an alpha-helix----beta-sheet conversion for a homologous, 28-residue, N-terminal fragment. *Biochemistry* **31:** 5621-5631

Zarei MM, Radcliffe KA, Chen D, Patrick JW, Dani JA (1999) Distributions of nicotinic acetylcholine receptor alpha7 and beta2 subunits on cultured hippocampal neurons. *Neuroscience* **88:** 755-764

Zhang M, Zhao J, Zheng J (2014) Molecular understanding of a potential functional link between antimicrobial and amyloid peptides. *Soft Matter* **10:** 7425-7451

Zhang S, Iwata K, Lachenmann MJ, Peng JW, Li S, Stimson ER, Lu Y, Felix AM, Maggio JE, Lee JP (2000) The Alzheimer's peptide a beta adopts a collapsed coil structure in water. *J Struct Biol* **130:** 130-141

Zheng F, Erreger K, Low CM, Banke T, Lee CJ, Conn PJ, Traynelis SF (2001) Allosteric interaction between the amino terminal domain and the ligand binding domain of NR2A. *Nat Neurosci* **4:** 894-901

Zou K, Gong JS, Yanagisawa K, Michikawa M (2002) A novel function of monomeric amyloid beta-protein serving as an antioxidant molecule against metal-induced oxidative damage. *J Neurosci* **22:** 4833-4841